Rubber Production in Continental Southeast Asia its Potentialities and Limitations

Reza Golbon

FACULTY OF AGRICULTURAL SCIENCES

University of Hohenheim

Rubber Production in Continental Southeast Asia

its Potentialities and Limitations

Dissertation
Submitted in fulfillment of the requirements for the degree
"Doktor der Agrarwissenschaften"
(Dr.sc.agr. / Ph.D. in Agricultural Sciences)

to the
Faculty of Agricultural Sciences

Institute of Agricultural Sciences in the Tropics

Agroecology in the Tropics and Subtropics

Prof. Dr. Joachim Sauerborn

Submitted by
Reza Golbon, M.Sc.
from Esfahan

Stuttgart, 2019

Institute of Agricultural Sciences in the Tropics
(Hans-Ruthenberg-Institute)

This thesis was accepted as doctoral dissertation in fulfilment of the requirements for the degree "Doktor der Agrarwissenschaften" (Dr.sc.agr. /Ph.D. in Agricultural Sciences) by the Faculty of Agricultural Sciences at the University of Hohenheim on June 13, 2019.

Date of oral examination: July 17, 2019

Examination committee

Supervisor and Reviewer	Prof. Dr. Joachim Sauerborn
Co-Reviewer	Prof. Dr. Hans-Peter Piepho
Additional Examiner	Prof. Dr. Joachim Müller
Head of Committee	Prof. Dr.-Ing. Stefan Böttinger

Author's Declaration

I, Reza Golbon, hereby affirm that I have written this thesis entitled "**Rubber Production in Continental Southeast Asia - its Potentialities and Limitations**" independently as my original work as part of my dissertation at the Faculty of Agricultural Sciences at the University of Hohenheim. All authors in the quoted or mentioned publications in this manuscript have been accredited. No piece of work by any person has been included without the author being cited, nor have I enlisted the assistance of commercial promotion agencies. This thesis has not been presented into other boards for examination.

Stuttgart 2019

Reza Golbon

Table of contents

Acknowledgements

First and foremost, I would like to express my sincere gratitude to my Supervisor Prof. Dr. Joachim Sauerborn for his continuous support during my Ph.D. study, for his patience, for his being always fair and receptive and for his appreciation of lateral and outside-the-box-thinking. To have been a member of his team was a high honor and many good memories will remain.

I cannot thank Dr. Marc Cotter and Dr. Joseph O. Ogutu enough for the important roles they played all along, helping me overcome the main obstacles and reach the end of this process.

Very special appreciations go out to PD Dr. Frank Rasche and Eva Schmidt for their kind and caring organizational and logistic support after Prof. Sauerborn's retirement.

I would also like to thank the members of my thesis committee: Prof. Joachim Müller and Prof. Dr. Hans-Peter Piepho for their insightful comments, encouragement and questions which helped me improve my research from several different perspectives.

A very special gratitude goes out to my friends who were with me in the ups and downs of this journey and contributed through inspiring, encouraging and invigorating exchanges: Shahin Ghaziani, Dr. Samira Sahami, Ziba Barati, Dr. Hossein Mahmoudi, Dr. Shahrokh Raei, Dr. Eskandar Abadi, Dr. Franziska Harich, Prof. Dr. Folkard Asch, Sabine Baumgartner, Irene Chukwumah, Dr. Michael Yongha Boh, Dr. Jan Bauer, Dr. Inga Häuser, Dr. Xueqing Yang, Kevin Thellmann, Benjamin Warth, Kristian Johnson, Dr. Sabine Stuerz, Dr. Christian Brandt, Dr. Carsten Marohn, Dr. Elena Jenssen, Johanna Schüssler, Dr. Solveig Franziska Bucher, Natalie Reinsch, Kerstin Hoffbauer, Ali Hoffbauer, Arvid Donert, Bernd Riehle, Vera Gillé, Tar Avidan, Ai Han-Jian, Jing-Xin Liu, Lai Han, Dr. Mehdi Mahbod, Dr. Iman Rastegar, Rahil Zabihi, Pedram Manavi, Elisabeth Zimmermann, Dr. Dorette Müller-Stöver, Dr. Eva Kohlschmid, Dr. Jan Grenz, Dr. Marie Joy Schulte and Dr. Konrad Martin.

Finally, I would like to thank my dear parents Mahin and Hamid and my dear sister Neda whose warm presence, even from far away, always provided me with moral and emotional support.

Summary

This thesis focuses on three climate-related aspects of Para rubber (*Hevea brasiliensis*) cultivation in areas where altitudes and latitudes higher than its endemic range create conditions which are labeled nontraditional, suboptimal or marginal for rubber cultivation: 1. rubber yield in relation to the meteorological conditions preceding harvest events, 2. potential geographical shifts in rubber cultivation through climate change and 3. assessment of climate driven susceptibility to South American leaf blight (*Pseudocercospora ulei*) of rubber.

Linear mixed models were developed and used to predict rubber yield in Xishuangbanna China (22°N 100°E and 900 m above sea level) based on the meteorological conditions to which rubber trees had been exposed for periods ranging from one day to two months prior to tapping events. Serial autocorrelation in the latex yield measurements was accounted for using random effects and a spatial generalization of the autoregressive error covariance structure suited to data sampled at irregular time intervals. Information theoretics was used to select models with the greatest strength of support in the data from a set of competing candidate models. The predictive performance of the selected best model was evaluated using both leave-one-out cross-validation and an independent test set. Moving averages of precipitation, minimum and maximum temperature, and maximum relative humidity with a 30-day lead period were identified as the best yield predictors. Prediction accuracy expressed in terms of the percentage of predictions within a measurement error of 5 g for cross-validation and also for the test dataset was above 99 %.

The second study focused on the potential shifts of rubber cultivation as a consequence of ongoing climate change within the Greater Mekong Subregion (GMS). Rule-based classification was applied to a selection of nine gridded climatic data projections (precipitation and temperature, and global circulation models (GCMs)). These projections were used to form an ensemble model set covering the representative concentration pathways (RCPs) 4.5 and 8.5 of the Fifth Assessment Report of the Intergovernmental Panel on Climate Change at three future time sections: 2030, 2050 and 2070. A post classification ensemble formation technique based on the majority outcome of the classification was used to not only provide an ensemble projection but also to spatially track and weight the disagreements between the classified GCMs. A similar approach was used to form an ensemble model aggregating the involved climatic factors. The level of agreement between the ensemble projections and GCM products was assessed for each climatic factor separately, and also at the aggregate level. Shifting zones with high confidence were clustered based on their land use composition, physiographic attributes and proximity. Following

the same ensemble formation technique and by setting a 28 °C threshold for annual mean temperature, areas prone to exposure to potentially excessive heat levels were mapped. Almost the entire shift projected with high certainty was in the form of expansion, associated with temperature and temporally limited to the 2030 time window, during which the total area conducive to rubber cultivation in the GMS is projected to exceed 50% by 2030 (from 44.3% at the turn of the century). The largest detected cluster (41% of the total shifting area), which also is the most ecologically degraded, corresponds to Northern Vietnam and Guangxi Autonomous Region of China. The area exposed to potentially excessive heat is projected to undergo a 25-fold increase under RCP4.5 by 2030 from 14568 km^2 at the baseline.

The third study focuses on South American leaf blight (SALB) of Para rubber trees. SALB is a serious fungal disease that hinders rubber production in the Americas and sustains concerns over the future of rubber cultivation in Asia and Africa. The existing evidence on the influence of weather conditions on SALB outbreaks in Brazil has prompted a number of assessment studies seeking to produce risk maps that reflect this relationship. Emerging hot spot analysis was applied to three decades of gridded daily precipitation and surface relative humidity data to illuminate the temporal and geographical patterns of these two factors in relation to the occurrence of weather conditions linked to SALB emergence. Inferential improvements through inclusion of the uncertainties and fine-scaled temporal breakdown of the evaluation were achieved in this section. Our findings support the notion that plenty of low risk areas exist within the rubber growing areas outside of the 10° equatorial belt.

With the work done over the course of the three studies on rubber presented within this thesis, I have been able to shed more light on a number of challenges and opportunities that the continuous production of this important natural and renewable resource is facing. Thorough assessment of preferable locations for optimal latex production is crucial for decision-makers in order to both maximize the yield and minimize unnecessary and undesirable impacts on the landscape level from poor choices of location. The approaches developed and presented are transferable to different regions and cropping systems if needed.

Zusammenfassung

Untersucht wurden im Rahmen der Dissertation drei klimabezogene Aspekte des Kautschukanbaus (*Hevea brasiliensis*) in Gebieten, die im Allgemeinen auf Grund ihrer geographischen Lage (nördl./südl. des 10. Breitengrades) als suboptimal, nicht-traditionell oder wenig geeignet beschrieben werden. Dabei stand die Bildung von Ertragsmodellen in direkter Abhängigkeit von lokalen Wetterbedingungen und die durch den Klimawandel entstehenden Optionen zur Expansion und/oder Reduktion der Flächen für den Kautschukanbau auf überregionaler Ebene, sowie die globale Risikobewertung für die Infektionswahrscheinlichkeit mit der südamerikanischen Blattfallkrankheit (*Pseudocercospora ulei*) im Zentrum der Arbeit.

Linear gemischte Modelle wurden verwendet, um den Latexertrag in der Präfektur Xishuangbanna, Provinz Yunnan, VR China (22°N 100°E und 900 m ü. d. M.) in Abhängigkeit der lokalen Wetterbedingungen zu prognostizieren. Hierfür wurde auch untersucht, welche Zeitintervalle der Wetterbeobachtung, von einem bis 60 Tagen vor dem Erntezeitpunkt, den ausschlaggebendsten Einfluss auf den Latexertrag haben. Um das Problem der Autokorrelation der Latexertragsmessungen zu bewältigen wurden „random effects“ und eine räumliche Verallgemeinerung der autoregressiven Fehlerkovarianzstruktur innerhalb der in unregelmäßigen Zeitabständen gesammelten Daten angewandt. Aus einer Reihe von konkurrierenden Modellen wurden daraufhin diejenigen mit der stärksten Erklärungskraft ausgewählt. Die Vorhersagekraft der Modelle wurde durch 'leave-one-out' Kreuzvalidierung sowie unter Zuhilfenahme eines unabhängigen Datensatzes evaluiert. Die gleitenden Durchschnitte von Niederschlag, Tageshöchst- und Tagesmindesttemperatur sowie die maximale Luftfeuchtigkeit, alle gemittelt über einen Zeitraum von 30 Tagen vor der Ernte, wurden als beste Ertragsprädiktoren identifiziert. Die prognostizierte Treffsicherheit, ausgedrückt als Prozentanteil der Vorhersagen innerhalb von 5 g Messungenauigkeit, war für die Kreuzvalidierung und den Testdatensatz jeweils mehr als 99 %.

Eine weitere Studie behandelte die klimawandel-bedingte Expansion oder Kontraktion der potentiell für den Kautschukanbau geeigneten Flächen im erweiterten Einzugsgebiet des Mekong (Greater Mekong Subregion, GMS). Rasterbasierte Temperatur- und Niederschlagsprognosen, hergeleitet aus einer Auswahl aus neun globalen Zirkulationsmodellen (GCMs) wurden regelbasiert klassifiziert. Die Zusammenführung der Zirkulationsmodelle stellte ein Ensemble-Model-Set dar, das die repräsentativen Kohlendioxid Konzentrationspfade (RCPs) 4.5 und 8.5 aus dem fünften Bericht des Zwischenstaatlichen Ausschusses für Klimaänderungen (IPCC) in drei zukünftigen Zeitabschnitten umfasst: 2030, 2050 und 2070. Dafür wurde eine Methode zum

Aufbau eines Modellensembles nach der Klassifizierung entwickelt, die in der Lage ist nicht nur die Zusammenstellung des Ensembles zu gewährleisten, sondern darüber hinaus auch die Entwicklung der GCMs und der Abweichungen zwischen den GCMs räumlich nachzuverfolgen und zu gewichten. Ein ähnlicher Ansatz wurde verfolgt, um die Zusammenstellung des Modellensembles für die beteiligten Klimakomponenten durchzuführen. Für jeden Klimafaktor wurde, sowohl separat als auch aggregiert, der Grad an Übereinstimmung zwischen den Projektionen der Ensembles und den GCMs untersucht. Zonen, in denen eine Änderung der Eignung für den Kautschukanbau mit hoher Sicherheit prognostiziert wurden, zeichneten sich durch die Bildung von Clustern hinsichtlich der Zusammenstellung der Landnutzung, physio-geographischer Attribute und Nähe zueinander aus.
Die gleiche Methodik wurde angewandt, um Gebiete mit einem prognostizierten erhöhten Risiko für übermäßige Hitze, basierend auf einem Schwellenwert von 28°C Jahresdurchschnittstemperatur, zu identifizieren. Die Auswertung ergab, dass der größte Anteil an erwartbarem Wandel in der potentiell nutzbaren Fläche für eine mögliche Expansion des Kautschukanbaus liegt. Mit hoher Sicherheit lässt sich sagen, dass bis zum Jahr 2030 die potentiell nutzbare Fläche (temperaturbedingt) innerhalb der GMS von 44.3% auf über 50% ansteigen wird. Das größte räumliche Kontinuum innerhalb dieser Übergangszone (41% des gesamten Wandels) befindet sich in den ökologisch am stärksten degradierten Gebieten Nordvietnams und der Autonomen Region Guangxi, VR China. Gleichzeitig deuten die Prognosen auf einen Anstieg der durch übermäßige Hitze gefährdeten Gebiete um das 25-fache, basierend auf dem RCP4.5 für 2030.

Die Südamerikanische Blattfallkrankheit beim Kautschuk (South American leaf blight, SALB) ist eine schwerwiegende Pilzerkrankung die den Kautschukanbau in Nord und Südamerika stark einschränkt und als eine ernste Bedrohung für den Kautschukanbau in Asien und Afrika anerkannt ist. Eine Reihe von Studien, basierend auf Belegen das bestimmte Witterungsverhältnisse einen ausschlaggebenden Einfluss auf großflächige Ausbrüche von SALB in Brasilien hatten, wurden durchgeführt, um eine Kartierung für das Infektionsrisiko zu erstellen,. Um kleinräumige Muster innerhalb von Untersuchungsobjekten mit sowohl dynamischen als auch zyklischen räumlichen und zeitlichen Eigenschaften erkennen zu können, müssen sowohl die zugrundeliegenden Daten als auch die Ergebnisse eine ausreichend feine räumliche Auflösung und temporäre Granulation aufweisen. Technische Barrieren wie unzureichender Zugang zu Daten oder geringe Rechenleistung, die bisher als Grund für die Nutzung von tendenziell zu stark generalisierten Proxi-Variablen herangezogen wurden, sind in letzter Zeit zunehmend abgebaut worden. In dieser Studie wurde eine „Emerging Hot Spot“ Analyse angewendet, um basierend auf einer Zeitreihe von 30 Jahren an täglichen Daten zu

Niederschlag und relativer Luftfeuchtigkeit, die zeitlichen und geographischen Muster dieser Faktoren im Zusammenhang mit dem Erscheinen von Wetterbedingungen, die einen Ausbruch von SALB unterstützen würden, zu beleuchten. Durch den konsequenten Umgang mit Unsicherheiten und einer detaillierten zeitlichen Aufschlüsselung der Auswertung konnte so eine deutliche Verbesserung der wissenschaftlichen Schlussfolgerungen erreicht werden. Die Ergebnisse unterstützen die Annahme, dass „SALB sichere" Anbaugebiete außerhalb des 10. Breitengrades und innerhalb der für den Kautschukanbau nutzbaren Zonen weltweit existieren.

Im Rahmen der drei Studien die innerhalb dieser Doktorarbeit vorgestellt wurden war ich in der Lage auf eine Reihe von Herausforderungen und Möglichkeiten einzugehen, die für den andauernden und zukünftigen Anbau dieser wichtigen, nachwachsenden Ressource von Bedeutung sind. Die Untersuchung umweltgerechter und geeigneter Anbaugebiete und -standorte für eine optimale und nachhaltige Latexproduktion können einen entscheidenden Informations- und Diskussionsbeitrag für Politiker und Entscheidungsträger auf lokaler und regionaler Ebene darstellen. Die Methoden, die im Rahmen dieser Studie entwickelt und vorgestellt wurden sind sowohl auf andere Weltregionen anwendbar, als auch wenn gewünscht, transferierbar auf andere Acker- und Waldbausysteme.

Overview of publications

Following the rules of the Faculty of Agricultural Sciences on cumulative PhD dissertations, chapters two to four of this manuscript have been published in the peer-reviewed journals which follow.

Chapter 2

Golbon R, Ogutu JO, Cotter M, Sauerborn J (2015) Rubber yield prediction by meteorological conditions using mixed models and multi-model inference techniques. Int J Biometeorol 59(12): 1747–1759. doi: 10.1007/s00484-015-0983-0.

Chapter 3

Golbon R, Cotter M, Sauerborn J (2018) Climate change impact assessment on the potential rubber cultivating area in the Greater Mekong Subregion. Environ Res Lett 13(8):084002. doi: 10.1088/1748-9326/aad1d1.

Chapter 4

Golbon R, Cotter M, Mahbod M, Sauerborn J (2019) Global Assessment of Climate Driven Susceptibility to South American Leaf Blight of Rubber using Emerging Hot Spot Analysis and Gridded Historical Daily Data. Forests 10(3): 203. doi:10.3390/f10030203.

Other peer-reviewed publications with Reza Golbon's participation:

Cotter M, Berkhoff K, Gibreel T, Ghorbani A, Golbon R, Nuppenau E, Sauerborn J (2014) Designing a sustainable land use scenario based on a combination of ecological assessments and economic optimization. Ecological Indicators 36, 779-787. doi:10.1016/j.ecolind.2013.01.017.

Yang X, Blagodatsky S, Marohn C, Liu H, Golbon R, Xu J, Cadisch G (2019) Climbing the mountain fast but smart: Modelling rubber tree growth and latex yield under climate change. Forest Ecology and Management 439:55–69. doi: 10.1016/j.foreco.2019.02.028.

Thellmann K, Golbon R, Cotter M , Cadisch G , and Asch F (2019) Assessing hydrological ecosystem services in a rubber-dominated watershed under scenarios of land use and climate change. Forests 10(2), 176. doi:10.3390/f10020176.

List of figures

List of tables

Abbreviations

AIC	Akaike information criterion
AICc	AIC corrected for small sample size
AR	autoregressive model
ARMA	autoregressive moving-average model
a.s.l.	above sea level
BII	biodiversity intactness index
BMBF	German federal ministry of education and research
CART	classification and regression tree analysis
CCAFS	climate change and food security program
CIAT	international center for tropical agriculture
CS	cold spot
DMC	dry matter content
EHSA	emerging hot spot analysis
ESRL	the earth system research laboratory
GADM	global administrative areas project
GBH	girth at breast height
GHG	greenhouse gas
GIS	geographic information systems
GMS	greater Mekong subregion
HS	hot spot
IPCC AR5	fifth assessment report of the intergovernmental panel on climate change
IRSG	international rubber study group
K-L	Kullback-Leibler distance
KMZ	keyhole markup language zipped
LGFG	Landesgraduiertenförderung Act
LILAC	living landscapes China project
LOOCV	leave-one-out cross-validation
LR	likelihood ratio
LRT	likelihood ratio test
MAE	mean absolute error
ML	maximum likelihood
MMI	multi-model inference

MSEA	mainland Southeast Asia
NCEP	national center for environmental prediction
NetCDF	network common data form
NOAA	national oceanic and atmospheric administration
NRWNNR	Naban river watershed national nature reserve
NSO	Thailand agricultural census
OAR	office of oceanic and atmospheric research
PLS	partial least squares
PNG	portable network graphic
PROBOR	programa de incentivo à produção de borracha vegetal
PSD	climate prediction center
RCP	representative concentration pathways
REML	restricted (residual) maximum likelihood
RH	relative humidity
RMSE	root mean square error
SALB	South American leaf blight
SMA	standard moving average
SNRi	sustainable natural rubber initiative
SP POW	spatial power covariance structure
SRTM	shuttle radar topography mission
SURUMER	sustainable rubber cultivation in the Mekong region project
T	temperature
VIF	variance inflation factor
VPD	vapor pressure deficit
XSBN	Xishuangbanna

1 General introduction

1.1 Rubber boom and its socio-economic and environmental impacts

Natural rubber is an important industrial commodity for which Para rubber tree (*Hevea brasiliensis* Muell. Arg.) is currently the only viable source. In spite of its tropical origin, the Amazon, *H. brasiliensis* possesses considerable climatic adaptability (Alam et al. 2005; Kositsup et al. 2009; Rao and Kole 2016) and has been cultivated in altitudes exceeding 1000m a.s.l. and latitudes over 25° (Priyadarshan et al. 2005) (see Figures 1.1 to 1.3). Driven by the growing global demand for this high-value raw material, rubber cultivation has been and still is quickly expanding in the tropics and subtropics, replacing forests and traditional agricultural practices (Chen et al. 2016b; Sarathchandra et al. 2018; Chakraborty et al. 2018; Xiao et al. 2019).

Although an overwhelming majority of the global rubber cultivation is in the hands of smallholders (Fox and Castella 2013), most often the spatial pattern in which rubber cultivation expands and solidifies its dominance over many tropical and subtropical landscapes, has undeniable similarities to typical large-scale commercial plantations: vast monocultures engulfing fragmented, shrinking and disconnected pieces of forest. Of course, large commercial plantations play a role too, as less developed countries such as Cambodia, Laos and Myanmar grant land concessions to foreign investments to establish large rubber plantations. Grogan et al. (2019) used remote sensing to reveal that more than 20% of the national forest cover in Cambodia has been cleared between 2001 and 2015, a fifth of which has been converted to rubber plantations..

This rubber boom has been accompanied by significant environmental and socio-economic change. Disturbed equilibrium in ecosystem functions and services caused by habitat and biodiversity loss (Li et al. 2013; He and Martin 2015; Warren-Thomas et al. 2015; Liu et al. 2016; Zhang et al. 2017; Rembold et al. 2017), deterioration of carbon stocks (de Blécourt et al. 2013; Yang et al. 2016; Min et al. 2019), soil erosion (Liu et al. 2015b, 2018c), hydrological cycle imbalance (Tan et al. 2011; Hardanto et al. 2017; Tarigan et al. 2018), and land and water pollution by fertilizers, pesticides and herbicides (Abdullah 1995) are only some of the environmental problems associated with this transformation. From the socio-economic point of view, poverty alleviation has been achieved through rubber production to different degrees (Liu et al. 2006; Fox and Castella 2013; Lu 2017; Andriesse and Tanwattana 2018). Yet, issues such as food insecurity due to subsistence crops being abandoned in favor of rubber (Behera et al. 2016; Thanichanon et al. 2018), income insecurity as a result of severe fluctuations in rubber price (Andriesse and Tanwattana 2018), and particularly in land concession cases, human rights violations (land

grabbing, poor working conditions and migrant workforce issues) have been documented (Kenney-Lazar 2012; Global Witness 2013; Baird et al. 2019).

Figure 1.1 Rubber dominated landscapes

Figure 1.2 Land use conversion to rubber
Freshly cleared hilltops in Xishuangbanna (China) with rubber seedlings in foreground

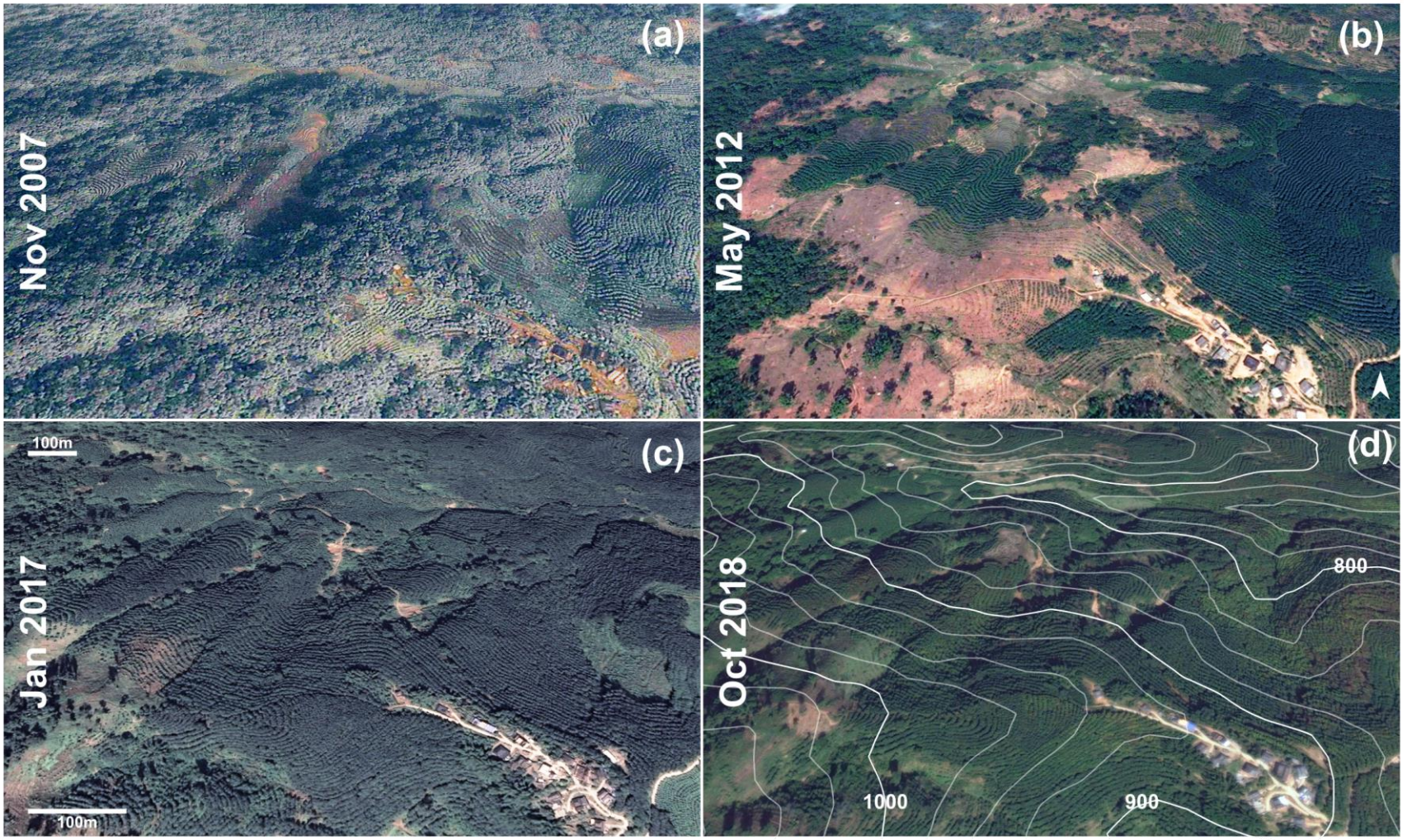

Figure 1.3 An example of land use change from forest to rubber cultivation in elevations verging 1000m a.s.l. in Xishuangbanna during the last decade. Screenshots were collected from Google Earth™. For more information on the location illustrated above, see Figure 2.1. The bird eye viewpoint is identical of all panels. Dual scale bars are used due to the non-vertical viewpoint. Contour lines were generated from STRM data (www.usgs.gov) using ArcGIS 10.2.2. The different components of the Figure were combined and arranged in Inkscape 0.92.

1.2 Mitigation of the negative environmental impacts of monoculture rubber cultivation

Ahrends et al. (2015) estimated that 57% of the continental Southeast Asian rubber cultivation is not sustainable. Production of natural rubber to meet raw material demand and mitigation of rural poverty, should not be at the cost of compromising current and coming generations' access to other ecosystem functions and services.

Policy makers and stakeholders have recently started to react to the environmental concerns raised through academic discourse on the expansion of rubber monocultures. Guidelines, action plans and initiatives have been proposed. The International Rubber Study Group (IRSG), an international organization based in Singapore, is composed of stakeholders involved in different parts of the natural rubber value chain. They introduced a set of standards in 2014 dubbed Sustainable Natural Rubber Initiative (SNRi), which seeks sustainability across the natural rubber sector (IRSG 2014). More recently, another collection of guidelines has been published by the Chinese Chamber of Commerce for Metals, Minerals and Chemicals Importers and Exporters (CCCMC) and seeks the same goal (CCCMC 2017). There is still a long way to go for such campaigns to translate to widespread practices and enforced standards.

Meanwhile researchers have been investigating more diversified and environmentally friendly ways to cultivate rubber through agroforestry schemes, such as exploring the possibility for rubber intercropping with other species, such as perennial tree crops (Righi et al. 2007, 2008, 2013; Snoeck et al. 2013; Partelli et al. 2014; Araújo et al. 2016; Novais et al. 2017), timber species (Somboonsuke et al. 2011; Jongrungrot and Thungwa 2013; Jongrungrot et al. 2014; Langenberger et al. 2017) and legumes as cover crop (Watson et al. 1964; Broughton 1976; Clermont-Dauphin et al. 2016, 2018). Besides contribution to the development of a more balanced ecosystem, intercropping can provide farmers with additional income sources and compensate some of the losses occurring due to rubber price fluctuations. Being able to reliably evaluate the feasibility of such plans and estimate the revenues from each of these cultivation methods in the context of the existing local environmental conditions, is essential for the exploration of alternatives, decision-making and land use planning. However, there are some significant knowledge gaps in regards to different aspects of rubber cultivation at high altitudes and latitudes, not only for the agroforestry schemes, but also for *H. brasiliensis*. This is a barrier to exploring more diversified cultivation systems.

1.3 Research gaps

This thesis addresses some of the research gaps existing in three identified domains in relation to rubber cultivation in mainland Southeast Asia.

A robust and parsimonious statistical model for estimation of latex yield in the above mentioned areas has so far been lacking. Some of the assumptions of normal regression methods, on top of them the independence of residuals, are typically missing in rubber yield data, which dictate the use of additional/alternative measures for such a purpose.

Studies investigating the effects of climate change on rubber cultivation and its potential spatial distribution are rare. Furthermore, some essential aspects of this topic have so far not been covered, including the uncertainties that can be traced through the disagreements among different climate change projections. Areas expected to be soon exposed to heat levels potentially harmful to rubber trees have not been mapped.

Risk assessment for introduction of South American leaf blight (SALB), the most serious disease known to *H. brasiliensis*, responsible for insignificant share of American tropics, to Asia and Africa have until recently not been made spatially explicit through the use of geographic information systems. Two major aspect of this issue have not yet been adequately addressed: the time steps involved in trend analysis, they need to be broken down to a reasonably fine scale, and the implausibly dichotomous 'safe' and 'risky' classifications should be revised by allowing for an 'uncertain' class.

1.4 Objectives

This thesis pursues the following objectives with geographical focus on continental Southeast Asia:

1. Modeling rubber yield in relation to meteorological conditions through
   1.1. identification of the meteorological covariates most influential in predicting rubber yield
   1.2. determination of the optimal lead periods to capture the lagged effects for covariates
   1.3. finding the appropriate way to account for serial autocorrelation in the latex yield data
   1.4. construction and validation of a robust and parsimonious rubber yield predicting model
2. Ensemble assessment of the expected impacts of climate change on the rubber cultivating area by
   2.1. mapping potential shifts of rubber cultivation
   2.2. geographically delineating the potential exposure to excessive heat levels

2.3. assessing the agreement level among the ensemble members
2.4. presenting the uncertainties raising from the ensemble members
3. Mapping the climate-driven susceptibility to South American Leaf Blight of rubber

1.5 Outline of the thesis

As a cumulative thesis, this dissertation is composed of a general introduction (current section), three chapters which have been published or submitted for publication as peer-reviewed articles (Chapters 2 to 4) and a general discussion (Chapter 5).

Chapter 2 presents modeling of rubber yield based on weather conditions occurring before harvest events using time series data and linear mixed models for rubber cultivating areas in high altitudes and altitudes of continental Southeast Asia.

Chapter 3 investigates the effects of climate change on potential spatial changes in areas conducive to rubber cultivation in continental Southeast Asia within the next five decades using an ensemble of gridded climatic data projections.

Chapter 4 focuses on the climate driven global risk assessment of exposure to South American leaf blight which is the most serious disease of rubber trees in a spatial context using emerging hotspot analysis on historical gridded data with daily temporal granulation.

Chapter 5 concludes this thesis by discussing the findings presented in Chapters 2 to 4 and their implications in a joint context.

2 Rubber yield prediction by meteorological conditions using mixed models and multi-model inference techniques

Reza Golbon[1*], Joseph Ochieng Ogutu[2], Marc Cotter[1] and Joachim Sauerborn[1]

[1] Institute of Plant Production and Agroecology in the Tropics and Subtropics, University of Hohenheim, Stuttgart, Germany

[2] Institute of Crop Science, University of Hohenheim, Stuttgart, Germany

*Correspondence: golbon@uni-hohenheim.de
Published online: 1 April 2015
doi: 10.1007/s00484-015-0983-0

Abstract

Linear mixed models were developed and used to predict rubber (*Hevea brasiliensis*) yield based on meteorological conditions to which rubber trees had been exposed for periods ranging from 1 day to 2 months prior to tapping events. Predictors included a range of moving averages of meteorological covariates spanning different windows of time before the date of the tapping events. Serial autocorrelation in the latex yield measurements was accounted for using random effects and a spatial generalization of the autoregressive error covariance structure suited to data sampled at irregular time intervals. Information theoretics, specifically the Akaike information criterion (AIC), AIC corrected for small sample size (AICc), and Akaike weights, was used to select models with the greatest strength of support in the data from a set of competing candidate models. The predictive performance of the selected best model was evaluated using both leave-one-out cross-validation (LOOCV) and an independent test set. Moving averages of precipitation, minimum and maximum temperature, and maximum relative humidity with a 30-day lead period were identified as the best yield predictors. Prediction accuracy expressed in terms of the percentage of predictions within a measurement error of 5 g for cross-validation and also for the test dataset was above 99 %

Keywords

Hevea brasiliensis, Yield, Prediction, Meteorological conditions, Mixed models, Multi-model inference

2.1 Introduction

The rubber tree *Hevea brasiliensis* (Willd. ex A. Juss.) Muell. Arg. is an important industrial crop which occupies more than 10 million ha of the terrestrial surface of the earth (Rivano et al. 2013) and provides more than 11 million tons of natural rubber per year (FAOSTAT 2015; IRSG 2015). The tree is a member of the family Euphorbiaceae and is native to the southern part of the Amazon basin (Priyadarshan and Goncalves 2003). Since the 1870s, attempts have been made to cultivate rubber outside of the South American humid tropics owing to the limitation of rubber cultivation by South American leaf blight (SALB) caused by the fungus *Microcyclus ulei*, recently renamed *Pseudocercospora ulei* (Henn.) by Hora Júnior et al. (2014). Rubber cultivation in the southern plateau of Brazil, where low temperatures and humidity create "escape areas" from SALB, has been practiced and studied since the 1980s (Ortolani et al. 1998; Clément-Demange et al. 2007). Today, nearly 97 % of the total global production comes from outside the Tropical Americas (Asia, 91.9 %, and Africa, 5.0 %) (FAOSTAT 2015).

Especially during the last decades and in response to driving forces such as increasing market demand, high value of natural rubber, governmental desire for self-sufficiency, and regional development policies (Rao et al. 1998; Fox and Castella 2013; Xu et al. 2014; Fox et al. 2014), rubber cultivation has expanded to areas farther away from suitable climatic conditions of the humid tropics. For example, according to Li and Fox (2012), more than 1 million ha of rubber plantations had been established in 2012 in nontraditional rubber-cultivating areas of China, Laos, Myanmar, Thailand, Vietnam, and Cambodia. This accounts for about 12 % of the total rubber-growing area in Southeast Asia, which is predicted to quadruple by 2050 (Fox et al. 2012).

Southern China and the northeastern states of India are the northernmost areas associated with rubber cultivation (Priyadarshan et al. 2005). Climatic conditions in continental southern margins of China are subtropical, fully humid in the eastern side (Guangxi and Guangdong), and subtropical winter dry in the central and western parts (southern Yunnan). Southern Yunnan Province has a hilly topography and hence strongly contrasts with the other subtropical Chinese rubber-producing regions. This results in considerable spatial variability in climatic conditions and potentially substantial changes in climate and microclimate-related qualities of land influencing rubber yield. Thus, for example, it is an established phenomenon that the gestation period (the time required by rubber trees to reach maturity as a perennial crop) increases from 5 years in optimal conditions of the equatorial belt (10° S to 10° N) to up to 8 years in sub-optimal areas with cold and dry month. Besides genotype, husbandry, and soil conditions, mainly the climatic setting defines the output of latex (Rao et al. 1998). Modeling the relationships between

climatic/meteorological covariates and rubber yield can therefore help differentiate and rank locations according to their potential for economic rubber production and guide land use planning.

Priyadarshan (2011) has reviewed the findings of a number of studies that have examined the optimal abiotic environmental conditions for rubber growth and development, net photosynthesis, and latex formation and latex flow at tapping (Pushparajah 1983; Haridas 1985; Monteny et al. 1985; Shangphu 1986; Shuochang and Yagang 1990; Sanjeeva Rao and Vijayakumar 1992; Ong et al. 1998). However, far fewer attempts have been made to predict rubber yield based on the environmental conditions to which rubber trees are exposed (Jiang 1988; Rao et al. 1998; Raj et al. 2005; Yu et al. 2014). Yu et al. (2014) studied the relationships between the rubber yield and climatic conditions using partial least squares (PLS) regression and classification and regression tree analysis (CART). Other methods used to predict latex yield consisted of correlation analysis, stepwise multiple regression, and identification of the ranges of meteorological variables associated with high yields. To investigate the lagged effects of meteorological conditions on rubber yield, some studies have introduced the standard moving average (SMA) variants of the meteorological variables as predictors in their models (Rao et al. 1998; Raj et al. 2005).

Findings of different studies have been mixed regarding the meteorological factors they have identified as being the most influential or best in predicting rubber yield. Meteorological factors identified as being the most predictive of latex yield include minimum and maximum temperatures (Rao et al. 1998), mean temperature (Jiang 1988; Raj et al. 2005; Yu et al. 2014), diurnal temperature variation (Jiang 1988; Raj et al. 2005; Yu et al. 2014), precipitation (Jiang 1988; Yu et al. 2014), soil moisture storage (Raj et al. 2005), evaporation (Rao et al. 1998; Raj et al. 2005), vapor pressure deficit (Rao et al. 1998), relative humidity (Ortolani et al. 1998; Yu et al. 2014), sunshine hours (Jiang 1988; Ortolani et al. 1998; Yu et al. 2014), and wind speed (Priyadarshan and Goncalves 2003). This is not surprising if differences inherent in the characteristics of the investigated genotypes (e.g., level of their resistance to different stress factors) and locations (e.g., soil and climate conditions) across different study sites are considered. A mechanistic understanding of how the influence of variation in meteorological covariates on latex yield is modified by the interaction between genotypes and the environment is essential for developing predictive models for rubber yield but is still in its infancy. Even so, several recent studies have focused on understanding the mechanisms through which fluctuations in particular climactic variables influence latex yield. So, for example, the effect of rainfall seasonality, mediated through seasonality in soil water status, has been associated with a strong seasonality in activities of different parts of the root system of *H. brasiliensis*. Most of the water and nutrient uptake by

this species takes place in the top soil where the highest concentration of fine roots is present, whereas the deep roots show high water uptake activity during the dry season, with a peak in water uptake coinciding with the transition period between the dry and rainy seasons (Gonkhamdee et al. 2009; Carr 2012; Liu et al. 2014; Kobayashi et al. 2014). This seasonality apparently underlies the stronger relationship between the fine root dynamics of *H. brasiliensis* in eastern Thailand and monthly meteorological data than finer-resolution (e.g., weekly) data, particularly soil water status, recently documented by Chairungsee et al. (2013). As a result, the generalizability of models for predicting rubber yield from meteorological covariates would seem to be limited both by the specific genotypes and geographical contexts considered.

Harvesting latex from rubber trees is always carried out repeatedly on the same trees over time. Therefore, if interest centers on latex yield from each harvest event (as in the present case), then the collection of data on the same measurement units (rubber trees) over time is inevitable. The resulting longitudinal data are thus likely to be serially correlated, requiring the use of mixed models to account for the autocorrelation.

In this study, we exploit the flexibility provided by mixed models, information-theoretic model selection criteria, and multi-model inference to identify the meteorological covariates most influential in predicting rubber yield in the southern Yunnan Province of China. The selected meteorological covariates are used to construct an empirical model for predicting rubber yield and the predictive accuracy of the model assessed by both cross-validation and an independent test dataset.

2.2 Materials and methods

2.2.1 Data collection

Data collection took place in the central part of the Naban River Watershed National Nature Reserve (NRWNNR), Xishuangbanna (XSBN), China (Figure 2.1). Data were obtained from two, 15-year-old rubber plantations of the cold-resistant clone GT1 at a density of about 470 trees per ha. Trees which provided the training dataset were located on a 41° south-facing slope at 900 m above sea level (m a.s.l.) (22° 9′ 45″, 100° 39′ 26″), while the test dataset was gathered on a 37° southeast-facing slope at 680 m a.s.l. (22° 10′ 02″, 100° 39′ 37″). Soil type was identified as an acrisol with clay (C) texture in the top 20 cm and silty clay (SiC) in the 20–77 cm depth (Wolff and Zhang 2010).

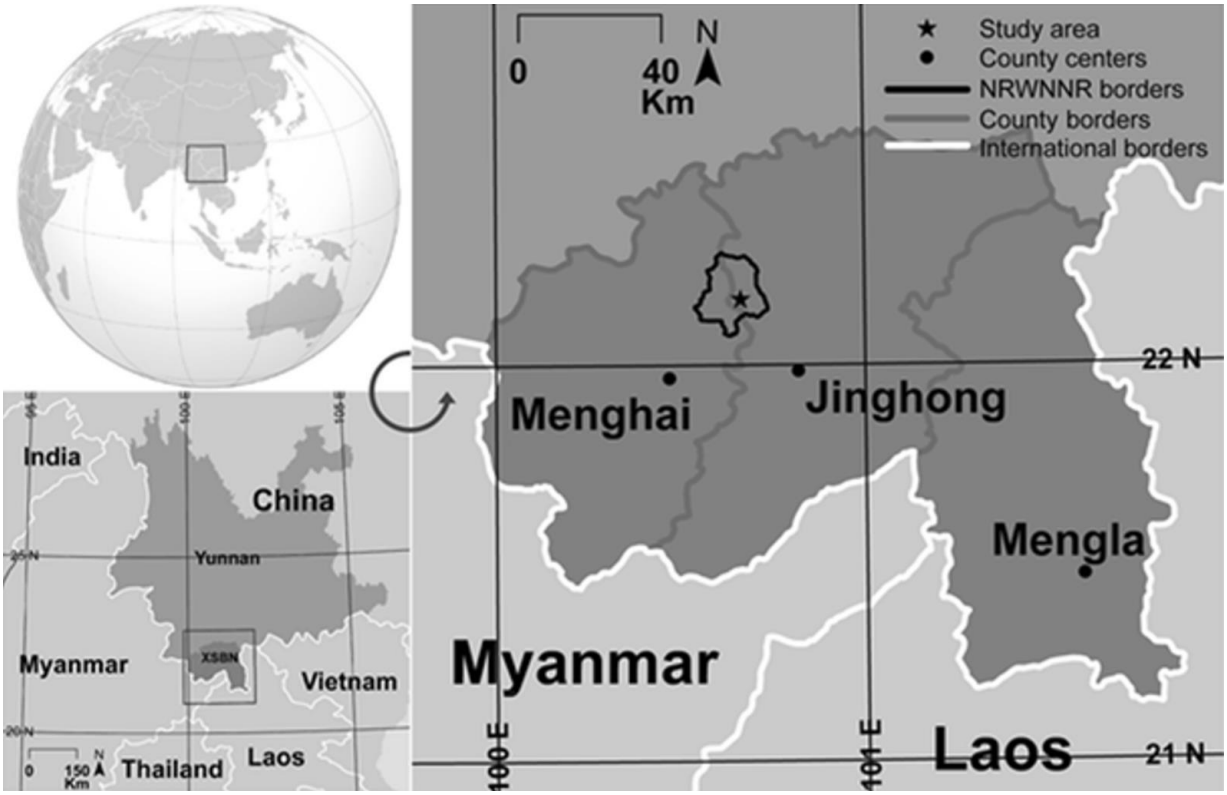

Figure 2.1 Location of the study area
The orthographic projection in the upper left corner is modified from Wikipedia (http://commons.wikimedia.org). Other maps were generated using ESRI ArcMap 10, and the shape files of the administrative borders are available at the website of Global Administrative Areas Project (http://www.gadm.org)

Rubber trees (n = 18) were randomly selected from each plantation. We chose girth at breast height (GBH) at 130 cm aboveground close to 55 cm (average girth for rubber trees of clone GT1 at age 15 as we found in a pilot study covering over 3000 trees in central NRWNNR) as a requirement for selection of the study trees. Rubber was planted in the mid-1990s and went through their 7th and 8th year of tapping during the data collection period (March 2009 to November 2010). Plantations were subject to comparable management regimes including tapping frequency, harvest time, and fertilization regime. These two plantations could also be considered representative of smallholder rubber cultivation practices in the region except for yield stimulation by bark treatment with Ethephon, a plant growth regulator stimulating latex flow. Upon our request, this treatment was not applied to trees selected for this study. The influence of the tapping practice on rubber yield has been reported to dominate the effects of genetics and the annual phenological stages (Silva et al. 2012). If tapping is carried out by different persons with differing skill levels, then this introduces an additional source of variation to the yield data which needs to be accounted for by prediction models. Accordingly, only one person experienced in tapping carried out all the tappings in the two plantations for consistency. We randomly assigned data from one of the plantations to the training set and the other dataset to the test set.

Fresh latex obtained from each tapping event was weighed at latex collection time (around 10 a.m.) on site using a hanging scale (Kern HDB 5K5N) with ±5 g precision. A mobile weighing station was used to avoid vibration while weighing. The changes in the length of the tapping line of each tree were measured throughout the harvest season. The latex yield from each tapping event for each tree was divided by the length of the corresponding tapping line used on the tapping day to correct for the effect of the length of injured area on yield. Latex yield for each tree is expressed as the weight of the fresh latex per tapping per unit length of the trees' tapping line (g cm−1 day−1). Dry matter content (DMC) of the fresh latex and its fluctuations influence the economic yield of rubber. If rubber is delivered in the form of fresh latex to processing factories or to middle men, it is regularly controlled for its viscosity, which, in turn, reflects the rubber content. To quantify latex dry matter content and its fluctuations during the data collection period, we collected weekly latex samples from rubber trees which were dried as thin films in glass petri dishes in an electric oven at 60 °C for 24 h. As the frequency of the DMC records was not equal to that of the latex data, we did not combine the two datasets prior to model building and prediction of dry matter yield. Nevertheless, the empirical estimates of the central tendency and dispersion for the dry matter content of latex are useful for estimating the expected ranges within which the dry matter content of the predicted latex yield should lie.

Temperature (T) and relative humidity (RH) at 3 m in height aboveground inside the leaf canopy were logged on an hourly basis by digital sensor-data loggers (Voltcraft DL-120TH). Daily precipitation (P) at the site was measured using graduated buckets on a 2-m-high platform in an open area next to the plantation. From the hourly logged temperature and relative humidity data, corresponding vapor pressure deficit (VPD) values were calculated. Likewise, the diurnal mean (Me), maximum (Mx), minimum (Mn), and the diurnal variation (daily maximum-minimum difference) (d) values were derived from the hourly logged T, RH, and VPD data, for a total of 13 daily covariates. The usual latex collection time (10 a.m.) was chosen as the beginning of each daily cycle.

As tapping is an activity usually repeated every 2 to 3 days, rubber yield and the factors responsible for its fluctuation are embedded in time. We accounted for potential cumulative, lagged, or delayed effects of variation in the climatic variables on latex yield using moving averages (SMA) of the meteorological variables (denoted as *M*) in our models. The moving average (m_t)for each of the 13 predictor variables (x_t) for day t was computed as

$$m_{t\,(k)} = \frac{1}{k}\sum_{i=2}^{k+1} x_{t-i+1} \quad (1)$$

where $-i+1$ is the lag in days from the date of the tapping events and k is the width in days of the time window covered by the moving average. Five window sizes without lag ($k = 3, 7, 15, 30,$ and 60 days and $l = i - 0$) and two window sizes with lags (k = 15, $l = i - 15$, and $k = 30$, $l = i - 30$) were considered. Hereafter, variables are subscripted by (k, l) to make the size of the window spanned by the moving average and the lag period explicit. Note that, using this notation, $M_{(30,0)} = 1/2\,(M_{(15,0)} + M_{(15,15)})$ and that $M_{(60,0)} = 1/2\,(M_{(30,0)} + M_{(30,30)})$. A total of 104 predictor variables (13 covariates plus 91 moving averages; i.e., 13 covariates × (5 SMAs without lags + 2 SMAs with lags)) were derived and used to relate latex yield to the meteorological covariates

2.2.2 Model development

Using the derived set of predictor variables, mixed models with single predictors were constructed. The multi-model inference (MMI) approach (Burnham and Anderson 2002) was used to select and evaluate the relative importance of the selected predictor variables. Specifically, the Akaike information criterion (AIC, (Akaike 1973)) and its second-order variant, AIC corrected for small sample size (AICc) (Sugiura 1978; Hurvich and Tsai 1989), were used. The maximum likelihood (ML) method was used to compute the information criteria used to select all the fixed effects (covariates). In contrast, the restricted (residual) maximum likelihood (REML) method was used to select the random effects and variance-covariance structures and to estimate parameters of the selected best model. REML is not suitable for selecting fixed effects because it eliminates fixed effects by construction (Wolfinger 1993).

The model with the smallest Akaike information criterion AIC_{min} was considered as the best fitting model within the set of candidate models, and the relative information loss associated with the other models AIC_i in comparison with the best model (known as Kullback-Leibler or K-L distance) was quantified as

$$\Delta_i = \mathrm{AIC}_i - \mathrm{AIC}_{min} \quad (2)$$

As AIC is -2 times the maximized log likelihood of the estimated model, the likelihood of each model (g_i), given the data, was recovered by

$$\mathcal{L}(\mathrm{g}_i|\mathrm{data}) = \exp(-1/2\,\Delta_i) \quad (3)$$

The Akaike weights (w_i) of the models, which are the likelihoods of the models scaled to add up to one, were then calculated as

$$w_i = \frac{\exp(-1/2\,\Delta_i)}{\sum_{i=1}^{R}\exp(-1/2\,\Delta_i)} \quad (4)$$

where w_i is the weight of evidence in favor of the model g_i, being the actual K-L best model within the set of R candidate models given the data at hand and Δ_i is defined as in (2). To formally evaluate the strength of evidence for models, evidence ratios were calculated as

$$\mathcal{L}(\mathrm{g}_i|\mathrm{data})/\mathcal{L}(\mathrm{g}_j|\mathrm{data}) = w_i/w_j \quad (5)$$

We selected the most predictive of the 104 derived meteorological covariates using a two stage process. In the first stage, the time window associated with the best fit was selected separately for each predictor using Akaike weights (w_i) for models containing only the predictor or one of its moving averages ($m_{t\,(k)}$) calculated as in (1) as the only fixed effect. Models based on the same predictor but differing only in terms of the span of the time window k over which the moving averages of the meteorological covariates (without lag) were computed were grouped together (13 groups corresponding to MnT, MeT, MxT, dT, MnRH, MeRH, MxRH, dRH, MnVPD, MeVPD, MxVPD, dVPD and P). For instance, $\mathrm{MxT}_{(k,l)}$ (with k = 3, 7, 15, 30 and 60 days and $l = i - 0$) formed one such group denoted as RMxT in (4). We ranked the models according to the Akaike weights (w_i) within each group and selected the time window associated with the best ranks across the groups as the best supported time window for use in fitting the subsequent multiple regression model incorporating all the best supported covariates in the second stage. Selection of one time window ensured that only variables from groups distinguished by different non-overlapping window sizes were selected. For example, the two variables $\mathrm{MnT}_{(30,0)}$ and $\mathrm{MxT}_{(60,0)}$ do not have non-overlapping window sizes because k =30 for the former is fully nested within k =60 for the latter. We thus expect variables averaged over the larger window to contain part of the information contained in the variables averaged over the shorter window, leading to undesirable redundancy.

The preceding procedure selected the best supported time window over which moving averages were calculated for each covariate. Since each selected time window was associated with only one of the 13 initial predictors, selection of a time window was equivalent to limiting the candidate

set of predictors to 13 covariates. The 13 selected variables were used to build an *a priori* set of multivariate regression models. We avoided data dredging by considering the likely influences of the predictor variables on the biology of latex production or the strength of correlations between the predictor variables before using them in different combinations to build full candidate models in the second stage. For example, while we simultaneously used maximum and minimum temperature as predictors in a number of candidate multivariate models, we avoided using mean temperature (MeT) in the same models with MnT and MxT because they are correlated by construction. By the same reasoning, the group of vapor pressure deficit variables was not used in candidate models containing both temperature and relative humidity from which they were derived.

To gain insights into the relative importance of the predictors (within the selected time window) inference was based on the whole set of candidate models (univariate regression models from the first stage and multiple regression models from the second stage), by accounting for model selection uncertainty and summing the Akaike weights across all models. The sum of Akaike weights over all models that include the predictor variable j, denoted $w_+(j)$, is given by

$$w_+(j) = \sum_{i=1}^{R} w_i I_j(\mathrm{g}_i) \tag{6}$$

where $I_j(\mathrm{g_i})$ is the indicator function and equals 1 if variable j is in model g_i, and 0 otherwise (Burnham and Anderson 2002). The resultant additional evidence for importance or triviality of each predictor was used to further reduce the final set of predictors from the initial set of 13. To evaluate the potential impact of lagged effects on the selected models, the evidence ratios for the selected models relative to those for models containing the same but lagged forms of the predictors were calculated and compared. The preceding multi model inference steps were repeated using AICc and the results compared with those for AIC to infer potential influences of sample size on the selected best model. To check for collinearity among the selected predictors, a variance inflation factor (VIF) for the selected predictors was calculated using

$$VIF_j = \frac{1}{1 - R_j^2} \tag{7}$$

where R_j^2 is the multiple coefficient of determination for variable j when it is regressed against other predictor variables, one at a time.

2.2.3 Covariance structure selection using likelihood ratio tests

The covariance structure which was used to account for serial autocorrelation in the yield records was a combination of random intercepts and spatial power (SP POW) covariance structure which is a spatial generalization of the first-order autoregressive error model appropriate for longitudinal measurements made at irregular time points. As harvest events occurred at unequal time intervals, other autoregressive covariance structures which require equal time steps between measurements (e.g., AR(1) and ARMA(1,1)) were ruled out of consideration. Likelihood ratio test was used to compare support for the models assuming (*i*) perfect independence of observations, (*ii*) added variance component due to random tree effects, and (*iii*) random tree effects plus serially autocorrelated residual errors. Within these three models, each of the more complex covariance structures contained the simpler ones, and therefore, the compared models were nested.

In case of random intercepts (random tree effects), the additional parameter in the model is a variance component which by definition is non-negative. This puts the parameter under the null hypothesis (H_0: variance component = 0) on the boundary of the parameter space (if a standard χ^2 distribution is used for the likelihood ratio (LR) test) which is not permissible. Under such conditions, a nonstandard mixture of two χ^2 distributions has to be used instead (Self and Liang 1987; Stram and Lee 1994; Verbeke and Molenberghs 2000). The test statistic in case (*i*) vs. (*ii*) is the difference in the REML estimates of −2 log likelihoods of two nested models which follows a mixture of two equally weighted (50:50) χ^2 distributions with 0 (has all its mass or probability at zero) and 1 degrees of freedom and denoted as $\chi^2_{0:1}$. For the spatial power part of the covariance structure in case (*iii*), the additional model parameter is a correlation coefficient which is not subject to the boundary problem. Nevertheless, in all the LR tests comparing pairs of cases (*i*) to (*iii*), at least one component of a pair used in the LR tests had the boundary problem. Mixture χ^2 distributions appropriate for LR tests comparing covariance structures (*ii*) vs. (*iii*) and (*i*) vs. (*iii*) were therefore $\chi^2_{1:2}$ and $\chi^2_{0:2}$, respectively. Following Wolfinger (1993), we used only models saturated with respect to the fixed effects, including all the fixed effects deemed to be relevant, when selecting the covariance structure using LRT.

2.2.4 Parameter estimation

Once the final covariance structure and fixed effects were selected, the final model parameters were estimated using the REML method. Residual diagnostics for the final model were performed on normal quantiles of raw residuals and studentized marginal and conditional residuals and influence diagnostics using studentized deleted residuals (i.e., residuals standardized by their

standard deviation and excluding the i^{th} observation) to assess the influence of individual observations and potential violation of the model assumptions, namely normality, homoscedasticity of residuals, and linearity of the assumed regression relationship (Su et al. 2012). Wilcoxon rank-sum test was used to compare the predictor variables between the training and test datasets. The predictive accuracy of the model was evaluated using leave-one-out cross-validation (LOOCV) (Stone 1974) on both the training and test sets. The mean absolute error (MAE), root mean square error (RMSE), and the percentage of predictions from the final model with measurement errors less than 5 g in absolute value were calculated to further assess the predictive power and robustness of the final model. The denominator degrees of freedom for significance tests of the fixed effects were synthesized using the method of Kenward and Roger (1997). All the models were fitted in the SAS procedures MIXED, GLIMMIX, and NPAR1WAY (SAS 2011).

2.3 Results

An overview of the latex yield records (training dataset) and the meteorological conditions during the data collection period is provided in Figure 2.2. A comparison of the monthly weather conditions in the study period with the weather conditions prevailing over the 20 years spanning 1989–2008 is provided in Appendix Figure A2.1. The annual harvest season for rubber in XSBN usually starts at the end of March. Due to logistical constraints, our yield measurements only started in the last week of May 2009 and mid-April for 2010. A total of 158 harvest events were recorded from the rubber plantations which provided the training dataset (64 events in 2009 and 73 events in 2010). Mean ± 1 SD values of latex yield (grams of fresh latex collected from 1 cm of tapped bark per day) over the course of the data collection periods were 4.82 ± 2.18 for the training set and 5.49 ± 1.82 for the test set. Mean ± 1 SD values of the length of the tapping line were 34.0 ± 3.53 and 31.6 ± 2.89 cm, respectively. There was an unusual rainfall shortage at the beginning of the harvest season in 2010 (April), which extended up to the month of July and seemed to be associated with a change in latex yield. This coincided with the first 29 records in 2010 (training set). This fact motivated the idea of testing for the need of a class variable representing three levels for the three resulting periods (2009 and wet and dry periods in 2010) in the regression model.

Subdivision of the study period into three blocks, allowing fitting of a model with three levels for the study period turned out to be significant only for regression models with fixed effects consisting of the daily variables or moving averages with short window spans (up to 2 weeks). Even so, the supported models had poorer fits than those consisting of predictors averaged over

either 30 or 60 days. For the models with predictors averaged over 30 days, the weight of evidence in favor of models with three levels for the study period was merely about one quarter of those for the models with only one level.

Weekly collected and oven-dried latex samples (388 samples from 23 tapping events) had mean ± 1 SD dry matter contents (%) of 33.1 ± 8.90 in 2009, 37.2 ± 9.77 in the dry period of 2010, and 33.7 ± 8.46 for the rest of the harvest season in 2010. A plot of the DMC against time (Appendix Figure A2.2) suggested no significant temporal pattern.

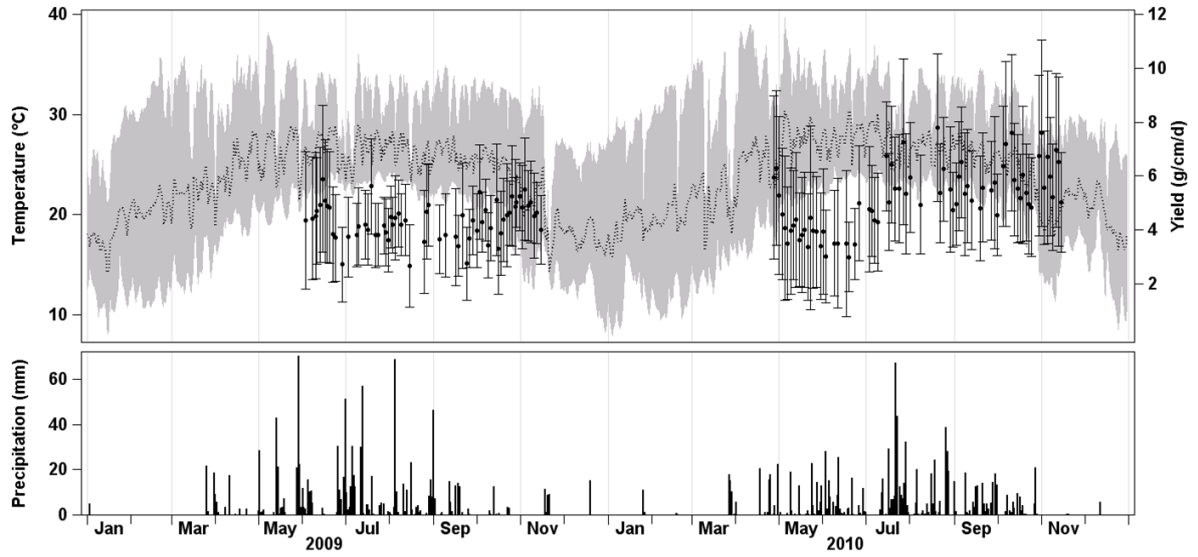

Figure 2.2 Temporal variation in the yield records and two of the meteorological variables over the course of the data collection periods
The dotted line shows the daily mean temperature, the gray-shaded area shows the diurnal temperature range, and the dots show the mean of the latex yield from 18 trees (standard deviation given as error bars). Daily rainfall is presented in the lower panel

Model selection identified models with moving averages of the meteorological covariates calculated over 30-day window spans as having the strongest support in the data in six out of the total of 13 candidate time windows considered. The three top-tanked covariates were $MnT_{(30,0)}$, $MeT_{(30,0)}$, and $dT_{(60,0)}$. The 60-day window was selected as the best in four of the 13 time window-differentiated groups of models. This was reaffirmed by the Akaike weights of 0.887 for the 30-day window and 0.123 for the 60-day window. The two Akaike weights jointly constitute a 100 % confidence set on the selected best models and thus virtually preclude all the other models from consideration. Because the weight of evidence for the models for the 30-day window alone is almost 90 %, we limited the candidate set of predictors considered in subsequent model selection steps to the moving averages of covariates computed over this time window alone.

We attempted to establish if the selected time window represented lagged effects which acted additively or independently. We did this by first subdividing the 30-day window for the best-supported models into smaller component windows and then comparing the support for the model based on the 30-day window vs. the multiple regression model containing all the resultant component windows, each treated as a separate variable. For simplicity and brevity, we only considered a partition of the 30-day window into two parts of 15-day span each. Comparing the single-predictor 30-day models with their 15 + 15-day counterparts, Akaike weights showed weaker support for the models containing the 13 covariates based on the 30-day span (0.09) than for the models containing the same covariates but represented by two separate 15-day components (0.91). This supports the hypothesis of independent over additive lagged effects or using covariates based on the two 15-day component windows separately rather than the combined 30-day window. Despite the greater support for the partitioned lags in simpler models, the Akaike weights of models with 15 + 15-day predictors diminished heavily when multiple regression models were added to the set of models compared within the MMI scheme (0.868 vs. 0.132 in favor of the 30-day time window). As a result, we opted to retain the covariates based on the 30-day windows in the MMI evaluation of the multiple regression models.

The *a priori* set of candidate multiple regression models (without interaction) consisted of 55 models. Two models had the strongest support within the set of the 30-day multiple regression models. They differed only in that one had one less fixed effect ($P_{(30,0)}$) and hence lower weight of evidence (0.403 vs. 0.595) than the other.

We chose to keep the precipitation effect ($P_{(30,0)}$) in the candidate variable set while exploring potential interactions between the covariates in the final model. Inclusion of the interaction effect $MnT_{(30,0)} \times P_{(30,0)}$ improved model fit the most compared to all the other interactions considered (with $\Delta_i = 5.1$ compared to the next best fitting model). We then kept this interaction in the model and added the next best-supported interaction effect to the model. The improvement in model fit due to adding further interaction terms did not exceed the selection threshold of $\Delta_i = 2$. Therefore, we retained $MnT_{(30,0)} \times P_{(30,0)}$ as the only interaction effect among the fixed effects in the final model. This increased the number of candidate model set to 56, with a confidence set on models exceeding 98.8 %. The covariates selected by multi-model inference are presented in Table 2.1 as mean ± 1 SD for both the training and test sets together with the Wilcoxon rank-sum tests comparing the two datasets.

Table 2.1 Descriptive statistics for the predictor variables selected for the final model

Variable name†	Training set	Test set	Wilcoxon rank-sum test
	Mean (SD)	Mean (SD)	P value
P(30,0)	5.10 (2.76)	5.38 (2.95)	0.47
MnT(30,0)	20.80 (1.93)	21.04 (1.81)	0.18
MxT(30,0)	28.70 (2.52)	28.66 (1.45)	0.051
MxRH(30,0)	90.92 (2.43)	91.75 (3.15)	6.5×10^{-05}

†Daily precipitation (P), minimum daily temperature (MnT), maximum daily temperature (MxT) and maximum relative humidity (MxRH) averaged over the 30 days leading to the tapping event with no lag (30,0) were the selected predictors for the final model. Wilcoxon rank-sum test checks if the weather conditions prevailing in the two plantations were similar

The coefficients for the predictor variables estimated using the REML method are presented in Table 2.2 and in Eq. 8. Coefficients for the standardized covariates are also provided as a means for comparing the relative contribution of the fixed effects to the total fit (as coefficient sizes are not affected by the measurement scale of individual variable) and to simplify their potential use with future datasets with standardized covariates. Since one model scored more than 90 % of the total Akaike weights, this ruled out the need for model averaging. VIF related to the predictors are presented in Table 2.2. More details such as significance tests and confidence intervals for the fixed effect coefficients are available in Appendix Table A2.1.

$$\text{Yield} = 23.6 - 0.37 \times \text{MnT}_{30,0} - 0.05 \times \text{MxT}_{30,0} - 0.11 \times \text{MxRH}_{30,0} + 0.6 \times \text{P}_{30,0} - 0.03 \times \text{MnT}_{30,0} \times \text{P}_{30,0} \quad (8)$$

Table 2.2 Coefficient estimates for fixed effects

Fixed Effect	Original variables		Standardized variables		VIF
	Estimate	SE	Estimate	SE	
Intercept	23.593	1.875	4.733	0.234	–
$\text{MnT}_{(30,0)}$	-0.366	0.038	-29.859	3.100	2.33
$\text{MxT}_{(30,0)}$	-0.051	0.013	-6.068	1.551	1.57
$\text{MxRH}_{(30,0)}$	-0.109	0.021	-12.884	2.523	4.22
$\text{P}_{(30,0)}$	0.633	0.185	84.151	24.640	1.92
$\text{MnT}_{(30,0)}$*$\text{P}_{(30,0)}$	-0.028	0.008	-83.725	25.434	–

Coefficients estimated for selected model parameters (daily precipitation (P), minimum daily temperature (MnT), maximum daily temperature (MxT) and maximum relative humidity (MxRH) averaged over 30 days leading to the tapping event with no lag (30,0)). Coefficients for standardized variables were computed from models incorporating covariates standardized to zero mean and unit variance.

LR tests which were performed to choose an appropriate variance-covariance structure strongly supported a variance-covariance structure consisting of random tree effects (denoted as RandInt) plus a SP POW structure for accounting for serial autocorrelation. Further enrichment of the variance-covariance structure by adding random slopes for individual trees did not lead to any discernible improvement in model fit. Table 2.3 presents the LR test results for the three models for the variance-covariance, including (*i*) a fixed effects-only model with no random effects and homogeneous residual errors (denoted as fixed), (*ii*) fixed + RandInt model, and (*iii*)

fixed + RandInt + SP POW model. As the fixed + RandInt + SP POW model contains the fixed + RandInt model, which, in turn, contains the fixed effects-only model, an LR test is permissible. The estimated covariance component (for random intercepts for rubber trees) equaled 0.92, whereas the temporal autocorrelation parameter was 0.76^{d}, where *d* is the time in days separating a pair of latex measurements. AIC and AICc had identical performance in all steps of the model selection.

Table 2.3 Likelihood ratio (LR) tests for variance-covariance structure selection

Variance-covariance structure			-2 ln (λ_N)	Asymptotic null distribution	*P* value
Fixed	**vs.**	**Fixed+RandInt**	584.1	$\chi^2_{0:1}$	5.6×10^{-130}
Fixed+RandInt	**vs.**	**Fixed+RandInt+SP(POW)**	737.0	$\chi^2_{1:2}$	3.6×10^{-162}
Fixed	**vs.**	**Fixed+RandInt+SP(POW)**	1321.1	$\chi^2_{0:2}$	2.4×10^{-289}

The contrast between candidate covariance structures is tested in three levels. Simpler covariance structures are nested in the more complex covariance structures. The test statistic -2 ln (λ_N) is -2 times the difference between the maximized restricted log likelihoods of the two candidate models being compared. The asymptotic null distribution of -2 ln (λ_N) is a mixture of two equally weighted chi-square distributions used for the LR test with the indicated degrees of freedom.

Residual and influence diagnostics suggested no violation of model assumptions (normality, homoscedasticity, and linearity of residuals) (Appendix Figure A2.3). Variance inflation factors were all below the threshold value of 10 (Table 2), suggesting an absence of substantial multicollinearity. Results of the LOOCV of the full model and its reduced forms consisting only of single predictors are summarized in Table 2.4. All the five models in Table 2.4 are based on the same variance-covariance structure selected as described above.

Table 2.4 Evaluation of the prediction performance of the final model and its reduced forms in leave-one-out cross-validation

Model components	Correlation		Mean absolute error (MAE)	Root mean square error (RMSE)	% of predictions within ± 5g range of the measured yield
	$r_{Pearson}$	$\rho_{Spearman}$			
Full model	0.78	0.78	0.95	1.32	99.56
$MnT_{(30,0)}$	0.78	0.78	0.98	1.36	99.53
$MxT_{(30,0)}$	0.70	0.72	1.10	1.55	98.89
$MxRH_{(30,0)}$	0.71	0.74	1.08	1.52	98.98
$P_{(30,0)}$	0.72	0.73	1.05	1.45	99.25

Performance of the full model and its reduced forms consisting of individual covariates based on the correlation between the measured and the predicted yield, prediction error indices (MAE and RMSE) and the percentage of predictions within the measurement accuracy range of the weighting scale used in the field of 5 grams.

Predicted vs. measured latex yields showed a fairly uniform error distribution over the prediction range (Figures 2.3 and A2.4 for the measurement-unit-specific plots). To assess the uniformity in prediction across different rubber trees, we visually inspected the tree-specific prediction errors. The behavior of the measurement units under cross-validation is depicted in Figure 2.4. No obvious pattern or grouping was noticeable. The full model had the smallest prediction error with 99.5 % of the predictions falling within the expected measurement accuracy range of 5 g (Table

4). The single-predictor models had larger prediction errors. Nevertheless, their predictions fell within the expected measurement error range of 5 g, and hence, their performance was not that much inferior to that of the full model.

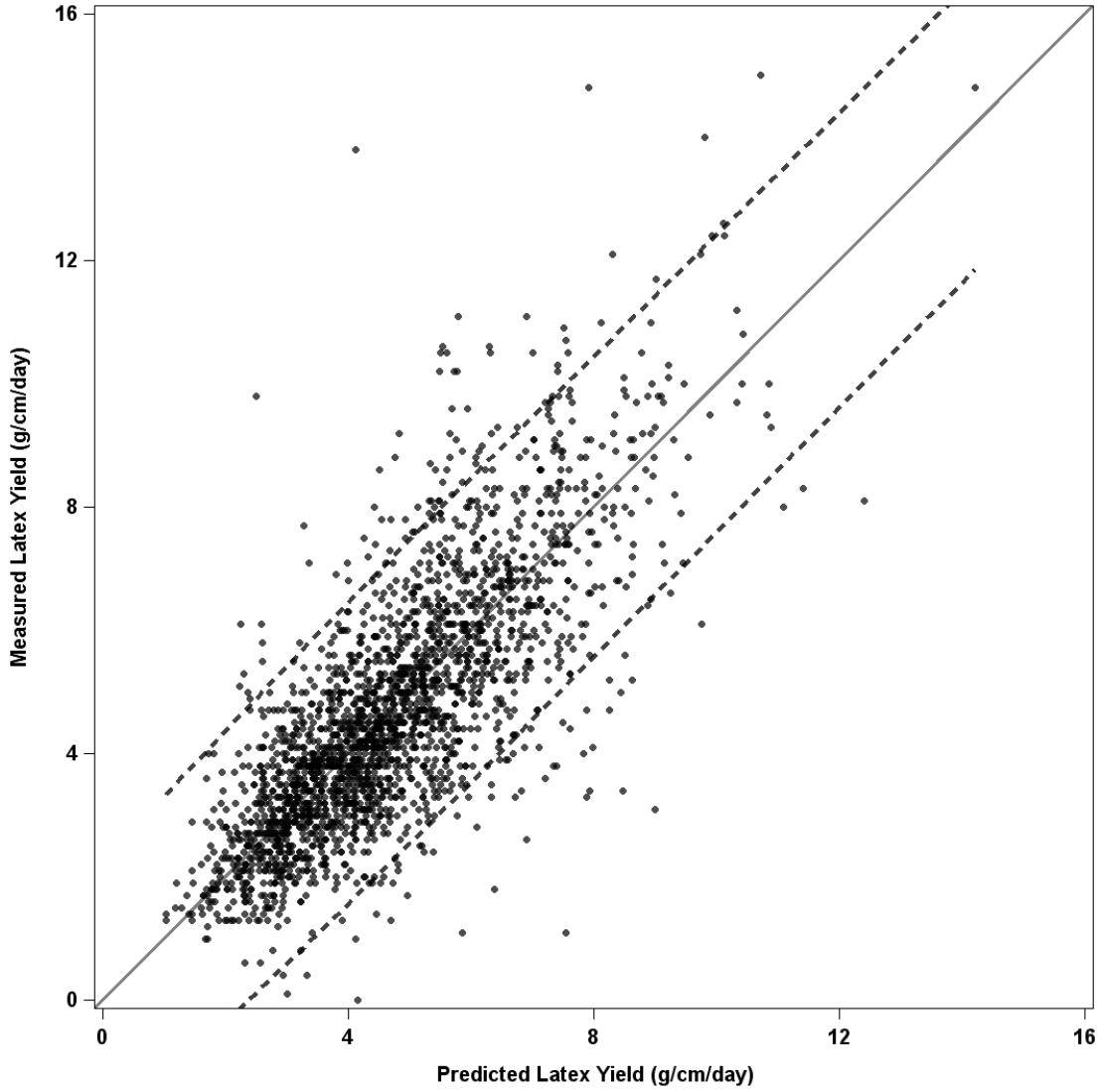

Figure 2.3 Predicted vs. measured latex yield
The dashed lines are the pointwise 95 % prediction bands obtained by leave-one-out cross-validation and subjected to spline smoothing

The Wilcoxon rank-sum tests (Table 1) failed to reject the null hypothesis of equal means for the training and test datasets for precipitation and maximum and minimum temperatures but rejected this hypothesis for the maximum relative humidity. Application of the model coefficients obtained from the training dataset to assess model performance on the external (test) dataset would be reasonable if corresponding variables in both datasets come from the same underlying population, but the contrary would justify validation on the test dataset using the fixed effects at hand and re-estimating the model coefficients. Predictive accuracy of the developed model was evaluated by both approaches to account for the potential type I error: direct application of

coefficients obtained from the training dataset to the test dataset and a round of LOOCV on the test dataset. Prediction accuracy on the test dataset (percentage of predictions within the expected measurement error range of 5 g) was 99.36 % when model parameters were those estimated on the training dataset and 99.81 % when the model parameters were re-estimated.

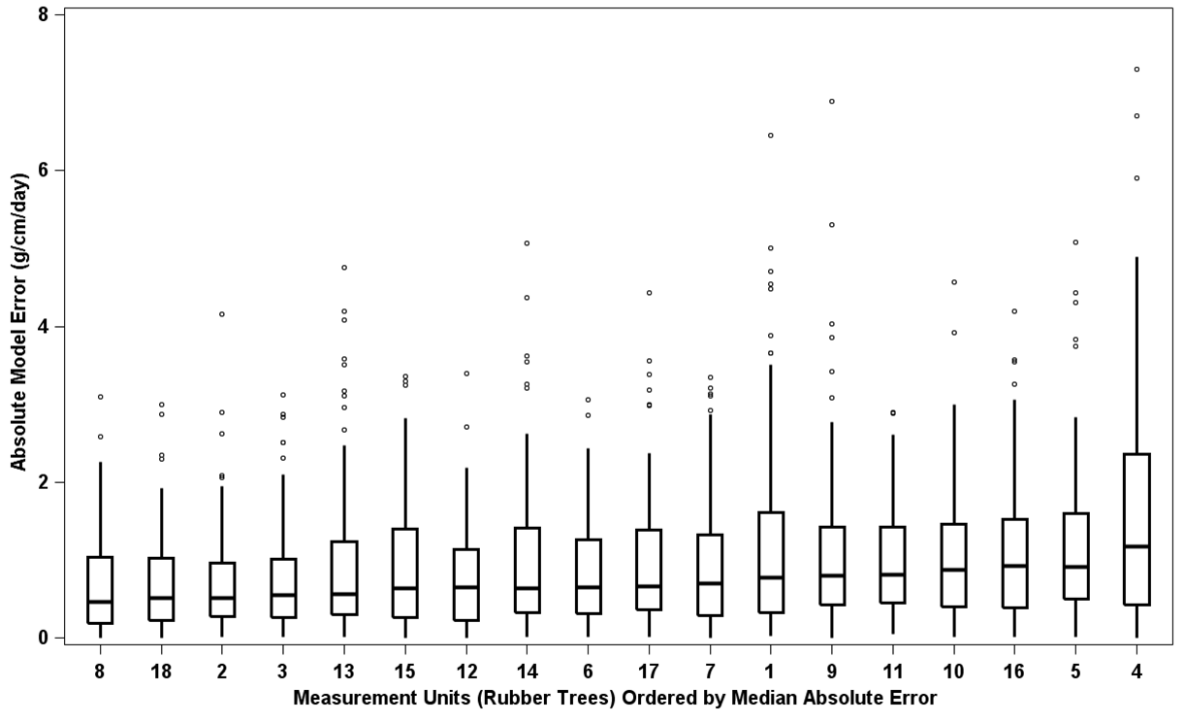

Figure 2.4 Distributions of tree-specific absolute model error in the test dataset

2.4 Discussion

In this study, we used daily latex yield data from rubber trees and records of the meteorological conditions prevailing in the plantations to identify suitable meteorological predictors of rubber yield. Model selection and multi-model inference techniques were used as aids in building a predictive model within a mixed model framework. We assessed the predictive accuracy of the resulting model using both cross-validation and a test dataset. We identified four meteorological variables, namely daily minimum and maximum temperatures, maximum relative humidity, and rainfall, all averaged over 30-day windows before tapping events as the best-supported predictors among the suite of 13 variables we investigated. The mean and diurnal variation in temperature (ranked by Akaike weights as the second and third best models in univariate regressions, respectively) and relative humidity were clearly outperformed by the selected predictors as were also the predictors measuring vapor pressure deficits. Minimum temperature, precipitation, and their interaction explained the largest part of the variation in the yield data. Precipitation was the

only factor with a positive effect on rubber yield, but its interaction with minimum temperature had a substantial and negative influence on yield (see coefficient estimates for the standardized fixed effects in Appendix Table A2.1). This suggests that the positive effect of rainfall on latex yield can be reduced or even negated under conditions of both high precipitation and low minimum temperatures within the range of values experienced by the rubber trees. Such significant interactions between different climatic factors influencing latex yield have only recently been indirectly suggested by Yu et al. (2014) using regression trees but have otherwise been largely overlooked by several earlier studies (Jiang 1988; Rao et al. 1998; Raj et al. 2005). The negative association we observed between the rubber yield and minimum temperature reinforces similar findings by Raj et al. (2005) and Yu et al. (2014). The regression trees developed by Yu et al. (2014) identified the mean temperature over the 30-day period preceding tapping events to be the most important factor in determining yield. However, their PLS yield prediction model identified the minimum temperature both a day before taping and averaged over the month leading to a tapping event to be the most influential (had the largest standardized coefficients) of all the predictors they considered. Our model also identified the 30-day average minimum temperature, but not the 30-day averaged mean temperature, as a relevant and important predictor of latex yield.

Other climatic factors that have been shown to have positive correlations with rubber yield are diurnal temperature variation and sunshine hours (Jiang 1988; Yu et al. 2014). Despite emerging as the third best-ranked factor in our univariate regression phase of model selection, diurnal temperature range had too weak a support in the multiple regression phase of model selection to merit inclusion in the final, selected best model. The negative relationship between the rubber yield and increase in minimum temperature most probably operates through diurnal temperature difference. Higher net gains occur as a result of efficient photosynthesis in the daytime and limited respiration in the nighttime due to low temperature, provided that the minimum and maximum temperatures remain within their tolerable limits (Jiang 1988) and that sufficient soil moisture is available to the plants during the warm hours of the day (Lotti et al. 2012).

Besides the photosynthetic (Satheesan et al. 1984; Senevirathna et al. 2003; Rodrigo 2007; Kositsup et al. 2009; Gunasekera et al. 2013) and phenological (Renner 2007; Yeang 2007; Guardiola-Claramonte et al. 2008, 2010) roles of solar radiation on rubber, there is clearly a strong correlation between the temperature and sunshine hours (Bristow and Campbell 1984; Thornton et al. 2000), which merits consideration especially if their mean over longer periods is to be used as a predictor variable. Rao et al. (1998), for instance, have reported Pearson correlation coefficients of as high as 0.86 between the 7-day mean of sunshine duration and the weekly mean maximum temperature in Kottayam (India). Our study did not measure sunshine duration due to

logistical constraints, thus precluding corroboration of the reported correlation for our study period and site. Nevertheless, the considerably high correlations reported by earlier studies imply that care needs to be taken to avoid including both temperature and sunshine in the same model or to adopt modeling strategies able to adequately handle high multicollinearity. Our modeling strategy aimed to identify the best and most parsimonious model for predicting rubber yield from meteorological covariates while also accounting for potential serial autocorrelation. Given the high correlation between the temperature and sunshine duration, it is likely that temperature and sunshine effects are substitutable so that the latter is likely to be excluded from models that already include temperature, as our best model did.

Models incorporating moving averages of metrological covariates computed over the 30-day window had stronger support in terms of the weight of evidence (w_i) and provided more accurate predictions than the other competing models. Also, partitioning the study period into three temporally distinct blocks distinguished by levels of rainfall or humidity did not enhance predictive accuracy relative to models including predictors with moving averages computed over shorter window spans, but with the study period not subdivided into finer time blocks. This is noteworthy and implies temporal generalizability and robustness of the selected best model to marked temporal variation in the meteorological covariates.

It is also noteworthy that moving average techniques are smoothing methods which are most often employed to reveal the underlying trends in time series subject to fluctuations. In such cases, the time series of interest is often the response, whereas in our work (but see also (Rao et al. 1998; Raj et al. 2005)), the SMA technique has been applied to the raw data to identify appropriate predictor variables (Eq. 1). The moving averages selected as the best predictors mean that k equally weighted consecutive measurements of a predictor variable x_j are used to predict latex yield. This provides a simple and biologically meaningful way of accounting for lagged effects as each of the k measurements are lagged by 1 to k time units (e.g., 1 to 30 days in the case of a predictor such as $MnT_{(30,0)}$).

The clearly superior support for covariates averaged over the 30-day window and, to a far lesser extent over the 60-day window, argued for using 30-day averaged covariates in building the final model for prediction and also suggested that considering windows wider than 60-days would seem unnecessary. This contrasts with and is somewhat longer than the 15–20-day lag reported for the yield of rubber trees in Agartala, Northeast India (Raj et al. 2005). Note that when the size of the time window over which moving averages are calculated increases, the information contained in the smoothed data tends to diminish due to stronger smoothing. Therefore, shorter time windows should be preferred. Comparing the $M_{(30,0)}$ class of models with those with separate

effects of $M_{(15,0)} + M_{(15,15)}$, the latter class of models allow for unequal weights for the two component windows. However, this increased flexibility comes at the cost of a larger number of parameters to be estimated and, therefore, higher penalty in calculating the corresponding AIC values, which adversely affect the Akaike weights of the models. The better fit of the $M_{(15,0)} + M_{(15,15)}$ class of models compared with the $M_{(30,0)}$ class was limited to the single-predictor models, but the $M_{(30,0)}$ covariates performed better in the multiple regression context, which is unsurprising, as $M_{(15,0)} + M_{(15,15)}$ models are far less parsimonious than the $M_{(30,0)}$ models. This points to redundancy of some of the differentially weighted lagged effects.

Likelihood ratio tests revealed substantial differences between the fixed effects-only model and its mixed model variants which we used to approximate the data. Random intercepts were used to estimate the added variance in latex yield measurements due to random variation among individual trees, including variation due to potentially influential but unmeasured tree-specific effects. However, adding random tree-specific regression slopes for predictors to the model for the variance-covariance structure did not improve model fit. Regarding the spatial power component of the covariance structure, the estimated correlation between consecutive records ($\rho = 0.7^d$ where d is the time in days separating a pair of records) supported the initial expectation that serial correlation was an important issue in the data that needed to be accounted for.

2.4.1 Strengths and limitations of the modeling approach

This study demonstrates how to exploit the power and versatility of mixed models and model selection based on information-theoretic criteria and the multi-model inferential paradigm to obtain valid prediction and minimize violations of model assumptions.

The data we used were observational, which naturally raises the question of whether the observed range of values and combinations of the variables observed at the data collection period can be considered as representative of the underlying truth. Since setting up an experimental study that mimics the particulars of a study such as the current one is likely to be very challenging, if not impractical, using data collected over long periods of time would seem to be the most promising path to improve the reliability of latex predictions.

This study was carried out on only one rubber genotype—the GT1—which is one of the old and internationally well-known clones often used by breeders as a reference to evaluate the performance of new genotypes (Clément-Demange et al. 2007; Gouvêa et al. 2013). Although expansion of this study to include more clones would help establish the generality of our results, we presume that the current results based on the preeminent clone (GT1) may be similarly applied to other clones based on the existing knowledge with success.

The hanging scales used in the field for data collection (fresh latex weight) were selected to match field conditions and yet have an acceptable measurement precision. A compromise between these two constraints led us to choose scales with an accuracy of 5 g. It is worth stressing that our evaluation of prediction quality as the percentage of the forecasts falling within the measurement precision of 5 g is bound to this sensitivity level. In other words, using a scale with higher sensitivity would lead to a narrower band, potentially covering a reduced number of predictions. When technical improvements permit higher precision in field measurements, it would be desirable to test the model prediction accuracy under stricter conditions. We acknowledge that our inferences are probably limited to the set of investigated variables and the data at hand, but the approach we present is very general and should be applicable in a variety of settings.

2.5 Conclusions

We present a modeling approach and a model able to accurately predict rubber yield (99 % of predictions within 5 g accuracy) using meteorological conditions prevailing during the 30 days immediately preceding tapping events. The model was calibrated and validated for the environmental setting in our study site in Xishuangbanna, China. Precipitation, minimum and maximum temperatures, and maximum relative humidity were identified as the best predictors from a set of candidate covariates. This study also highlights the relevance of interactions between meteorological variables as rubber yield predictors and confirms the necessity of accounting for serial autocorrelation in the latex yield data.

Acknowledgements

This study was financed by the German Federal Ministry of Education and Research (BMBF) (project number 0330797A) and the Landesgraduiertenförderung Act (LGFG) of the Ministry for Science, Research and Art Baden-Württemberg. We deeply appreciate the tireless efforts of Mr. Ai Han-Jian and Mrs. Lai Han who helped at the preparation and data collection stages of this study. We specially thank the administration of NRWNNR and the rubber farmers of NaBan village for their kind support. We are grateful to three anonymous reviewers for constructive criticisms and insights that helped improve an earlier draft of this paper.

3 Climate change impact assessment on the potential rubber cultivating area in the Greater Mekong Subregion

Reza Golbon*, Marc Cotter and Joachim Sauerborn

Institute of Plant Production and Agroecology in the Tropics and Subtropics, University of Hohenheim, Stuttgart, Germany

*Correspondence: golbon@uni-hohenheim.de

Received: 16 January 2018

Accepted for publication: 6 July 2018

Published: 20 July 2018

doi: 10.1088/1748-9326/aad1d1

Abstract

In order to map potential shifts of rubber (*Hevea brasiliensis*) cultivation as a consequence of the ongoing climate change in the Greater Mekong Subregion, we applied rule-based classifications to a selection of nine gridded climatic data projections (precipitation and temperature, Global Circulation Models (GCMs)). These projections were used to form an ensemble model set covering the Representative Concentration Pathways (RCPs) 4.5 and 8.5 of the Fifth Assessment Report of the Intergovernmental Panel on Climate Change at three future time sections: 2030, 2050 and 2070. We used a post classification ensemble formation technique based on majority outcome of the classification to not only provide an ensemble projection but also to spatially track and weight the disagreements between the classified GCMs. A similar approach was used to form an ensemble model aggregating the involved climatic factors. The level of parsimony between the ensemble projections and GCM products was assessed for each climatic factor separately, and also at the aggregate level. Shifting zones with high confidence were clustered based on their land use composition, physiographic attributes and proximity. Following the same ensemble formation

technique and by setting a 28°C threshold for annual mean temperature, we mapped areas prone to exposure to potentially excessive heat levels. Almost the entire shift projected with high certainty was in form of expansion, associated with temperature components of climate and temporally limited to the 2030 time window where the total area conducive to rubber cultivation in the GMS is projected to exceed 50% by 2030 (from 44.3% at the turn of the century). The largest detected cluster (41% of the total shifting area), which also is the most ecologically degraded, corresponds to Northern Vietnam and Guangxi Autonomous Region of China. The area exposed to potentially excessive heat is projected to undergo a 25-fold increase under RCP4.5 by 2030 from 14568 km^2 at the baseline.

Keywords

Multi-model ensemble, mapping of rubber, Para rubber tree, cash crops, geographic information systems, biodiversity, deforestation, Mekong Region, Mainland Southeast Asia

3.1 Introduction

Natural rubber is a key industrial commodity with wide application in manufacturing of a very diverse range of products. Although rubber-bearing plant species such as *Taraxacum kok-saghyz* and *Parthenium argentatum* have lately reemerged on the research and development scene as potential alternative sources of natural rubber (van Beilen and Poirier 2007a, b; Rasutis et al. 2015; Kreuzberger et al. 2016; Dong et al. 2017; Ramirez-Cadavid et al. 2017; Soratana et al. 2017), the Para rubber tree *(Hevea brasiliensis)* has retained its status as the sole viable source of natural rubber, which does not seem to change in the close future (Cornish 2017). Global consumption of natural rubber has exceeded 12 million metric tons in the last three years according to the International Rubber Study Group (IRSG 2017). Raising demand has been matched and to some extent surpassed by increases in production. Global trends of the natural rubber production and consumption and the harvested area are illustrated in Figure 3.1.

Recent decades have been associated with expansion (and to some extent shift) of rubber cultivation zones from the traditional rubber growing regions (the 10°S to 10°N equatorial belt) to higher latitudes and longitudes (Priyadarshan et al. 2005; Ziegler et al. 2009; Li and Fox 2012; Ahrends et al. 2015; Chen et al. 2016a, b). Thailand, the leading rubber producing country since 1990, which also has had the highest share of the global area converted each year to rubber cultivation (30% on average since the turn of the century), can well illustrate the situation (Figure 3.2).

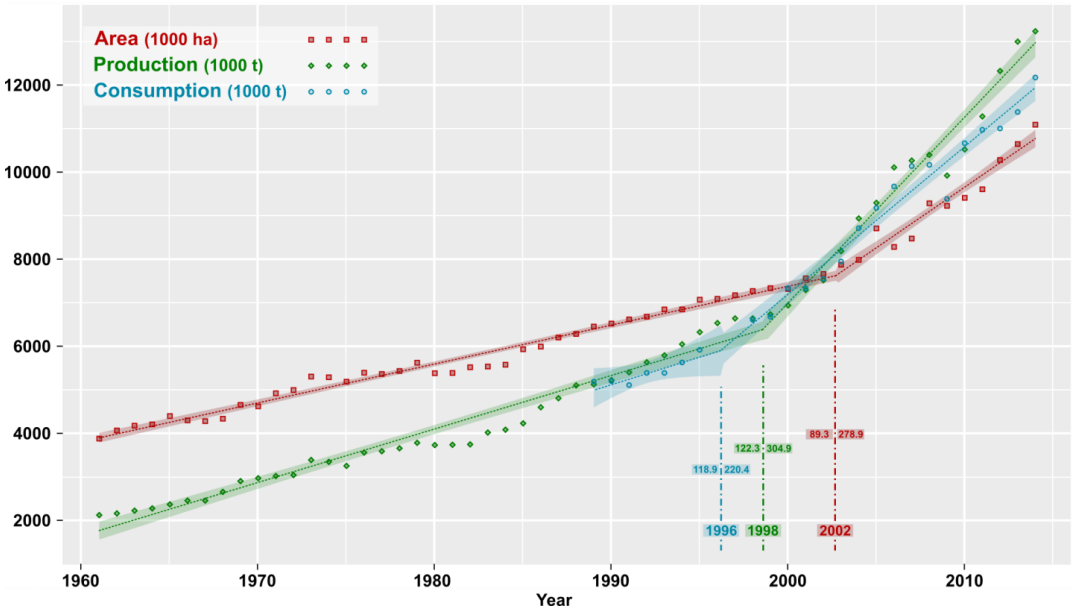

Figure 3.1 Global trends for consumption, production and area under rubber cultivation
Segmented regression lines reveal the shifts in trends: 1996 is the estimated year before which a 118.9 thousand ton increase per year explained the growing consumption trend, accelerating to 220.4 thereafter while for production, the slope has shifted from 122.3 to 304.9 thousand tons per year by 1998 and year 2002 appears to be the most efficient breakpoint explaining the increasing trend of the global area under rubber cultivation, surging from 89.3 to 287.9 thousand hectares added each year. We have used R package 'segmented' (Muggeo 2003) version 0.5-1.4 to generate this figure from FAOSTAT (production and area) and IRSG (consumption) data (FAOSTAT 2017; IRSG 2017). Inkscape 0.91 was used for visual optimization.

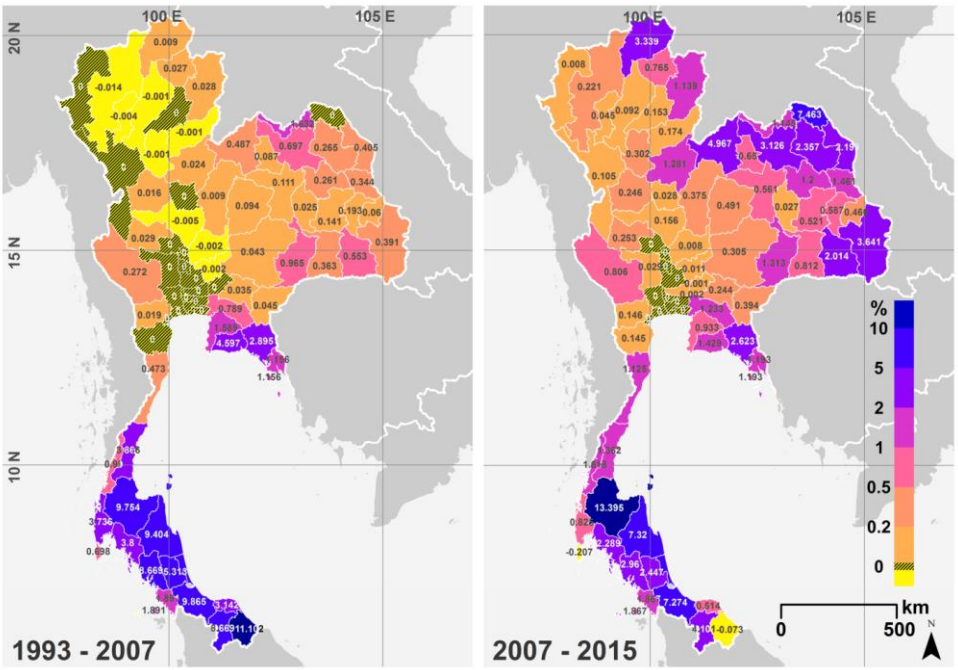

Figure 3.2 Temporal dynamics of the expansion of rubber cultivation in Thailand
The provincial share of the Thai national increase in the area under rubber cultivation in two time sections: from 1993 to 2007 (3158 km²) and from 2007 to 2015 (12485 km²). The 1993 Thailand Agricultural Census (NSO 1994) and the agricultural statistics yearbooks of Thailand (2009 and 2015) data (available at www.oae.go.th) and the GADM administrative divisions' shapefiles (2.8) were used. Maps were generated in ArcGIS 10.2.2 and visually optimized in Inkscape 0.92.

The Greater Mekong Subregion (GMS) is an economic cooperation program consisting of six nations: China (Yunnan province and Guangxi autonomous region), Vietnam, Thailand, Laos, Myanmar and Cambodia. The GMS covers more than 2.5 million km^2 of the Mainland Southeast Asia (MSEA), about 84% of which overlaps with the Indo-Burmese mega biodiversity hotspot ((Myers et al. 2000; Mittermeier et al. 2004); Figure 3.3). It stands for a substantial share of global rubber production (46.7% in 2014)[1] almost exclusively coming from monocultures. Since its inception in the early 1990s, the GMS has in general, and its formerly isolated members (Myanmar, Laos and Cambodia) in particular, been undergoing rapid socio-economic change through regional development programs and transboundary investments in all conceivable sectors. At the same time, ecological degradation through accelerated landscape transformation has been observed. Heavy expansion of rubber monocultures and their spread to new areas have had a notable contribution to deforestation, habitat fragmentation and biodiversity loss (Li et al. 2007; Ahrends et al. 2015; He and Martin 2015; Häuser et al. 2015).

In response to concerns about the ecological implications of the rapid expansion of rubber monocultures mostly replacing forests and swidden agriculture in MSEA, remote sensing techniques are regularly used to monitor land use conversion to rubber cultivation (e.g. (Li and Fox 2011a, b, 2012; Dong et al. 2012, 2013; Senf et al. 2013; Fan et al. 2015; Grogan et al. 2015; Li et al. 2015; Chen et al. 2016a, b; Kou et al. 2017)). More recently, remote sensing has been used to track additional details such as the rubber plantation age (Koedsin and Huete 2015; Kou et al. 2015; Beckschäfer 2017; Trisasongko 2017).

Climate is one of the defining factors of the potential geographic extent for cultivation of any crop, and Para rubber is no exception. Momentous ongoing change in Earth's climate attributed to human activity (Collins et al. 2013; Kirtman et al. 2013; Lewandowsky et al. 2016; Thorne 2017; Medhaug et al. 2017; Berger et al. 2017) is comprehensively acknowledged by the scientific community (Cook et al. 2016). Some forecasts of the future potential geographical range for Para rubber in different parts of MSEA, mainly based on ecological niche modeling (Ray et al. 2014, 2016a, b; Ahrends et al. 2015; Liu et al. 2015a) and bioclimatic stratification (Zomer et al. 2014) have recently been published.

[1] This figure is mainly based on FAOSTAT data. As two Chinese provinces of Hainan and Guangdong contribute to the Chinese national production, their share (46.2% in 2014 as mentioned in the China Statistical Yearbook 2016 www.stats.gov.cn) has been deducted. In case of Laos for which FAO data is not available, United Nations Commodity Trade Statistics Data (comtrade.un.org) was used in combination with the historical commodity prices (www.indexmundi.com) to estimate the national rubber production: 56 thousand tons.

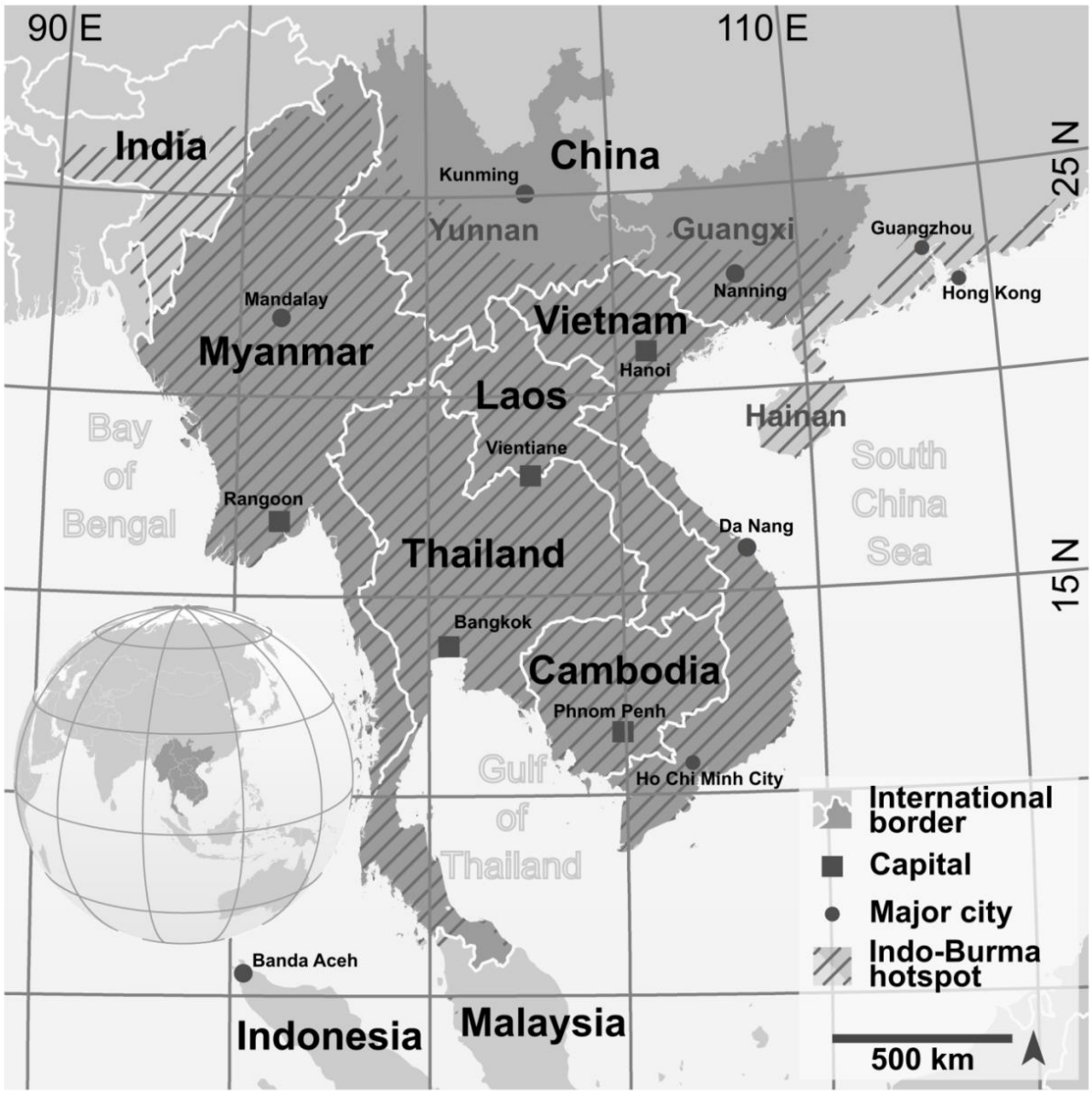

Figure 3.3 Geographical extent covered by this study
The orthographic projection in the upper left corner is modified from Wikipedia (http://commons.wikimedia.org). Other maps were generated using ESRI ArcMap 10, and the shape files of the administrative borders are available at the website of Global Administrative Areas Project (http://www.gadm.org)

Gridded data of climatic factors simulating likely future conditions are essential inputs for forecasts. Global Circulation Models (GCMs) are useful sources of information commonly exploited to assess the potential impacts of climate change. Various institutions are engaged in creating such datasets and provide dozens of potential choices as input. Variations among GCMs, which mainly rise from structural and parameterization differences (Semenov and Stratonovitch 2010), can help to provide a means to capture and explore some of the projection uncertainties which have to be accounted for in order to obtain a realistic and scientifically sound image. Variabilities observed in sets of comparable simulations prompt some key choice questions, starting with whether a single simulation would suffice or a multi-member ensemble is needed

for a reasonably robust forecast. In the latter case, can using the largest possible ensemble be a legitimate decision or could a reduced set of simulations perform better while minimizing the computational cost? Based on what criteria should a shortlisting take place? Should an average of all set members be used as ensemble or (considering the spatial nature of the data) is there a better option? How to handle the uncertainties (dispersion) inherent in the input differences (an important but so far overlooked factor)? And how to communicate these uncertainties in a comprehensive and useful way?

Potential phytosanitary deficiencies as well as growth and yield failures due to crop exposure to excessive levels of ambient temperature are some of the more unsettling aspects of climate change. Despite the existing evidence for this matter (Abd Karim 2008; Kositsup et al. 2009; Yu et al. 2014; Golbon et al. 2015; Jayasooryan et al. 2015; Nguyen and Dang 2016), setting a clear-cut threshold for heat stress is still a debatable subject.

Here, we apply rule-based geographical classification to a selection of the downscaled IPCC AR5 climatic projections in order to map the potential geographical zones projected to be climatically suitable for Para rubber cultivation, or exposed to excessive heat, in MSEA in three time sections centered on 2030, 2050 and 2070 while accounting for and presenting the classification uncertainty.

3.2 Data and methods

3.2.1 Data

We used the WorldClim dataset (version 1.4, (Hijmans et al. 2005)) to generate the baseline climatic map and an ensemble of nine GCMs under the Fifth Assessment Report of the Intergovernmental Panel on Climate Change (IPCC AR5) as simulations forecasting the climatic conditions for three 20-year time periods centered on 2030, 2050 and 2070. Facing the choice questions mentioned in the introduction section 3.1, we referred to McSweeney et al. (2015), which ranked IPCC AR5 GCMs according to their regional performances and recommended a subset of 8-10 GCMs, avoiding the least realistic models while retaining the maximum plausible dispersion. Nine GCMs were selected using the regional plausibility rankings: ACCESS1.0 (Bi et al. 2013; Dix et al. 2013), CCSM4 (Gent et al. 2011), IPSL-CM5A-LR (Dufresne et al. 2013), NorESM1-M (Bentsen et al. 2013), GFDL CM3 (Donner et al. 2011), BCC_CSM1.1 (Xin et al. 2013), MRI-CGCM3 (Yukimoto et al. 2012), HadGEM2-ES (Martin et al. 2011) and MPI-ESM-LR (Giorgetta et al. 2013). The GCM data were provided by the Climate Change and Food Security (CCAFS) Program data

portal of the International Center for Tropical Agriculture (CIAT) (available at www.ccafs-climate.org) and were downscaled to 30 arc sec (~1 km) resolution using delta method (Ramirez-Villegas and Jarvis 2010). Two of the four main climate change scenarios recognized by the IPCC AR5 were considered in this study: Representative Concentration Pathways (RCPs) 8.5 and 4.5. RCP 8.5 is a high greenhouse gas (GHG) emission scenario comprising no stabilization of the atmospheric GHG concentrations leading to 8.5 Wm^{-2} of radiative forcing by 2100 and a globe over 4°C warmer than the pre-industrial era. RCP 4.5 is a moderate scenario accommodating GHG concentration stabilization by 2070 and radiative forcing of 4.5 Wm^{-2} (2.5° C temperature rise) by the end of the 21st century (Riahi et al. 2011; Thomson et al. 2011). Land use data (see 7 Appendix Figure A3.1 available at stacks.iop.org/ERL/13/084002/mmedia , (Hoskins et al. 2016)), the Biodiversity Intactness Index (BII) created by Newbold *et al* ((Newbold et al. 2016), Appendix Figure A3.2) and the USGS GTOPO30 digital elevation model were used to cluster and describe the potential future expansion/retraction zones. We have also used the administrative divisions (GADM) shapefiles (available at www.gadm.org) in this study.

3.2.2 Methods

Five climatic suitability criteria adapted from Rivano et al. (2015) listed in Table 3.1 were used in this study. As mentioned by Thompson et al. (2013) and Stephens et al. (2012) it is essential to avoid averaging for ensemble formation as it leads to information loss on variation. Here we conducted the complete classification process on the involved gridded variables separately for each GCM and formed the ensemble product by the majority outcome for each grid cell overlaid with a simple uncertainty measure reflecting the strength of the majority. The total annual precipitation and the mean annual temperature layers were directly categorized to optimal, suboptimal and prohibitive ranges for each GCM, time section and scenario. The ensemble suitability projections were generated for each 'criterion × time section × scenario' combination consisting of the suitability class returned by the majority of the GCMs for every grid cell and a corresponding uncertainty layer reflecting the strength of the consensus on the class assigned to each ensemble grid cell ranging from full agreement (9/9) to mere majority (5/9). The monthly mean temperature and the monthly precipitation gridded data went through a similar process with two additional steps (see Figure 3.4), summarizing the intra-annual distribution of precipitation and temperature.

Table 3.1 Criteria and thresholds for classification of the gridded climatic data

Climatic criterion	Range			
	Prohibitive	Suboptimal	Optimal	Excessive
Annual mean temperature (°C)	< 23	23-25	25-28	> 28
Number of months with mean temperature below 23°C	> 5	1-5	0	-
Annual precipitation (mm)	< 1100	1100-1500	> 1500	-
Number of months with precipitation below 50mm	> 5	4-5	0-3	-

Thresholds used in this study are adapted from Rivano et al. (2015). The number of months with mean temperature below 23°C is referred to as intra annual temperature distribution and the number of months with precipitation below 50mm as intra annual precipitation distribution.

By overlaying the classification outcomes of the climatic layers, each grid cell was assigned one of the following summarizing classes: 'AllOpt' where all climatic layers returned an optimal classification, 'SubOpt' where at least one layer was described as suboptimal and none as prohibitive, 'SingProh' where only one layer was in prohibitive range and 'MultProh' with more than one climatic criterion in the prohibitive range. The aggregate uncertainty layers were also overlaid to produce an aggregate uncertainty layer in four levels: 1) full agreement among GCMs for all four criteria, 2) only one criterion projected with 7 or 8 from 9 majority (and all other criteria possessing stronger consensus), 3) only one criterion projected with 5 or 6 from 9 majority (and stronger consensus in all other criteria) and 4) two or more criterion projected with 5 or 6 from 9 majority.

A point shapefile representing grid cells in the raster data was created for the shift zones with high aggregate certainty (levels 1 and 2) to which the corresponding land use, BII, altitude, slope, longitude and latitude values both in original and standardized form were extracted. We used the Grouping Analysis tool of the ArcGIS 10.2.2 to form clusters based on the standardized attributes and illustrated the outcome using 'ggplot2' 2.1.0 package in R.

Sankey diagrams are illustration tools suitable for description of multidimensional and hierarchical categorical data and are most often used to show material or energy flows through network systems. Geographical classification dynamics over time can also be very efficiently presented by Sankey diagrams. As demonstrated by Cuba (2015), Sankey diagrams are superior to cross-tabulation matrices in reflecting land use dynamics, particularly when multiple time sections are of interest. We generated Sankey diagrams to illustrate the climatic suitability class shifts projected to occur under RCP 4.5 and RCP 8.5 for each adjacent pair of time sections using the D3.js JavaScript library developed by Bostock et al. (2011).

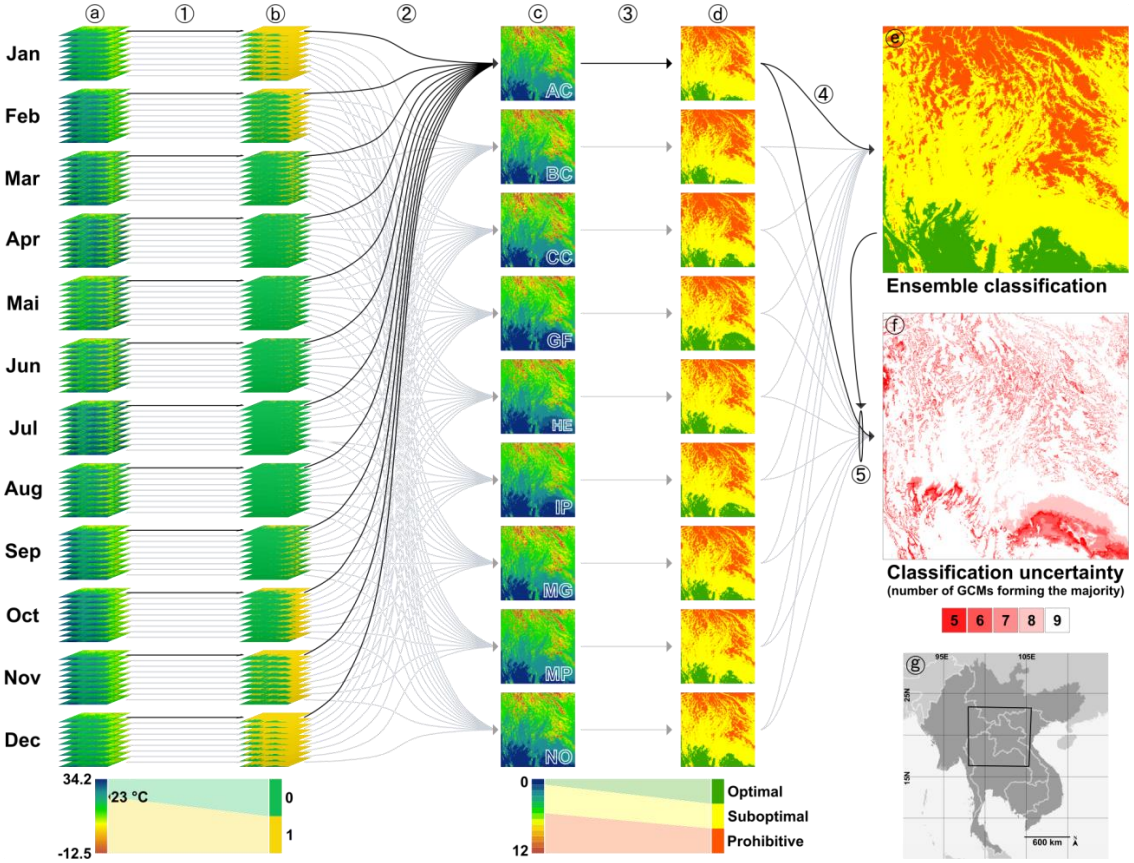

Figure 3.4 Steps involved in intra-annual temperature distribution suitability classification (as illustration case)

Continuous monthly mean temperature gridded data (Representative Concentration Pathway 4.5 for the 20 year period centered on 2030) ⓐ were used to generate binary layers ⓑ by setting a stress threshold ① (23° C). All 12 binary layers originating from the same Global Circulation Model (GCM) were summed ② to produce the layers reflecting the number of months projected to be below the threshold ⓒ (abbreviations AC to NO denote the corresponding GCMs). These layers were reclassified ③ to three levels: optimal, suboptimal and prohibitive ⓓ. The ensemble classification map ⓔ was generated by extracting the majority outcome of all GCMs for each grid cell ④. The uncertainty layer ⓕ reflects the consensus level among GCMs leading to the ensemble and was produced by counting the number of GCMs participating in the formation of the majority for each given grid cell ⑤. Panel ⓖ shows the geographic extents of the frame selected for illustration. All layers used in each step were assigned equal weights and the arrow color difference is only for visual clarity. ArcGIS 10.2.2 and Inkscape 0.91 were used for generation of this figure.

Using the ensemble formation technique, we created an 'excessive heat' layer distinguishing the area associated with annual mean temperature exceeding 28°C at the baseline and traced its potential expansion under the two RCPs overlaid with corresponding uncertainty layers. This criterion, however, was not used as an upper limit for transition to suboptimal or prohibitory conditions in the former steps.

3.3 Results

3.3.1 Single criterion classification

Climatic conditions in the study area at the baseline and the ensemble projections for the four climatic criteria (separately classified) are presented in Figures 3.5 and 3.6. Largest projected shifts (expressed as proportion of the total studied area) are observed for the annual mean temperature and the intra-annual temperature distribution moving from baseline to the 20 year time window centered on 2030. Considering the annual mean temperature, 25.13 % of the total area (642416 km^2 from 2556370 km^2) is projected (21.79 % projected with full GCM consensus) to migrate from prohibitive and suboptimal range to classes more conducive to rubber cultivation under RCP 4.5. The RCP 8.5 ensemble projection suggests this figure to be 28.55 % (23.38 % with full agreement). For intra-annual temperature distribution, 20.18 % (16.59 % with full agreement) of the total area is observed to experience such a transition under RCP 4.5 and 23.96 % (17.67 %) under RCP 8.5 from baseline to the 2030 period. Moving to 2050 and 2070 time periods, the emerging more suitable areas regarding the two aforementioned factors are of much smaller size and paired with higher degrees of uncertainty. The persistence of the new conditions in an area which has gone through climatic shift is relevant but not necessarily traceable in Sankey diagrams (Figure 3.5). Considering annual mean temperature under RCP 4.5, 14.17 % of the total area is projected with high certainty to remain in the new class after shifting from prohibitive to suboptimal or suboptimal to optimal range and 16.58 % under RCP 8.5. For the intra-annual temperature distribution, these figures are projected to be 14.17 % and 16.55 % respectively. Unlike temperature components of climate, the projected shifts observed in precipitation components were bilateral, associated with low certainty (i.e. high disagreement among GCMs) and smaller in size. The largest area projected to experience shifts in the precipitation class by 2030 was observed for intra-annual precipitation distribution summing to 7.02 % of the total investigated area (6.01 % moving from prohibitive to suboptimal or suboptimal to optimal and 1.01 % vice versa). 80.63 % of it (equal to 5.66% of the total area) has been projected by mere majority (i.e. the lowest possible certainty level).

Comparing single criterion GCM projections with their corresponding ensembles (Table 2) reveals that ACCESS1.0 has returned the closest single criterion maps to the ensemble with an average overlap of 92.42 % across all 24 possible criterion-RCP-time period combinations followed by BCC_CSM1.1, MPI-ESM-LR and CCSM4.

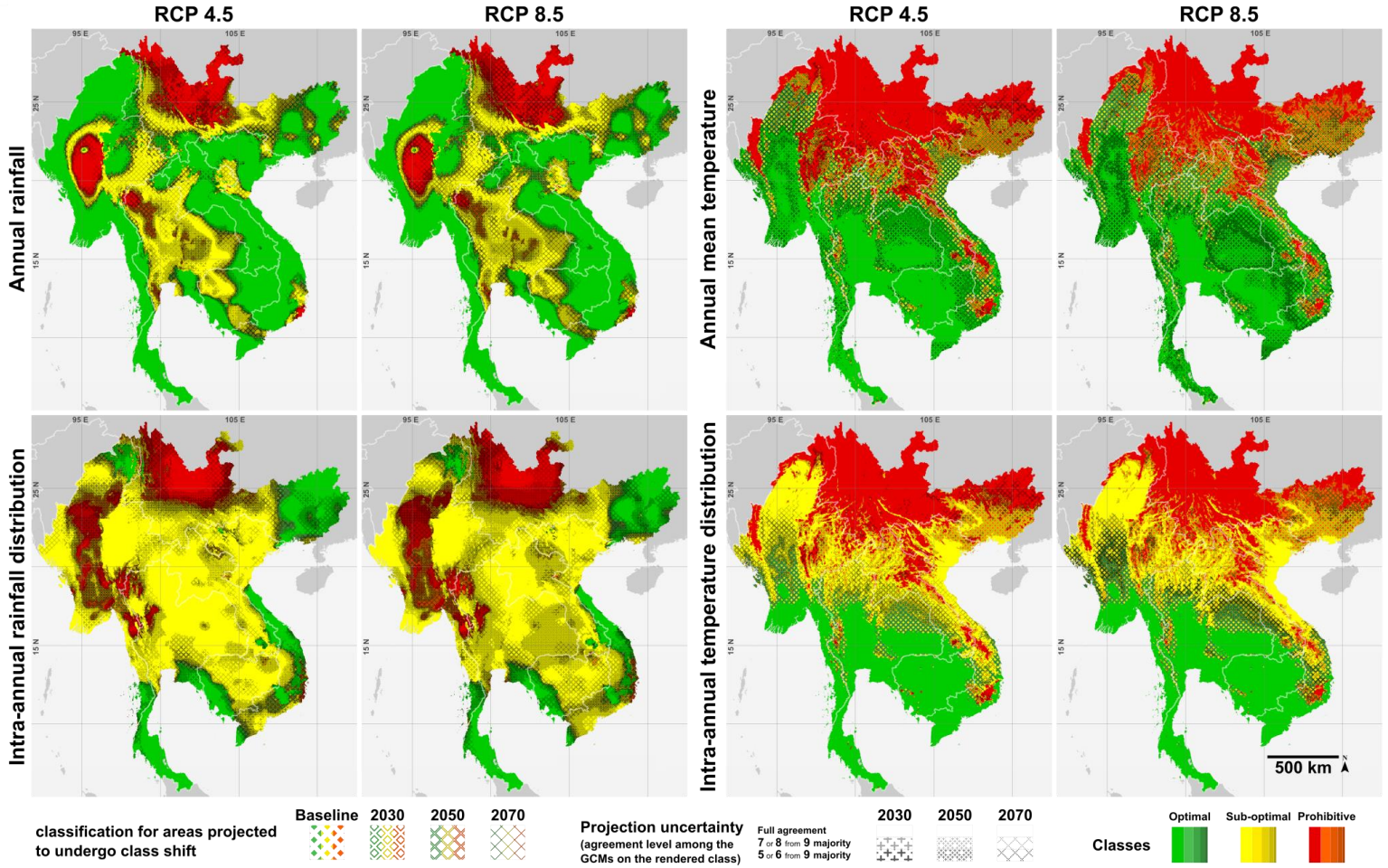

Figure 3.5 Baseline and projected single criterion climatic class dynamics maps
The classification dynamics for the climatic criteria considered in this study cover baseline and the ensemble future projections. Each panel contains seven (1+3+3) layers of information: suitability class at the baseline (×1), projected class shifts between the four time sections (×3), and the strength of the ensemble majority suggesting the change/no-change (×3). Please view this figure in original resolution and consult the usage guide provided in the Appendix (Figure A3.10) for clarifications. Maps were generated in ArcGIS 10.2.2 and visually optimized in Inkscape 9.2.

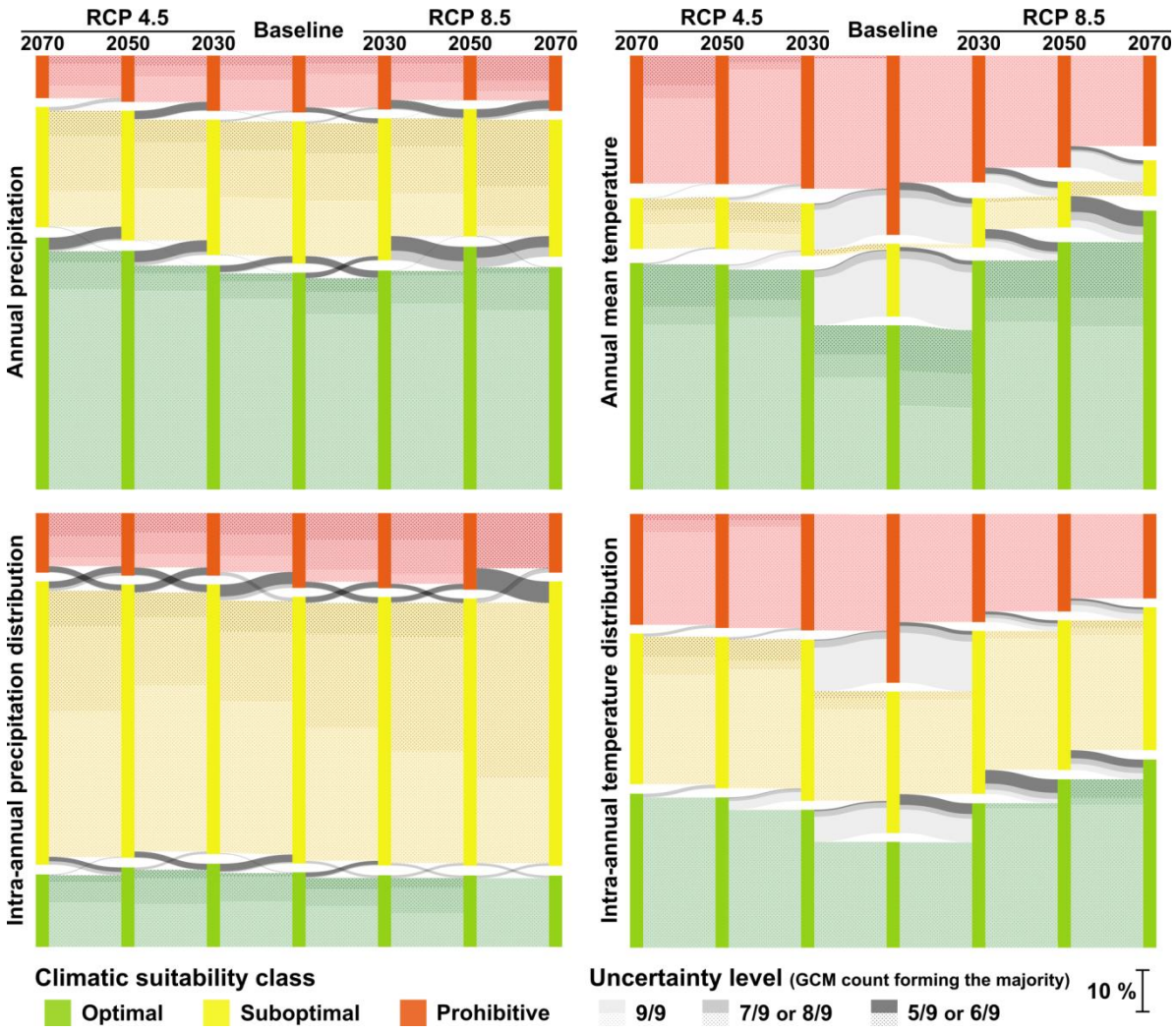

Figure 3.6 Baseline and projected single criterion climatic class dynamics
The classification dynamics for the area associated with the climatic criteria considered in this study at the baseline (2000) and the ensemble future projections correspond to the maps presented in Figure 3.5. For more details on the use of Sankey diagrams in illustration of geographic shifts, view the dedicated article: Cuba (2015). Sankey charts were produced in D3.js JavaScript library (Bostock et al. 2011) and visually optimized in Inkscape 9.2.

3.3.2 Aggregate classification

The geographical and temporal dynamics of the projected climatic suitability classes at the aggregate level are illustrated in Figures 3.7 and 3.8. The area projected to retain its aggregate climatic class across the investigated time span (by 2070) is projected to be 72.83% of the total area under RCP 4.5 and 66.23% under RCP 8.5. By the time window centered on 2050 these projections sum to 74.98% and 72.89% and by 2030 to 77.63% and 78.22% of the total area respectively. From the total projected class-shifting area by 2030, 26.78% (6.01% of the studied area) was projected with maximum certainty (i.e. full agreement among GCMs in all four criteria) under RCP 4.5 and 26.50% (5.77%) under RCP 8.5. It was projected to decline to 14.09% (3.53%) and 17.39% (4.71%) for the baseline to 2050 time period and further reduction to 9.49% (2.58%) and 7.10% (2.40%) for 2070 respectively. Performance similarity of single GCM aggregate

classification maps with the ensemble is presented in Table 3.3 where ACCESS1.0 returned the closest results to the ensemble.

Table 3.2 Classification agreement between the single criterion climatic data simulations and their ensemble

Criteria	RCP	Period	Climatic data simulations								
			AC	BC	MP	CC	NO	MG	IP	HE	GF
Annual precipitation	4.5	2030	93.9	91.2	93.7	89.6	89.8	90.3	94.7	88.1	85.8
		2050	93.7	94.6	91.5	91.7	89	89.1	90.1	90.7	88.0
		2070	92.6	85.7	91.1	93.8	83.2	92.8	90.5	86.7	91.7
	8.5	2030	94.0	88.7	91.1	88.8	88.8	89.7	92.7	88.5	84.6
		2050	93.2	92.7	90.0	92.2	90.6	87.6	89.1	88.1	84.7
		2070	89.2	84.1	88.6	89.6	85.9	92.5	87.2	83.2	89.1
Intra-annual precipitation distribution	4.5	2030	90.5	85.0	91.0	84.7	89.5	92.6	88.2	92.5	79.1
		2050	91.1	88.6	87.8	87.0	89.6	90.7	86.3	87.7	85.4
		2070	90.4	81.1	89.2	89.7	84.5	87.3	87.1	89.2	87.1
	8.5	2030	92.4	87.2	90.6	88.0	89.3	83.6	75.2	88.2	86.3
		2050	92.6	83.3	90.7	88.1	79.4	91.6	72.5	83.3	88.0
		2070	91.7	87.5	86.2	86.4	81.9	87.9	64.7	84.0	82.5
Annual average temperature	4.5	2030	91.5	99.2	82.3	91.3	92.2	90.3	87.5	90.1	86.4
		2050	91.2	99.3	89.0	91.9	93.6	88.7	88.6	85.4	80.8
		2070	81.5	99.2	86.4	95.9	92.8	90.7	86.3	73.2	77.0
	8.5	2030	96.6	96.5	97.8	92.2	87.3	85.0	90.2	89.5	93.4
		2050	91.6	95.7	98.8	90.3	89.1	80.7	86.9	85.5	87.8
		2070	92.1	93.7	98.6	86.2	85.5	78.0	87.6	80.6	89.7
Intra-annual temperature distribution	4.5	2030	97.0	96.1	92.4	98.2	96.1	95.0	94.7	96.7	94.0
		2050	96.0	96.5	92.2	97.4	96.4	93.3	96.0	93.3	90.8
		2070	90.5	96.6	92.1	97.7	96.1	92.8	95.2	86.8	88.8
	8.5	2030	95.7	95.8	97.0	98.6	94.7	93.6	96.5	93.9	96.7
		2050	94.6	93.5	97.3	96.1	94.3	89.9	96.1	92.3	93.7
		2070	94.4	95.2	98.7	94.7	93.5	88.9	96.4	91.1	95.6

Resemblance of the climatic classification by each of the nine simulations used in this study with their ensemble is expressed as proportion (%) of the sum of the areas with matching classification to the total area. Color-code reflects five levels: below 75%, 75 - 90%, 90.1 - 95%, 95.1 - 99% and above 99%. Maximum and minimum of each row are underlined. Nine IPCC AR5 simulations of representative concentration pathways RCP 4.5 and RCP 8.5 were used, here abbreviated as AC: ACCESS1.0 (Bi et al. 2013; Dix et al. 2013), CC: CCSM4 (Gent et al. 2011), IP: IPSL-CM5A-LR (Dufresne et al. 2013), NO: NorESM1-M (Bentsen et al. 2013), GF: GFDL CM3 (Donner et al. 2011), BC: BCC_CSM1.1 (Xin et al. 2013), MG: MRI-CGCM3 (Yukimoto et al. 2012), MP: MPI-ESM-LR (Giorgetta et al. 2013) and HE: HadGEM2-ES (Martin et al. 2011). Each time period corresponds to a 20 year (averaged) time section centered on the mentioned year. GCMs are rank-sorted from left to right by their overall resemblance to ensemble.

Restricting the investigated time window to the 20 year period centered on 2030 and the area to where climatic conditions are projected with high (the upper two levels) certainty to shift from prohibitive to rubber cultivation to suboptimal or optimal, our projections detected 195928 km^2 (7.70% of the total investigated area) under RCP 4.5 and 238734 km^2 (9.38%) under RCP 8.5 which are presented in Figure 3.8. Using Grouping Analysis we detected eight major clusters based on land use composition, physiographic attributes and proximity. Northernmost potential expansion was projected to verge on 27°N of the Irrawaddy basin and the altitudinal limit to exceed 1400 m a.s.l. in clusters 7 (Bilauktaung range Thailand-Myanmar border between 15.56 °N and 18.10 °N) and 8 (Cardamom Mountains of Cambodia) (Figure 3.9). The overall baseline

state of biodiversity in these clusters is presented in Figure 3.10 using the biodiversity intactness index (BII). (Steffen et al. 2015) have proposed a safe limit value of 0.9 (maximum 10% decline) for BII. The largest cluster (cluster 1) corresponding to Guangxi Autonomous Region of China and Northern Vietnam is the most ecologically degraded and accommodates 92.47% of the area already below the safe threshold.

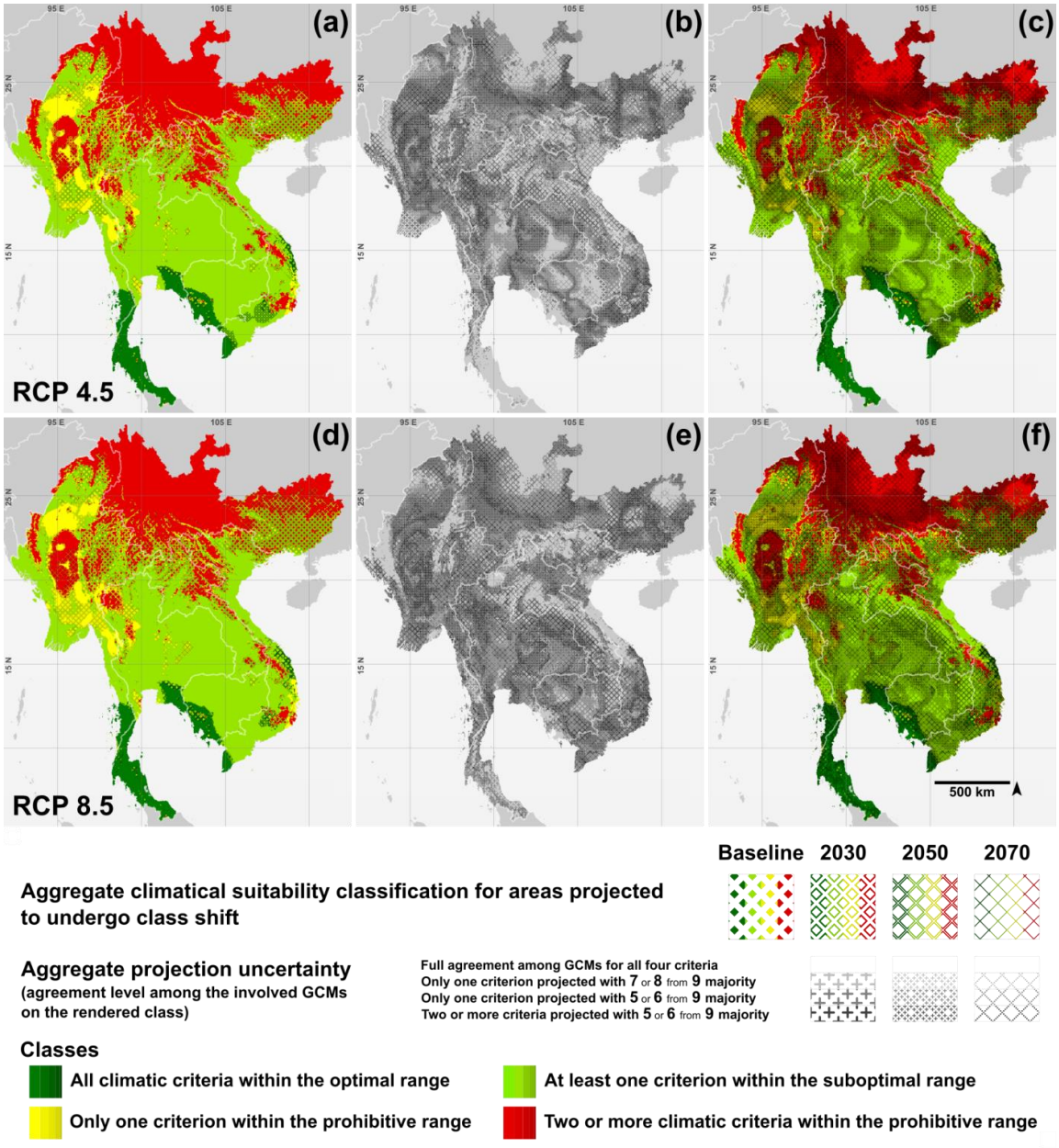

Figure 3.7 Aggregate climatic classification maps
Panels (a) and (d) reflect four (1+3) layers of information: the aggregate suitability class at the baseline (×1) and the projected class shifts between the four time sections (×3). Panels (b) and (e) demonstrate the strength of the ensemble majority suggesting the change/no-change (×3) between temporally adjacent time sections. Aggregate classification layers (a) and (d), and the corresponding uncertainty layers (b) and (e) are overlaid to produce panels (c) and (f). Please view this figure in original resolution and consult the usage guide provided in the Appendix (Figure A3.10) for clarifications. Maps were generated in ArcGIS 10.2.2 and visually optimized in Inkscape 9.2.

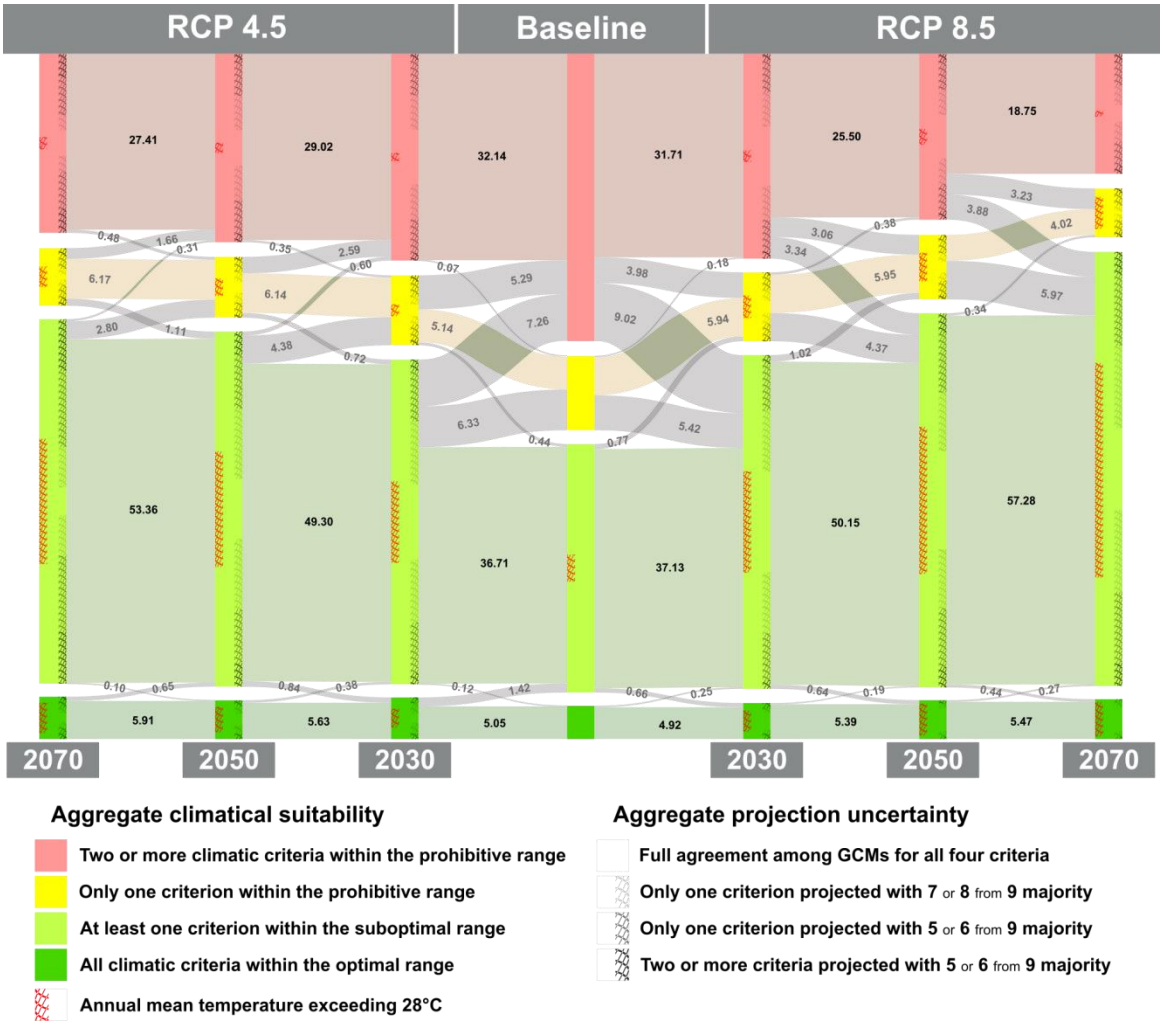

Figure 3.8 Baseline and projected aggregate climatic suitability dynamics
Baseline (2000) classification and future projections for three time sections under two IPCC AR5 representative concentration pathways 4.5 and 8.5 are reflected proportional (%) to the total investigated area. Inter-nod connections (flows) smaller than 0.05 % are not demonstrated. For more details on the use of Sankey diagrams in illustration of geographic shifts, view the dedicated article: Cuba (2015). Sankey diagram was produced in D3.js JavaScript library (Bostock et al. 2011) and visually optimized in Inkscape 9.2.

Table 3.3 Classification agreement between the data simulations and their ensemble at the aggregate level

RCP	Period	Climatic data simulations								
		AC	CC	BC	MP	NO	MG	GF	HE	IP
4.5	2030	90.22	88.27	89.60	85.82	90.66	85.92	78.39	89.99	89.89
	2050	92.48	88.77	92.30	83.26	90.90	85.61	82.34	85.76	89.00
	2070	89.39	93.02	87.31	86.32	88.76	86.11	84.45	81.24	87.45
8.5	2030	92.87	89.35	88.20	90.73	89.27	84.20	84.89	83.19	76.61
	2050	91.20	88.66	87.58	91.69	82.76	87.11	86.60	79.35	74.54
	2070	91.21	88.41	88.57	88.06	83.26	84.48	82.52	78.32	65.90

Resemblance of the aggregate climatic classification by each of the nine simulations used in this study with their ensemble is expressed as proportion (%) of the sum of the areas with matching classification to the total area. Color-code reflects five levels: below 75%, 75 - 80%, 80.1 - 85%, 85.1 - 90% and above 90%. Nine IPCC AR5 simulations of representative concentration pathways RCP 4.5 and RCP 8.5 were used, here abbreviated as AC: ACCESS1.0 (Bi et al. 2013; Dix et al. 2013), CC: CCSM4 (Gent et al. 2011), IP: IPSL-CM5A-LR (Dufresne et al. 2013), NO: NorESM1-M (Bentsen et al. 2013), GF: GFDL CM3 (Donner et al. 2011), BC: BCC_CSM1.1 (Xin et al. 2013), MG: MRI-CGCM3 (Yukimoto et al. 2012), MP: MPI-ESM-LR (Giorgetta et al. 2013) and HE: HadGEM2-ES (Martin et al. 2011). Each time period corresponds to a 20 year (averaged) time section centered on the mentioned year. GCMs are rank-sorted from left to right by their overall resemblance to ensemble.

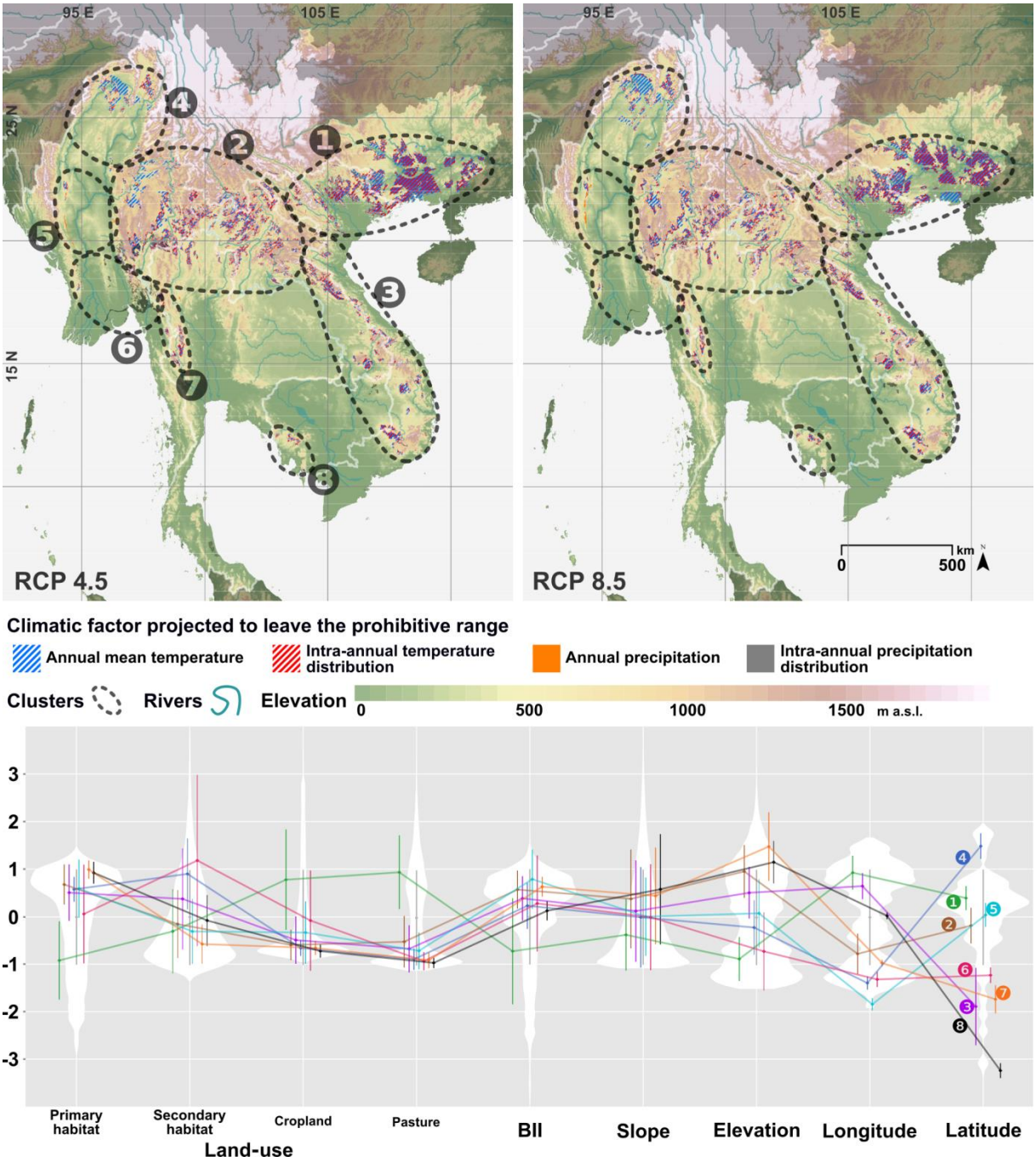

Figure 3.9 Areas projected with high certainty to become climatically suitable for rubber cultivation by 2030

Land use composition (Hoskins et al. 2016), physiographic composition (USGS GTOPO30) and biodiversity intactness index (BII) (Newbold et al. 2016) were used to group the parts of the study area which were projected with high ensemble consensus to become climatically suitable for rubber cultivation into eight clusters using the Grouping Analysis tool of ArcGIS 10.2.2. Violin plots (bottom panel) were generated using the 'ggplot2' 2.1.0 R package and visually optimized in Inkscape 9.2. Terms primary and secondary habitat represent 'undisturbed natural' and 'recovering, previously disturbed natural' habitats respectively. Variables shown above are adjusted to share zero mean and unit variance. For original scale, please see Appendix Figures A3.4 to A3.6.

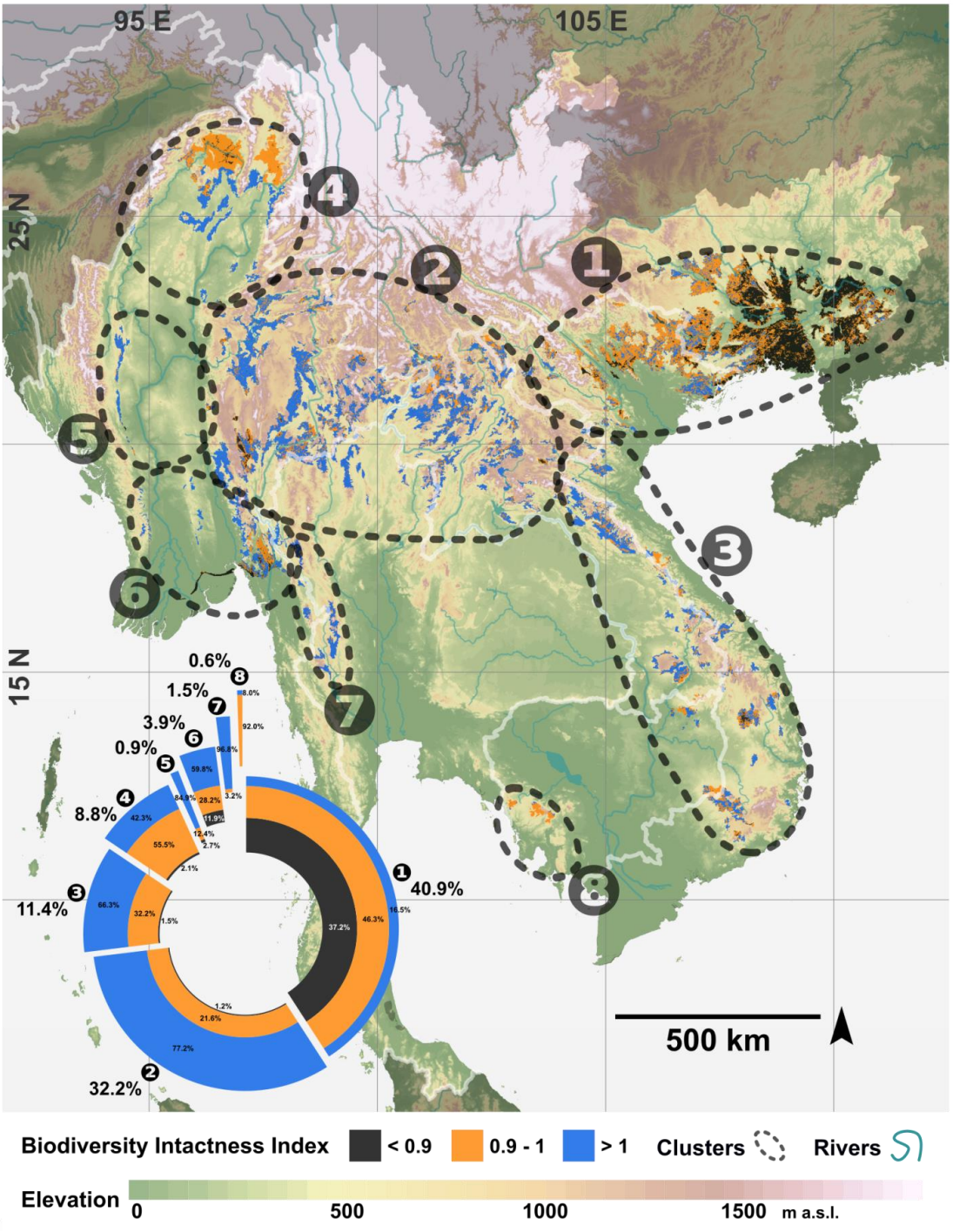

Figure 3.10 Biodiversity Intactness Index in high certainty shift zones
Biodiversity intactness index (BII) from Newbold et al. (2016) extracted for Areas projected with high certainty to become climatically suitable for rubber cultivation by 2030. See Appendix Figure A3.2 for complete frame coverage.

3.3.3 Exposure to excessive heat

Projected exposure to annual mean temperature levels exceeding 28°C in the study area is presented in Figure 3.11. Based on WorldClim data, total baseline area with this characteristic is limited to 14570 km² (less than 0.6 % of the total investigated area) located between 12.33 °N, 100°E and 16.33 °N, 101.50 °E in Thailand. Ensemble projections based on 7/9 to 9/9 majority classification suggest that by 2030, under RCP 4.5 this area may increase 25 fold (14.3% of GMS) and 35 fold (20.5% of GMS) under RCP 8.5 stretching northwards to 22°N in the central parts of the Irrawaddy basin. By 2050 however, this criterion may be associated with 23.2% of the total area under RCP 4.5 and 31.2 % under RCP 8.5 increasing respectively by 2070 to 26.5% and 38.9%.

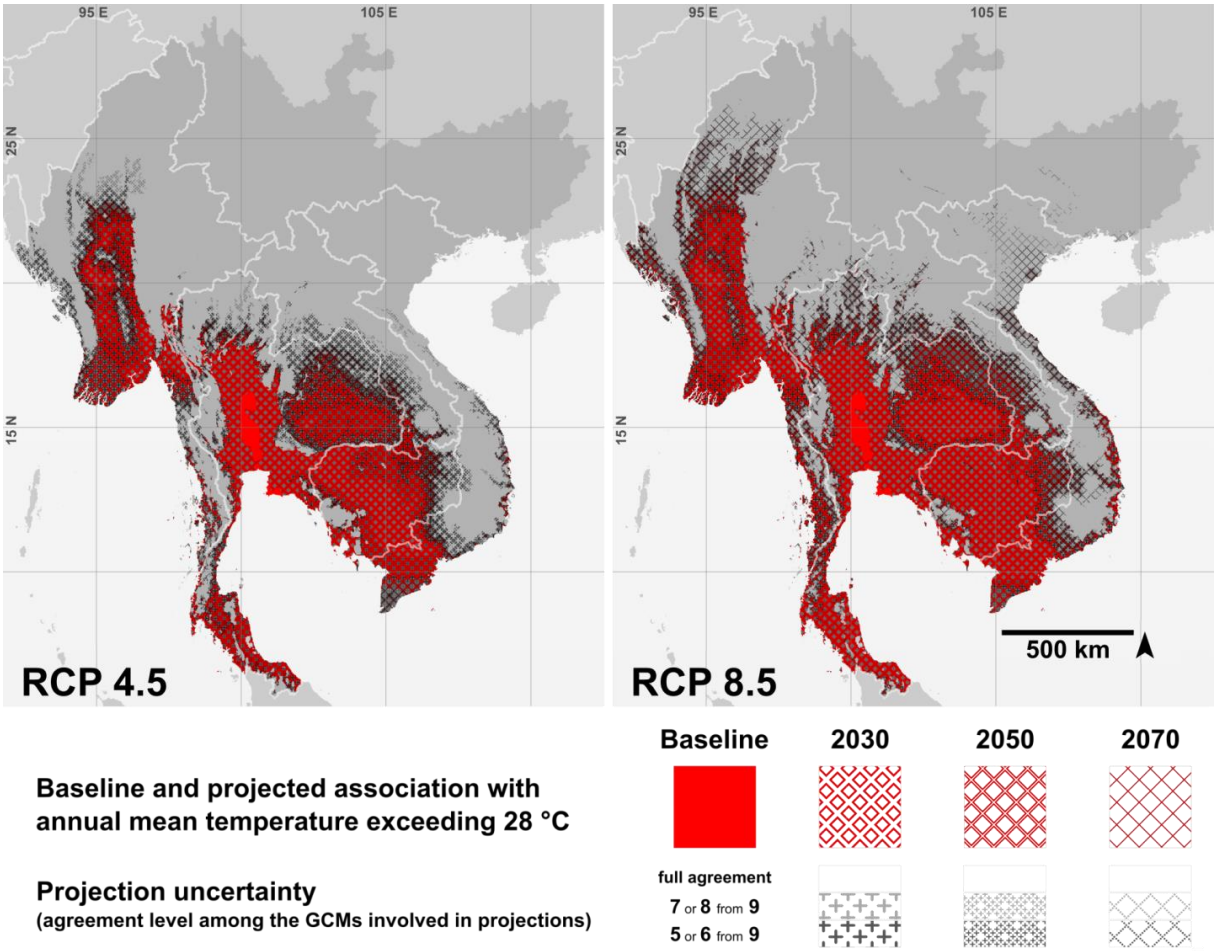

Figure 3.11 Baseline and projected extent of the exposure to mean annual temperature above 28°C
Each panel contains seven (1+3+3) layers of information: exposure to mean annual temperature above 28°C at the baseline (×1), projected shifts between the four time sections (×3), and the strength of the ensemble majority suggesting the shift/no-shift(×3). Please view this figure in original resolution and consult the usage guide provided in the Appendix (Figure 3.10) for clarifications.

3.4 Discussion

3.4.1 Contrasts and conjunctions with comparable studies

Zomer et al. (2014) conducted a study focusing on the potential changes in the area conducive to rubber cultivation in Xishuangbanna, Yunnan, China using environmental stratification while averaging all four AR5 RCPs which suggested an increase from 33.5% to 74.5% of the total prefecture area by 2050. Our findings for the same temporal and spatial frame are 52.5% (43.7% with high certainty) under RCP 4.5 and 83.1% (60.1%) under RCP 8.5. Ray et al. (2016a, b) used MaxEnt ecological niche modeling tool exploring the rubber producing Western Ghats and the North-East regions of India and noted a substantial attachment of the projection outcome to the region used for calibration. If Amazonia was used for model calibration, only a very limited southern part of Western Ghats was returned as suitable by MaxEnt while established rubber growing regions were left out. They observed the same limited transferability pattern while calibrating MaxEnt with each of two Indian rubber producing regions projecting for the other, one at a time. They reached plausible projections only by pooled occurrence points for parameter estimation. Ahrends et al. (2015) investigated the expansion trends of rubber cultivation in roughly the same geographical frame as this study and concluded that this land use is stretching into increasingly less suitable zones jeopardizing biodiversity and landscape functions. They included a typhoon damage risk assessment based on historical tropical cyclone tracks which, when compared with the area projected with high certainty in this study to become climatically conducive to rubber cultivation by 2030, suggests current typhoon risk zones to overlap only with parts of clusters one (13.2%) and three (2.2%). This overlapping area in cluster one is limited to a 50 km inland buffer of the Guangxi coastline between 106.50°E and 109.66°E. Recent studies on the influence of climate change on western North Pacific tropical cyclone tracks however project reductions in both frequency and intensity of typhoons in future for our area of interest mainly due to northward diversion (Colbert et al. 2015; Kossin et al. 2016; Zhang and Wang 2017). Liu et al. (2015a) projected the change in the area with potential for Para rubber cultivation in China covering all five provinces with rubber cultivation background (Hainan, Yunnan, Guangdong, Guangxi and Fujian) using ecological niche modeling to and reported a 15% increase by 2050 from about 400000 km^2 in 2010.

With the exception of cluster 1, which encompasses a major biotically compromised (BII<0.9) area share, most of the regions projected to gain climatic potential for rubber cultivation are chiefly composed of intact primary habitats (Figure 3.10 and Appendix Figure A3.4). In these areas land use modifications of significant scale require serious attention to the potential impacts on the

ecological integrity and ecosystem functions and services. The ongoing improvements in the scientific understanding and practice of concepts such as rubber based agroforestry systems (Langenberger et al. 2017) and Green rubber eco-certification (Kennedy et al. 2017) offer promising options for environmentally friendly rubber cultivation, particularly as support from smallholder side for participation in ecosystem protection appears to grow (Wigboldus et al. 2017; Min et al. 2018).

3.4.2 Strengths and limitations of the projection approach

Hevea brasiliensis is not only a plant and therefore a sessile species but also a crop subject to non-natural sources of influence (e.g. breeding and crop management), which may affect the reliability of species distribution models if based on biased presence and pseudo-absence records. From our point of view rule-based models tend to be less prone to circular reasoning but risk engaging non-accurate classification rising from misestimated or dated tolerance thresholds (e.g. due to breeding).

We chose to assign equal weights to the climatic criteria involved in this study, and also to the GCMs forming the ensemble single criteria layers. However, we acknowledge that a non-equal weight approach based on justified quantification of the influence associated with each criterion or its ensemble projection homogeneity (in case of GCMs, based on data quality) is plausible.

Non-climatic factors (e.g. soil conditions, land physiography, labor and market access) which are known to be decisive in suitability for rubber cultivation were not involved in this study. Coverage of a broad range of suitability determining factors in a single study faces serious technical challenges. Different variables can often not be processed with a general approach as the scale relevant for some factors may not necessarily match the scale suitable for the others. The availability and quality of data in a standardized form are also two crucial limiting features. However, some factors relevant in smaller scale (e.g. soil properties) can be nested in those relevant in larger scale (e.g. climatic conditions) by subsequent localized assessments. This requires the provision of the outputs of studies such as this in a modular form exploitable for third parties. The KMZ files accompanying this manuscript do not only provide the findings unchained from resolution loss, but can also be used by future studies as a base to expand upon.

Although recent trajectories of GHG emissions are closest to the RCP 8.5 (Appendix Figure A3.7), this climate change scenario incorporates some assumptions concerning the use of fossil energy resources which are in the long-run technically improbable (Capellán-Pérez et al. 2016; Ritchie and Dowlatabadi 2017a, b; Wang et al. 2017). In view of the concerns and evidence regarding rapid changes in land use and climate, it is counterintuitive to use the early years of the last decade

as baseline. Nevertheless, most required underlying data components are being revised not with emphasis on updating but on resolution (e.g. (Newbold et al. 2016)) or precision (e.g. (Fick and Hijmans 2017)).

Compared with the lower temperature tolerance limits known for Para rubber, upper thresholds and consequences of exposure to high levels of ambient temperature are not well understood. The global area already exposed to annual mean temperature above 28° C (Appendix Figure A3.9) does not match typical rubber growing regions. In case of the GMS, a comparison between Figures 3.2 and 3.11 underlines this point. Mesocosm experiments (Stewart et al. 2013; Bestion et al. 2015; Fordham 2015) and other manipulation methods which have recently gained prominence in studies aiming at a better understanding of the responses of the organisms to a warming climate can illuminate the way for *H. brasiliensis* as well.

The methods developed in this article are applied to a relatively restricted case study, rubber cultivation in the GMS. Nevertheless, the potential for transferability to other world regions and other cropping systems is very high, as the vast majority of datasets used is freely available for scientific purposes. The phenological and physiological crop specific background data for other crop plants can be collected from text books and literature reviews. Potential applications that come to mind might be the potential suitability for oil palm plantation systems, coffee agroforestry or bio-economically important crops such as sugar cane and maize and its´ potential northern distribution limits.

In order to broaden the audience of this study and to facilitate the use of its outputs for potential decision makers, we have produced two KMZ files (one for each RCP) which summarize the information behind Figures 3.5, 3.7 and 3.11, covering the baseline and the 2030s time windows. These files can easily be loaded in Google Earth™ to check the conditions for a given location by clicking. The KMZ files and all of the figures in high resolution are available on zenodo.org (https://doi.org/10.5281/zenodo.1312769).

3.5 Conclusion

Even though the climatic change in the GMS is projected to be predominantly in the direction of higher suitability for rubber cultivation, the expansion of climatically optimal area is projected to be minimal. When including the exposure to annual mean temperatures exceeding 28°C (current estimate of excessive heat for *Hevea* rubber), as a limiting factor, then even a heavy reduction in the total climatically optimal area is likely to occur (see Figure 3.8).

Across the time span investigated in this study (limited to 2070), about half of the new area with climatic potential for rubber cultivation is projected to emerge by 2030, near half of which is ecologically pristine (see Figure 3.10). This pattern, in combination with factors encouraging rubber cultivation in higher altitudes and latitudes underscores the urgency and importance of careful future land use planning. Local and regional decision-makers can use mid- to (more cautiously) long-term assessment such as this to develop policy guidelines and decision support mechanism that can take the occurrence of potential new land use and land management systems into account. Either to prepare a certain region for potential innovations regarding the demands to local infrastructure, or to put necessary guidelines and rules into place to "soften the blow" these innovations might have on traditional systems or biodiversity and nature conservation.

Acknowledgements

The authors want to thank the German Ministry of Science and Technology for supporting the research that led to this publication under the LILAC and SURUMER projects (grant numbers FKZ 0330797A and FKZ 01 LL 0919) as well as for funding its open access publication. We deeply appreciate the raw data provision by all sources mentioned in this article. We are grateful to Kevin Thellmann, Benjamin Warth and the anonymous referees for their constructive criticisms and insights which helped us improve an earlier draft of this paper.

Competing Interests: The authors declare they have no competing interests.

4 Global Assessment of Climate Driven Susceptibility to South American Leaf Blight of Rubber using Emerging Hot Spot Analysis and Gridded Historical Daily Data

Reza Golbon[1]*, Marc Cotter[1], Mehdi Mahbod[2] and Joachim Sauerborn[1]

1 University of Hohenheim, Institute of Agricultural Sciences in the Tropics (Hans-Ruthenberg-Institute), Agroecology in the Tropics and Subtropics Garbenstr. 13, 70599, Stuttgart, Germany

2 Department of Water Sciences & Engineering, College of Agriculture, Jahrom University, Jahrom 74131-88941, Iran

*Correspondence: golbon@uni-hohenheim.de

Received: date; Accepted: date; Published: date

Abstract:

South American leaf blight (SALB) of Para rubber trees (*Hevea brasiliensis* Muell. Arg.) is a serious fungal disease that hinders rubber production in the Americas and raises concerns over the future of rubber cultivation in Asia and Africa. The existing evidence of the influence of weather conditions on SALB outbreaks in Brazil has motivated a number of assessment studies seeking to produce risk maps that illustrate this relationship. Subjects with dynamic and cyclical spatiotemporal features need to embody sufficiently fine spatial resolution and temporal granulation for both input data and outputs in order to be able to reveal the desired patterns. Here, we apply emerging hot spot analysis to three decades of gridded daily precipitation and surface relative humidity data to depict their temporal and geographical patterns in relation to the occurrence of weather conditions that may lead to the emergence of SALB. Inferential improvements through improved handling of the uncertainties and fine-scaled temporal breakdown of the analysis have been achieved in this study. We have overlaid maps of the potential distribution of rubber plantations with the resulting dynamic and static maps of the SALB hot spot analysis to highlight regions of distinctly high and low climatic susceptibility for the emergence of SALB. Our findings highlight the extent of low-risk areas that exist within the rubber growing areas outside of the 10° equatorial belt.

Keywords: *Pseudocercospora ulei*, *Microcyclus ulei* phytopathology, geographic information systems, GIS

4.1 Introduction

Natural rubber is an essential raw material for the production of a wide range of goods and also the provision of numerous services (transportation above all). The Para rubber tree (*Hevea brasiliensis* Muell. Arg.) remains the unrivaled source for natural rubber. Although rubber trees originate from the Amazon basin, the Americas contribute only a fraction of the global rubber production (4.3% of 14.2 million tons in 2017) (FAOSTAT 2019). This is due to South American leaf blight (SALB), the most serious disease affecting rubber trees. It is caused by the fungus *Pseudocercospora ulei* P. Henn. (Hora Júnior et al. 2014), which induces lesions on young leaves, leading to defoliation that, in multiple cycles, weakens and eventually destroys the trees. SALB has so far been confined to the Americas, but its threat haunts Asian and African rubber production. The established high-yielding clones that are the source for most of the rubber produced worldwide have a very narrow genetic base (Besse et al. 1994; Le Guen et al. 2000). They originate from a region in Para state of Brazil where the natural resistance to SALB among wild rubber trees is the lowest compared to populations growing in other areas within the endemic range of *H. brasiliensis* (Le Guen et al. 2002, 2003, 2015). The genetic erosion associated with decades of selection and breeding in a SALB-free environment has also contributed to the vulnerability of the Asian clones (Varghese 1992; Onokpise 2004; Priyadarshan 2016). By contrast, the evolutionary potential of *P. ulei* has been observed to be vigorous (Barrès et al. 2012). The ongoing genetic improvement programs aiming to develop genotypes with stable resistance to SALB have yet to overcome this challenge (Guyot and Le Guen 2018). The destructive capacity of SALB, paired with the importance of its target crop (Häuser et al. 2015) and the lack of effective and both environmentally and economically (Evans 2002; Le Guen et al. 2008) acceptable countermeasures have earned *P. ulei* the status of a latent biological agent (Onokpise and Louime 2012; Miedaner 2017). Asian rubber-producing countries have implemented various measures to prevent the introduction of SALB and have developed contingency plans for its control in the case of an outbreak (LebaiJuri et al. 1997; Evans 2002; Asna and Ho 2005; Hashim 2012). Regional conferences and workshops backed by the FAO (Asia and Pacific Plant Protection Commission) have aimed to increase knowledge sharing and action harmonization among the participating countries.

In the 1970s and 1980s, a series of programs encouraging natural rubber production (Programa de Incentivo à Produção de Borracha Vegetal—PROBOR) was conducted by the Brazilian government to increase national self-sufficiency, and although not successful, revealed that rubber trees could be grown in some areas of Brazil (mainly in some parts of São Paulo State) without being affected by SALB (Furtado et al. 2015). These “escape zones” are colder and

experience an annual dry period that coincides with the refoliation period of the rubber trees (Rivano et al. 2015).

The 'disease triangle + time' conceptual model in plant pathology (Francl 2001; Agrios 2005) describes disease emergence as the result of the convergence of a susceptible host and a pathogen under favorable environmental conditions over a sufficient period of time. The absence of any of those elements would restrain disease development. Humidity, temperature, and light conditions have been reported to play a role in creating the conditions for SALB infection by influencing release, viability, and germination of spores and facilitating penetration of host tissues (Langford 1945; Holliday 1969; Chee 1976a; Gasparotto and Junqueira 1994; Evans 2002; Guyot et al. 2010, 2014). Among them, long lasting humid conditions leading to several hours of continuous "leaf wetness" is the point on which consensus among old and new literature exists.

Mature rubber trees go through an annual defoliation and refoliation cycle as opposed to seedlings, which within the first four to five years produce multiple leaf flushes throughout the growing season. Young rubber leaves are susceptible to SALB until up to three weeks after bud-break (Marattukalam and Saraswathyamma 1992; Lieberei 2007; Priyadarshan 2011) when they reach their physiological and structural maturity (Garcia et al. 1995; Fang et al. 2016).

A few studies based in geographic information systems (GIS) exist that focus on mapping SALB "escape zones", but on a relatively small scale (de Camargo et al. 2003; Silva et al. 2013; Rivano et al. 2015; Jaimes et al. 2016). Roy et al. (2017) expanded the covered geographical evaluation span to a global scale and took the effects of different phenological behavior of mature and immature trees into consideration. However, the limitation in this study is the time steps, which are monthly, and considering the pace at which the refoliation process and SALB infection evolve, lacks the requisite detail. The annual and monthly variables and their corresponding thresholds used in comparable studies are practically used as proxies attempting to capture the effects of the underlying daily variations. However, thanks to improved access to spatiotemporal historical data with finer temporal granulation (see Section 4.2.1) and an increase in computational power, the use of such proxies is more and more avoidable. Extraction of trends from weather records should account for and present the inherent uncertainties for highly dynamic variables, such as precipitation.

In this study, we applied emerging hot spot analysis, which is based on the Getis-Ord Gi* statistic (Getis and Ord 1992; Ord and Getis 1995), to three decades of gridded daily precipitation

and surface relative humidity data in order to reveal temporal (in daily steps over the yearly cycle) and geographical patterns that link weather conditions to the likelihood of SALB emergence.

4.2 Data and Methods

4.2.1 Data

We used the CPC (Climate Prediction Center) global unified gauge-based analysis of daily precipitation data (CPC 2018) and the NCEP (National Center for Environmental Prediction) global reanalysis daily surface relative humidity data (NCEP 2018), which are both available at the website of the Physical Sciences Division of the Earth System Research Laboratory under the Office of Oceanic and Atmospheric Research—National Oceanic and Atmospheric Administration (NOAA/OAR/ESRL PSD). These two data sources have been evaluated and used for long-term trend analysis of humidity and precipitation with reasonable results in different parts of the world (Dessler and Davis 2010; You et al. 2015; Ashouri et al. 2015; Cui et al. 2017; Villamil-Otero et al. 2018). The CPC precipitation data and the NCEP relative humidity data have spatial resolutions of 0.5 and 2.5 decimal degrees, respectively. We chose a 30-year period from 1988 to 2017 as the time frame for our input data. Based on the global climatic suitability map for rubber cultivation (Figure 4.1), we limited the geographical coverage of this study to the 30° north and south latitudes in which 0.5 decimal degrees range from about 55.6 km at the equator to 47.3 km at 30°.

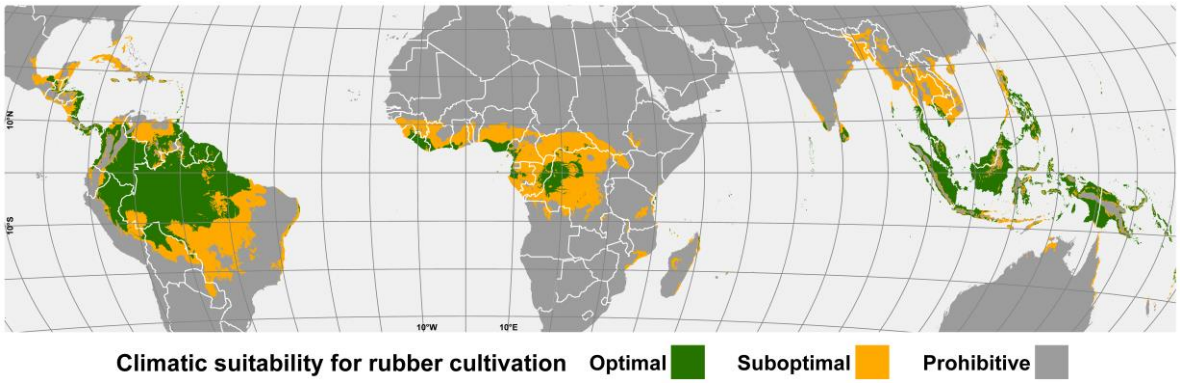

Figure 4.1 Global distribution of climatic suitability for rubber cultivation.
This map is based on four temperature and precipitation criteria: annual mean temperature, intra-annual temperature distribution, annual precipitation, and intra-annual precipitation distribution Rivano et al. (2015) applied to Worldclim V2 (Fick and Hijmans 2017) gridded climatic data. The process for generation of this map is described in detail in Golbon et al. (2018).

4.2.2 Methods

Our aim here is to explore the spatiotemporal patterns for high relative humidity and rainfall, which, when combined, represent the long-lasting hours of leaf wetness, facilitating SALB

establishment. Daily precipitation and relative humidity records in the continuous form were extracted from the NetCDF (Network Common Data Form) files. Surface relative humidity layers were resampled to match the spatial resolution of the precipitation data. Using conditional expressions applying thresholds of 1 mm for precipitation (representing precipitation incidence regardless of the quantity) and 90% for relative humidity (standing for close to saturation air humidity) (Roy et al. 2017), we converted the continuous data to binary layers (0 for values lower than the threshold and 1 for otherwise). These binary raster files were converted to point shapefiles. The points corresponding to waterbodies and areas with latitudes beyond 30° N and 30° S were eliminated. We added a new date-type field to the attribute table of each point shapefile and populated it with the corresponding date value. Point shapefiles affiliated with each day of the year (e.g., all the 30 files related to Jan 01 from 1988 to 2017) were merged, and the resulting shapefile was projected using the Hammer–Aitoff projection, which is metric and global. The Emerging Hot Spot Analysis (EHSA) tool of ArcGIS does not process the usual raster and vector inputs directly. Point shapefiles containing the temporal information (described above) need to be aggregated into NetCDF data structures called space-time cubes, which in addition to the coordinates, stores the time dimension information. This three-dimensional data structure has spatial units (bins) that can be in the form of either squares or hexagons. The projected point shapefiles were used to create space-time cubes containing the temporal and spatial information on events of precipitation and high surface relative humidity. We chose the hexagonal form for the space-time bins and, based on the resolution of the precipitation data (see Section 4.2.1), fixed the neighborhood distance (the height of the hexagons) to 90 km. The space-time cubes were used as input for the EHSA.

EHSA uses the Getis-Ord Gi* statistic (Getis and Ord 1992; Ord and Getis 1995) to evaluate the spatiotemporal patterns of occurrence/absence of an event of interest (precipitation and high relative humidity in the current case), verifying them versus the probability of the observations being outcomes of random processes (Getis and Ord 1992; Nelson and Boots 2008; Harris et al. 2017). EHSA returns three possible main categories for each space-time bin: cold spot, hot spot, or no pattern. In the context of this study, area units (hexagons) defined as hot spots are rendered to be associated with conditions favorable to the pathogen activity (incidence of rainfall or high relative humidity) as opposed to cold spots, for which the investigated criterion was detected not to be within the favorable range for the pathogen. The ‘no pattern’ category allows for the indeterminate conditions in which the data at hand supports neither a hot nor a cold spot category. The cold and hot spots were each divided into eight subcategories differing in their observed temporal stability and if applicable, the shifting direction detected for them

over time. However, for the purposes of this study, we focused on the hot and cold spots with significant trends (Mann-Kendall trend test z-scores with p-values smaller than 0.05) regardless of their subcategories in the subsequent steps and referred to them with acronyms “HS” (hot spot) and “CS” (cold spot), respectively. We handled the areas for which no pattern was detected and those with statistically nonsignificant trends equally and labeled them with “NS” (no pattern/nonsignificant trend). The EHSA output attributes were simplified from the original 17 possible outcomes to these three simplified categories. In order to homogenize the day by day changes in the geographical delineation of the HS/CS/NS hexagons, we extracted the majority outcome for each hexagon over a moving seven-day time window centered on the target day of the year (e.g., 28 Dec to 04 Jan for 01 Jan).

The day-to-day maps for both relative humidity and precipitation were date-tagged, laid out and exported as image files. We used Blender 2.79 to render an animated map with these 365 frames to be played as a 15 second long video. We further simplified the dynamic map in two steps. First, by adding a new field to the attribute table of each shapefile and merging the HS/CS/NS information of both criteria from which six possible classes ensued (HS + HS, HS + NS, NS + NS, CS + NS, CS + CS, and HS + CS). Finally, we added another field to the attribute tables and populated them with two possible classes: hexagons for which at least one of the two criteria was a significant cold spot (=1) and otherwise (=0) as the alternative. Finally, the resulting binary values for each hexagon were summed up over the whole year and for the refoliation periods to produce two static summary maps. In order to secure the coverage of the refoliation periods, we applied the time window of Feb–Apr for the Northern Hemisphere and Aug–Oct for the Southern Hemisphere. We have also created keyhole markup language zipped (KMZ) files corresponding to all of the daily maps from which the three mentioned videos were produced.

4.3 Results

The key outputs of this study are the daily spatial classifications presented as three animated maps (Videos A4.1 to A4.3), which require some direct engagement by the users (navigating through the time frames for an area of interest) to reveal the desired information. Video A4.1 presents the detected trends for both relative humidity and precipitation, while Video A4.2 simplifies that content by reflecting only the six possible class combinations regardless of their origin (i.e., which class belongs to which criterion). Video A4.3 focuses on the significant cold spots and combines the hot spots with the no pattern/not significant class. Although further compression of the outputs into single frame maps summarizing the patterns occurring over

longer time periods may seem to be in conflict (by forcing potentially arbitrary time frames and risking overgeneralization) with the goals of such a study, it is prudent to describe the extremes observed over the complete year cycle and the approximate leaf flushing period (Figure 4.2). Areas for which no significant cold spots (for neither of the two criteria) were detected across the yearly cycle were confined to the Asian and American tropics between 9° N and 8° S (Figure 4.2a). The other extreme outcome—the entire yearly cycle covered by a significant cold spot for at least one of the two criteria—was mostly returned for Asian, Pacific, and Caribbean islands and peninsular relatively narrow land strips.

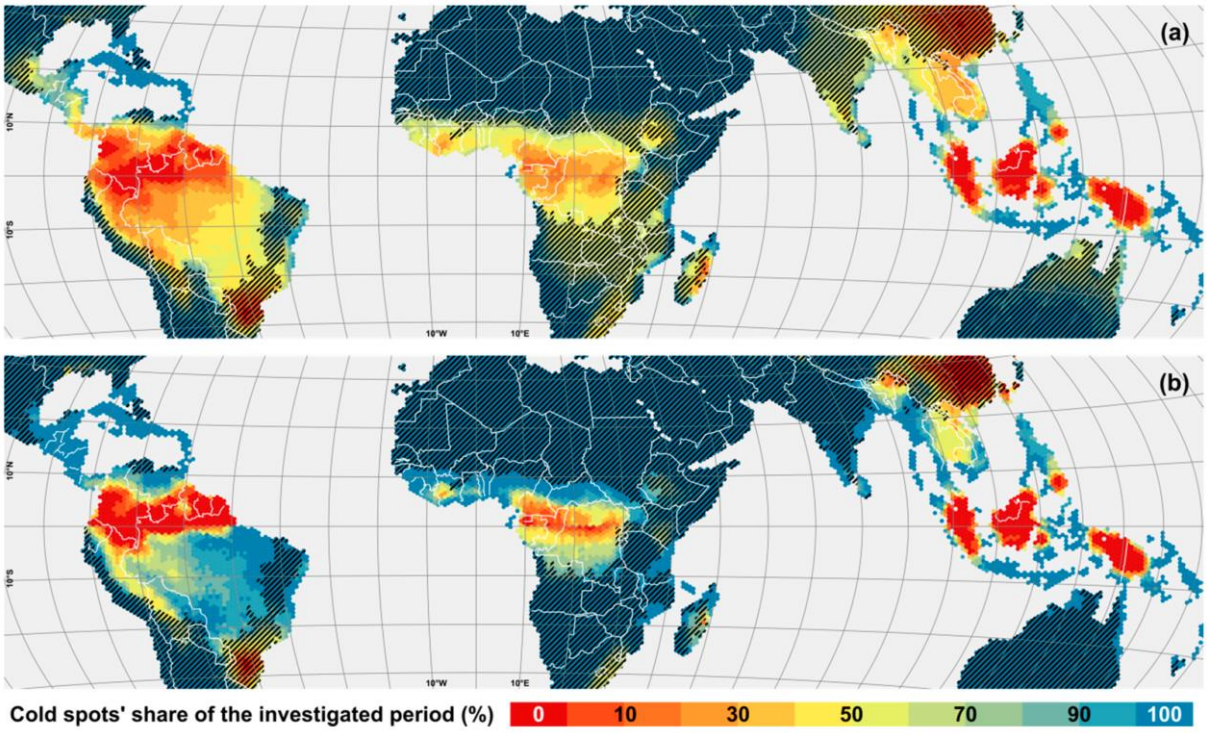

Figure 4.2 Summary maps of the cold spot occurrence
Days for which at least one of the two criteria considered in this study was detected to be a significant cold spot from the complete year cycle (a) and the approximate refoliation period (b) (Feb–Apr for the Northern Hemisphere and Aug–Oct in the Southern Hemisphere) are reflected in a proportional form. In this figure, similar to Video A4.3, we have pooled hot spots and the uncertain areas distinguishing them from cold spots which form an 'unsafe/uncertain' vs. 'safe' dichotomy. Therefore, 0% cold spot means 100% hot spot/uncertain. The non-hatched area reflects the zones climatically conducive to rubber cultivation (for more details see Figure 4.1)

Limiting the time window of interest to the approximate refoliation period for mature trees (Figure 4.2b), we found an increase in the area for which no significant cold spots were detected in the American tropics from the equator to the 8° N latitude. Within the same temporal frame, this pattern emerged around the African equatorial line from longitudes 8° E to 20° E. The outcome for the aforementioned insular and peninsular areas was very similar to findings on the annual cycle. In addition to what was indicated for the year-round summary, the following areas were found to be characterized throughout the refoliation period by at least one of the two criteria as a significant cold spot: in Asia, coastlines of the two Indian states of Kerala and Karnataka (8°

N to 14° N) and the eastern Indian coasts from 11° N to 13° N and 18° N to 21° N; in Africa, the area enclosed within 11° N, 15° W and 31° E, 4° N and at the eastern African coastlines from 5° S to 8° S (Tanzania) and 17–18° S (Mozambique); and in South America, northern Venezuela, Brazilian coastline from 6° S to 18° S and 42° W to 50° W stretching deep into Maranhão and Pará states and a large cluster in the southern parts of Mato Grosso state. In general, the share of the two extremes (all days vs. no days associated with a significant cold spot) from the total area climatically conducive to rubber cultivation is larger for the refoliation period than the annual cycle, reflected by the higher contrasts in panel b than a of Figure 4.2 and the transition from potential risk zones to safe zones occurs in shorter distances.

4.4 Discussion

The climatic risk analysis of SALB by Roy et al. (2017) is the only publication comparable to this study in regards to the time dimension during data processing and inference, the similarities in the covered geographical span, and the similarly rough spatial resolution of the input data. That study diverges from this work in three major points: exclusion of temperature variables from analysis, data processing method (EHSA vs. rule-based classification), and the level of temporal granulation (daily vs. monthly time slices). The temperature ranges reported in scientific literature for *P. ulei* (Holliday 1970; Chee 1976b; Liyanage and Jacob 1992) focus mainly on the optimal conditions for the pathogen, which cannot be used as impeding thresholds. Moreover, low temperature appears not to be a limiting factor for *P. ulei* within the geographical range that is climatically suitable/bearable for *H. brasiliensis* (Langford 1945). Figure A4.1 in the Appendix demonstrates how the spatial limits set by relative humidity and precipitation are completely nested within the space outlined by the temperature limits. Therefore, temperature turns to a superfluous criterion. There are precedents for the temporary loss of immunity to SALB in some established Brazilian 'escape zones' due to unusually humid weather conditions (Furtado et al. 2015), but cases relating to temperature anomalies have not been reported.

We chose to use EHSA, which not only accommodates temporal trends but also can allow for uncertainties and avoid potentially overgeneralized inferences based on vague dichotomies. Technical barriers, such as insufficient access to data and computational power, which are often the reasons for resorting to using proxy variables, are being progressively alleviated thanks to recent advances.

As opposed to small-scale and local studies, investigations with global coverage help provide a bigger picture. This broad overview comes at the cost of the potential loss of details compared to the reality, such as missed smaller but not necessarily insignificant pockets of land with conditions

contrasting the dominant neighboring land use and shifts in some of the detected borderlines. The broad overview mentioned above is helpful in evaluating the plausibility of the findings and the performance consistency of the data and methods in a general glimpse and also as an informal cross-validation. For instance, persistent cold spots assigned to the Caribbean and small Asian islands (see Figure 4.1 and Videos A4.1 to A4.3 on page 96) are dubious considering the stagnation of the class attributed to them over the year cycle and in relation to the conditions reflected in their immediate vicinity. This situation is probably caused by spatial isolation (shortage of neighboring points) of the corresponding space-time bins.

Ideally, a map that encapsulates the trends for the approximate annual refoliation period should restrict the summarized values assigned to each grid cell to the dates specifically relevant for the corresponding location. The surprisingly scarce and to some extent speculative literature that exists in regards to the processes and triggers of the phenological behavior of Para rubber (de Lemos Filho et al. 1993, 1997; Yeang 2007) does not aggregate to a solid base to link refoliation to the geography through the natural annual cycles. As an alternative, metadata gathered from studies that report both refoliation dates and the corresponding geographical coordinates from different locations should serve as an alternative for producing a time map for refoliation. The existing literature which report both refoliation dates and coordinates (Whaley 1948; Montény et al. 1985; Ortolani et al. 1998; Priyadarshan et al. 2001; Omokhafe 2004; Fernando et al. 2012; Liu et al. 2014; Maeght et al. 2015; Zhai et al. 2017; Liyanage et al. 2018) are not abundant enough and the indicated refoliation dates are often formulated in too much a loose range to be applicable to our purpose. As a result, the map which summarizes the situation over the refoliation period (Figure 4.2b) inevitably suffers from overgeneralization of the time frame. Nevertheless, this problem is tackled using the dynamic maps (Videos A4.1 to A4.3 on page 96). This requires users to navigate through the dates (video frames) of interest for a given area. A media player that permits the frame by frame viewing of the video should be used for that purpose. We suggest GOM media player (available at www.gomlab.com), which permits frame by frame navigation by pressing the 'f' key on the keyboard.

Roy et al. (2017) reported all mature trees in Indian rubber growing areas to be safe from SALB. Our findings support this assessment for the Western Ghats, where cold spots disappear in mid-May and reappear in November, and for the Odisha State where the low humidity period is even longer, stretching from October to June. However, the identified trends in the northeastern region of India are associated with considerable uncertainty. Moving further to the east, Roy et al. (2017) describe most of the rubber growing areas in China, Thailand, Cambodia, Laos, and Vietnam as low-risk, and parts of Philippines, Malaysia, and Indonesia as high-risk zones. We reached

comparable outcomes for these areas. For the continental parts of Southeast Asia, however, the time gap between the end of the refoliation period and the start of the humid season tends to be narrow. Roy et al. (2017) applied a blanket refoliation time window of February–March for their assessment of SALB risk for mature rubber trees in Africa. In areas south of the equator, this is not consistent with their refoliation rule of thumb, March–May for the Northern Hemisphere and September–November for the Southern Hemisphere. With using the dual time window, our findings suggest that the conditions during the refoliation season over large areas north of 5° N from Guinea to the Central African Republic and east of 30° E from Mozambique to Kenya (Figure 4.2b) tend to not support leaf wetness.

The thresholds applied in this study represent conditions leading to long hours of leaf wetness through the coincidence of rainfall and high relative humidity. However, other conditions causing leaf wetness (e.g. dew in place of rainfall) are also possible. Despite the fact that by the three levels of simplification applied to the dynamic maps some flexibility for more stringent examination of the outputs has been preserved, the thresholds applied to the raw data are fixed.

For studies relating to subjects concerning alien species, such as this one, the following seven measures suggested by Groom et al. (2017) should be followed: (1) creation of data management plans, (2) increasing interoperability of information sources, (3) documentation of data through metadata, (4) formatting data using existing standards, (5) adoption of controlled vocabularies, (6) increasing data availability, and (7) ensuring long-term data preservation. We have achieved points (2) and (4) by providing the KMZ outputs of our study to the public, and points (3), (5), (6), and (7) by archiving these files on zenodo.org (https://doi.org/10.5281/zenodo.2576857) data repository. These KMZ files can be used by any interested party regardless of their expertise, examined by individuals of no familiarity with geographic information systems (dragging and dropping in GoogleEarth™), or exploited by GIS-savvy researchers for further developments.

4.5 Conclusions

Incorporation of daily time steps in the risk evaluation is a tedious process but achievable. The uncertainties rising from the natural overtime variabilities in observations can be accounted for using EHSA. For rubber trees past their multiple-leaf-flush life stage, several areas safe from SALB (regarding the leaf wetness during the refoliation period) appear to exist in the areas outside of the 10° equatorial belt.

Funding

The authors appreciate the support provided by the German Federal Ministry of Education and Research which made this study possible through the LILAC and SURUMER projects (grant numbers FKZ 0330797A and FKZ 01 LL 0919 as well as post-grant open access funding 16PGF0104) and also the Deutsche Forschungsgemeinschaft supporting this work via project number 404870679.

Acknowledgments:

We also thank the National Oceanic and Atmospheric Administration of the United States for the raw data provision. We are grateful to Kristian Johnson for English editing of this paper and the anonymous reviewers for their constructive comments which helped us improve our initial manuscript.

5 General discussion

This thesis is devoted to three aspects of rubber cultivation in regions of the world which are considered suboptimal for rubber cultivation due to climatic characteristics different from the origin of Para rubber tree. Yield modeling for rubber based on meteorological conditions was pursued in the first study (Chapter 2). Meteorological covariates most influential in predicting rubber yield were identified, the optimal lead periods that capture the lagged effects for the predictor covariates were determined, serial autocorrelation in the input time series data was corrected, and a model was constructed and validated. Potential spatial shifts in rubber cultivation under the influence of climate change in continental Southeast Asia were investigated in the second study (Chapter 3) using an ensemble set of climate projections for the approaching five decades. Exposure of rubber trees to potentially excessive heat levels and also uncertainties inherent in the disagreements among the ensemble members were presented. In order to convey these contents efficiently to all readers regardless of their academic background, innovative methods were developed for both spatial data processing and output illustration. Finally, in Chapter 3, the climate-driven susceptibility to South American Leaf Blight of rubber was investigated on a global scale using 30 years of gridded precipitation and surface relative humidity data with daily temporal granulation. As each of the above mentioned chapters is a complete and independent work containing a dedicated discussions subsection, the rest of this general discussion will focus only on the common thread running through Chapters 2-4 and their collective implications while taking the relevant literature into consideration.

Humankind modifies ecosystems in order to harvest higher levels of provisioning services and boost the economic gains. However, short-sighted and inadequately informed decisions which do not take the true capacities and tolerance limits of ecosystems into account, endanger and destroy the resilience of ecosystems. Various computer models have been developed in recent years (see Christin et al. 2016; Dunford et al. 2017; Grêt-Regamey et al. 2017) that try to represent natural and man-made conditions and processes in a simplified and workable manner, facilitating the exploration of competing scenarios. This is in order to detect or develop plans which, in the ideal case, when implemented, result in a balanced and resilient system, redressing potential underperformance in gains from provisional ecosystem services or, at the other side of the spectrum, mitigate the negative effects of overexploitation through implementation of well-chosen tradeoffs among different ecosystem services in land management.

Ecosystem service assessment models require parameterization and therefore depend on statistical models that capture and quantify relationships between variables relevant for them.

Chapter 2 takes part in this domain by providing a validated instrument of rubber yield estimation in connection with climatic settings in high altitudes and latitudes of mainland Southeast Asia. The modeling method used in Chapter 2 (e.g. correction for autocorrelation and inclusion of random effects) yield robust models which compared with modeling methods missing these measures are more generalizable and less likely to produce widely outlying estimates once tried in circumstances varying from its training dataset. Yet, further spatiotemporal broadening of the input data (i.e. time series data collected over longer time periods from a broad range of locations) would add to this robustness. Applying the same methods in a standardized way to non-monoculture rubber growing alternatives in order to model their performance, is essential to the validity of the comparisons.

Finding the applicability thresholds for each variable space and spatiotemporal frame within which inferences are valid is also a crucial prerequisite for putting models to practice (Václavík et al. 2016). A direct connection between Chapters 2 and 3 is their complementary role respecting the similarity between areas projected to become climatically conducive to rubber cultivation by 2030 (Figure 3.9, clusters 2 and 3), with the site conditions from which the yield prediction model (Chapter 2) was constructed and validated. It means that the yield predicting statistical model is a good candidate for evaluation of the revenues which are to be expected from rubber cultivation in these areas. Yet, as it is acknowledged in subsection 3.4.1, non-climatic factors influencing the suitability of a location for rubber cultivation also need to be considered.

Besides climate change, further developments in genomics and breeding (Cheng et al. 2015, 2018; Deng et al. 2017; Nóia Júnior et al. 2018; Chen et al. 2019) are expected to contribute to the expansion of the geographical extent conducive to rubber cultivation by higher cold tolerance. Following this parallel, Figure 3.9 can be used to look for directions and approximate areas which may become host to prospective more cold-resistant genotypes.

By overlaying the delineations of the emerging cultivable areas with the current land use composition (Figure A 3.1) and the associated biodiversity losses (Figure A 3.2), any given location will be recognizable somewhere on a spectrum ranging from pristine to heavily degraded. Rubber plantations in their currently widespread form (monocultures) are rated to be ecologically inferior to forest but preferable to arable land use (Blagodatsky et al. 2016; Cotter et al. 2017). It would mean that in heavily degraded areas (e.g. cluster 1 in Figure 3.10) rubber cultivation, even in the conventional monoculture form, may lead to a more balanced relationship between ecosystem services. Conversely, conversion of ecologically pristine areas (e.g. clusters 2 and 3 in Figure 3.10) replaces a natural equilibrium with a man-made system which, when not composed carefully of appropriate components into a proper spatial configuration, will be imbalanced and

in the long run counterproductive (Liu and Slik 2014). Effects of the spatial configuration of manipulated ecosystems are still under vigorous debate (see Fletcher et al. 2018 and Fahrig et al. 2019). Tarigan et al. (2018) found that a minimum of 30% forest cover is needed for sustainable water flow regulation of a watershed in areas subject to cultivation of natural rubber and oil palm. After finding a 'common denominator' value for the share of undisturbed original land use (which would be in most cases related to our topic, forest) from the total area to satisfy the necessary balance between all ecosystem services, the challenge of selection of the best spatial configuration of land use mosaics and landscape matrix needs to be settled.

Tables 3.2 and 3.3 reflect the level of similarity between ensemble members and the ensemble itself. This ex post evaluation of similarities can be used as a basis in comparable studies to further reduce the number of ensemble members especially when limited time and high computational costs (low processing power) impose a compromise.

The validity of the inferences made on the potential geographical shifts due to climate change in the areas suitable for rubber cultivation (Chapter 3) are contingent upon the quality of the input ensemble members. Having used a set of projections which themselves are nominated by virtue of their high regional plausibility was a measure to minimize the risk of a biased outcome. Nevertheless, if the majority of the ensemble members happen to be biased to the same direction, use of multiple inputs will not mitigate the problem. Whether the ensemble set of climatic projections used here suffers from this problem will be clarified over time.

Other plant sources of natural rubber such as Russian dandelion *Taraxacum kok-saghyz* (van Beilen and Poirier 2007a, b; Kreuzberger et al. 2016; Ramirez-Cadavid et al. 2017; Panara et al. 2018), guayule *Parthenium argentatum* (van Beilen and Poirier 2007a, b; Rasutis et al. 2015; Soratana et al. 2017; Ilut et al. 2017; Kajiura et al. 2018; Bates and Cornish 2018; Stonebloom and Scheller 2019) and hardy rubber tree *Eucommia ulmoides* Oliver (Chen et al. 2012; Wang et al. 2016; Liu et al. 2018b) have received, specially recently, broad attention as potential alternatives for Para rubber. However, the struggle to overcome the inefficiency gap between them and *H. brasiliensis* has yet to come to a tangible success.

The '-omics' branches of biology have picked up the challenge of natural rubber biosynthesis using modified microorganisms (Steinbüchel 2003; Yang et al. 2012; Liu et al. 2018a; Men et al. 2019) and also its in vitro production (Yamashita et al. 2016). If these efforts lead to a breakthrough, the subsequent developments may turn the tables on the natural rubber business in a fashion that would be, to a degree, reminiscent of the paradigm shift which followed the discovery of Haber's process (generating ammonia from the atmospheric nitrogen).

The approach used in Chapter 4 is in essence spatiotemporal trend analysis applied to gridded time series to detect the annually recurring weather conditions which permit the outbreak of South American Leaf Blight (SALB), across the tropical and subtropical zones of the world. This chapter has contributed to a better understanding of SALB risk through three main technical improvements: use of a reasonably fine temporal granulation (daily time steps) for analysis, global coverage and permitting not just for 'risky' and 'safe' classes but also an 'uncertain' category for spatially explicit risk assessment. The findings of this chapter suggest much of the areas dubbed climatically suboptimal for rubber cultivation, to be unfavorable for SALB development within the susceptible annual refoliation period.

It is important to make findings and outputs of scientific studies truly accessible and open to future development. In cases involving spatial data analysis, if outputs are presented only in form of conventional maps with resolution imposed by the limited capacities of paper and ink, the potential for further development will reach a dead-end and important details will be lost. Fortunately, we are no more limited to paper and ink to deliver the outputs of spatial studies. Advanced but easy-to-use means such as KMZ files (see Chapters 3 and 4) make it possible to retain and deliver the spatial resolution of the original data to the end user. Depending on their needs and skills, users may benefit from these files as simple, but free of resolution loss maps or in case of more advanced users, they may further process the maps for their purposes.

The gridded time series used in Chapter 4 continue to grow by time. A cloud-based GIS application capable of streamlined processing of the up-to-date data which also permits its users to modify the applied thresholds deserves to exist. This would make the maps updateable and the methods accessible not only to similar spatial assessments for other crops but also to a wide range of topics concerning climate-driven stresses sources for different living beings.

References

Abd Karim Y (2008) Static modelling approaches to predict growth (girth) of *Hevea brasiliensis* as tools for extension activities in Malaysia. J Rubber Res 11:171–186

Abdullah AR (1995) Environmental pollution in Malaysia: trends and prospects. TrAC Trends Anal Chem 14:191–198. doi: 10.1016/0165-9936(95)91369-4

Agrios GN (2005) Plant pathology, 5th ed. Elsevier Academic Press, Amsterdam ; Boston

Ahrends A, Hollingsworth PM, Ziegler AD, et al (2015) Current trends of rubber plantation expansion may threaten biodiversity and livelihoods. Glob Environ Change 34:48–58. doi: 10.1016/j.gloenvcha.2015.06.002

Akaike H (1973) Information theory and an extension of the maximum likelihood principle. In: Petrov BN, Csaki F (eds) 2nd international symposium on information theory. Akademia Kiado, Budapest, pp 267–281

Alam B, Nair DB, Jacob J (2005) Low temperature stress modifies the photochemical efficiency of a tropical tree species Hevea brasiliensis: effects of varying concentration of CO2 and photon flux density. Photosynthetica 43:247–252. doi: 10.1007/s11099-005-0040-z

Andriesse E, Tanwattana P (2018) Coping with the End of the Commodities Boom: Rubber Smallholders in Southern Thailand Oscillating Between Near-poverty and Middle-class Status. J Dev Soc 26

Araújo AV, Partelli FL, Oliosi G, Pezzopane JRM (2016) Microclimate, development and productivity of robusta coffee shaded by rubber trees and at full sun. Rev Ciênc AGRONÔMICA 47:. doi: 10.5935/1806-6690.20160084

Ashouri H, Sorooshian S, Hsu K-L, et al (2015) Evaluation of NASA's MERRA Precipitation Product in Reproducing the Observed Trend and Distribution of Extreme Precipitation Events in the United States. J Hydrometeorol 17:693–711. doi: 10.1175/JHM-D-15-0097.1

Asna BO, Ho HL (2005) Managing Invasive Species: the Threat to Oil-palm and Rubber - the Malaysian Plant Quarantine Regulatory Perspective. In: The unwelcome guests - Proceedings of the Asia-Pacific Forest Invasive Species Conference. FAO, Kunming, China, pp 32–38

Baird IG, Noseworthy W, Tuyen NP, et al (2019) Land grabs and labour: Vietnamese workers on rubber plantations in southern Laos. Singap J Trop Geogr 40:50–70. doi: 10.1111/sjtg.12261

Barrès B, Carlier J, Seguin M, et al (2012) Understanding the recent colonization history of a plant pathogenic fungus using population genetic tools and Approximate Bayesian Computation. Heredity 109:269–279. doi: 10.1038/hdy.2012.37

Bates GM, Cornish K (2018) Rapid and complete removal of guayule (Parthenium argentatum) leaves by cryodefoliation, and freeze and thaw induction of rubber particle coagulation. Ind Crops Prod 125:491–495. doi: 10.1016/j.indcrop.2018.09.041

Beckschäfer P (2017) Obtaining rubber plantation age information from very dense Landsat TM & ETM + time series data and pixel-based image compositing. Remote Sens Environ 196:89–100. doi: 10.1016/j.rse.2017.04.003

Behera RN, Nayak DK, Andersen P, Måren IE (2016) From jhum to broom: Agricultural land-use change and food security implications on the Meghalaya Plateau, India. Ambio 45:63–77. doi: 10.1007/s13280-015-0691-3

Bentsen M, Bethke I, Debernard JB, et al (2013) The Norwegian Earth System Model, NorESM1-M – Part 1: Description and basic evaluation of the physical climate. GeosciModel Dev 6:687–720. doi: 10.5194/gmd-6-687-2013

Berger A, Yin Q, Nifenecker H, Poitou J (2017) Slowdown of global surface air temperature increase and acceleration of ice melting. Earths Future 5:811–822. doi: 10.1002/2017EF000554

Besse P, Seguin M, Lebrun P, et al (1994) Genetic diversity among wild and cultivated populations of *Hevea brasiliensis* assessed by nuclear RFLP analysis. Theor Appl Genet 88:. doi: 10.1007/BF00225898

Bestion E, Teyssier A, Richard M, et al (2015) Live Fast, Die Young: Experimental Evidence of Population Extinction Risk due to Climate Change. PLOS Biol 13:e1002281. doi: 10.1371/journal.pbio.1002281

Bi D, Dix M, Marsland SJ, et al (2013) The ACCESS coupled model: Description, control climate and evaluation. Aust Meteorol Oceanogr J 63:41–64

Blagodatsky S, Xu J, Cadisch G (2016) Carbon balance of rubber (Hevea brasiliensis) plantations: A review of uncertainties at plot, landscape and production level. Agric Ecosyst Environ 221:8–19. doi: 10.1016/j.agee.2016.01.025

Bostock M, Ogievetsky V, Heer J (2011) D3: data-driven documents. IEEE Trans Vis Comput Graph 17:2301–2309. doi: 10.1109/TVCG.2011.185

Bristow KL, Campbell GS (1984) On the relationship between incoming solar radiation and daily maximum and minimum temperature. Agric For Meteorol 31:159–166. doi: 10.1016/0168-1923(84)90017-0

Broughton WJ (1976) Effect of various covers on soil fertility under Hevea brasiliensis muell. arg. and on growth of the tree. Agro-Ecosyst 3:147–170. doi: 10.1016/0304-3746(76)90113-X

Burnham KP, Anderson DR (2002) Model selection and multimodel inference: a practical information-theoretical approach, 2nd edn. Springer, New York

Capellán-Pérez I, Arto I, Polanco-Martínez JM, et al (2016) Likelihood of climate change pathways under uncertainty on fossil fuel resource availability. Energy Environ Sci 9:2482–2496. doi: 10.1039/c6ee01008c

Carr MKV (2012) The water relations of rubber (*Hevea brasiliensis*): A review. Exp Agric 48:176–193. doi: 10.1017/S0014479711000901

CCCMC (2017) Guidelines for Sustainable Development of Natural Rubber. In: Chin. Chamb. Commer. Met. Miner. Chem. Import. http://www.cccmc.org.cn/docs/2017-11/20171107204714430892.pdf. Accessed 10 Jan 2019

Chairungsee N, Gay F, Thaler P, et al (2013) Impact of tapping and soil water status on fine root dynamics in a rubber tree plantation in Thailand. Front Plant Sci 4:. doi: 10.3389/fpls.2013.00538

Chakraborty K, Sudhakar S, Sarma KK, et al (2018) Recognizing the Rapid Expansion of Rubber Plantation – A Threat to Native Forest in Parts of Northeast India. Curr Sci 114:207. doi: 10.18520/cs/v114/i01/207-213

Chee KH (1976a) Factors affecting discharge, germination and viability of spores of *Microcyclus ulei*. Trans Br Mycol Soc 66:499–504

Chee KH (1976b) Factors affecting discharge, germination and viability of spores of *Microcyclus ulei*. Trans Br Mycol Soc 66:499–504

Chen B, Li X, Xiao X, et al (2016a) Mapping tropical forests and deciduous rubber plantations in Hainan Island, China by integrating PALSAR 25-m and multi-temporal Landsat images. Int J Appl Earth Obs Geoinformation 50:117–130. doi: 10.1016/j.jag.2016.03.011

Chen H, Yi Z-F, Schmidt-Vogt D, et al (2016b) Pushing the limits: The pattern and dynamics of rubber monoculture expansion in Xishuangbanna, SW China. PLoS ONE 11:. doi: 10.1371/journal.pone.0150062

Chen R, Harada Y, Bamba T, et al (2012) Overexpression of an isopentenyl diphosphate isomerase gene to enhance trans-polyisoprene production in Eucommia ulmoides Oliver. BMC Biotechnol 12:78. doi: 10.1186/1472-6750-12-78

Chen W-J, Wang X, Yan S, et al (2019) The ICE-like transcription factor HbICE2 is involved in jasmonate-regulated cold tolerance in the rubber tree (Hevea brasiliensis). Plant Cell Rep. doi: 10.1007/s00299-019-02398-x

Cheng H, Cai H, Fu H, et al (2015) Functional Characterization of Hevea brasiliensis CRT/DRE Binding Factor 1 Gene Revealed Regulation Potential in the CBF Pathway of Tropical Perennial Tree. PLOS ONE 10:e0137634. doi: 10.1371/journal.pone.0137634

Cheng H, Chen X, Fang J, et al (2018) Comparative transcriptome analysis reveals an early gene expression profile that contributes to cold resistance in Hevea brasiliensis (the Para rubber tree). Tree Physiol 38:1409–1423. doi: 10.1093/treephys/tpy014

Christin ZL, Bagstad KJ, Verdone MA (2016) A decision framework for identifying models to estimate forest ecosystem services gains from restoration. For Ecosyst 3:. doi: 10.1186/s40663-016-0062-y

Clément-Demange A, Priyadarshan PM, Thuy Hoa TT, Venkatachalam P (2007) *Hevea* Rubber Breeding and Genetics. In: Janick J (ed) Plant Breeding Reviews. John Wiley & Sons, Inc., Hoboken, NJ, USA, pp 177–283

Clermont-Dauphin C, Dissataporn C, Suvannang N, et al (2018) Intercrops improve the drought resistance of young rubber trees. Agron Sustain Dev 38:56. doi: 10.1007/s13593-018-0537-z

Clermont-Dauphin C, Suvannang N, Pongwichian P, et al (2016) Dinitrogen fixation by the legume cover crop Pueraria phaseoloides and transfer of fixed N to Hevea brasiliensis—Impact on tree growth and vulnerability to drought. Agric Ecosyst Environ 217:79–88. doi: 10.1016/j.agee.2015.11.002

Colbert AJ, Soden BJ, Kirtman BP (2015) The impact of natural and anthropogenic climate change on western North Pacific tropical cyclone tracks. J Clim 28:1806–1823. doi: 10.1175/JCLI-D-14-00100.1

Collins M, Knutti R, Arblaster J, et al (2013) Long-term climate change: projections, commitments and irreversibility. In: Stocker TF, Qin D, Plattner G-K, et al. (eds) Climate Change 2013: The Physical Science Basis. Contribution of Working Group I to the Fifth Assessment Report of the Intergovernmental Panel on Climate Change. Cambridge University Press, Cambridge, United Kingdom and New York, NY, USA, pp 1029–1136

Cook J, Oreskes N, Doran PT, et al (2016) Consensus on consensus: a synthesis of consensus estimates on human-caused global warming. Environ Res Lett 11:048002. doi: 10.1088/1748-9326/11/4/048002

Cornish K (2017) Alternative Natural Rubber Crops: Why Should We Care? Technol Innov 18:245–256. doi: 10.21300/18.4.2017.245

Cotter M, Häuser I, Harich FK, et al (2017) Biodiversity and ecosystem services−A case study for the assessment of multiple species and functional diversity levels in a cultural landscape. Ecol Indic 75:111–117. doi: 10.1016/j.ecolind.2016.11.038

CPC (2018) Global Unified Gauge-Based Analysis of Daily Precipitation. In: CPC Glob. Unified Gauge-Based Anal. Dly. Precip. https://www.esrl.noaa.gov/psd/data/gridded/data.cpc.globalprecip.html. Accessed 21 Aug 2018

Cuba N (2015) Research note: Sankey diagrams for visualizing land cover dynamics. Landsc Urban Plan 139:163–167. doi: 10.1016/j.landurbplan.2015.03.010

Cui W, Dong X, Xi B, Kennedy A (2017) Evaluation of Reanalyzed Precipitation Variability and Trends Using the Gridded Gauge-Based Analysis over the CONUS. J Hydrometeorol 18:2227–2248. doi: 10.1175/JHM-D-17-0029.1

de Blécourt M, Brumme R, Xu J, et al (2013) Soil Carbon Stocks Decrease following Conversion of Secondary Forests to Rubber (Hevea brasiliensis) Plantations. PLoS ONE 8:e69357. doi: 10.1371/journal.pone.0069357

de Camargo ÂP, Marin FR, de Camargo MBP (2003) Zoneamento Climático da Heveicultura no Brasil. Embrapa (Brazilian Agricultural Research Corporation), Campinas, São Paulo, Brazil

de Lemos Filho JP, Nova NAV, Pinto HS (1997) A model including photoperiod in degree days for estimating *Hevea* bud growth. Int J Biometeorol 41:1–4. doi: 10.1007/s004840050045

de Lemos Filho JP, Nova NAV, Pinto HS (1993) Base temperature and heat units for leaf flushing emission and growth of *Hevea brasiliensis* Muell. Arg. Int J Biometeorol 37:65–67

Deng XM, Wang JX, Li Y, et al (2017) Characterization of a cold responsive HbICE1 gene from rubber trees. Trees 31:137–147. doi: 10.1007/s00468-016-1463-9

Dessler AE, Davis SM (2010) Trends in tropospheric humidity from reanalysis systems. J Geophys Res Atmospheres 115:. doi: 10.1029/2010JD014192

Dix M, Vohralik P, Bi D, et al (2013) The ACCESS coupled model: Documentation of core CMIP5 simulations and initial results. Aust Meteorol Oceanogr J 63:83–99

Dlugokencky E (2017) Trends in atmospheric methane. In: Natl. Ocean. Atmospheric Adm. Earth Syst. Res. Lab. NOAAESRL Glob. Monit. Div. https://www.esrl.noaa.gov/gmd/ccgg/trends_ch4/. Accessed 13 Oct 2017

Dlugokencky E, Tans P (2017) Trends in atmospheric carbon dioxide. In: Natl. Ocean. Atmospheric Adm. Earth Syst. Res. Lab. NOAAESRL Glob. Monit. Div. https://www.esrl.noaa.gov/gmd/ccgg/trends/global.html. Accessed 13 Oct 2017

Dong J, Xiao X, Chen B, et al (2013) Mapping deciduous rubber plantations through integration of PALSAR and multi-temporal Landsat imagery. Remote Sens Environ 134:392–402. doi: 10.1016/j.rse.2013.03.014

Dong J, Xiao X, Sheldon S, et al (2012) Mapping tropical forests and rubber plantations in complex landscapes by integrating PALSAR and MODIS imagery. ISPRS J Photogramm Remote Sens 74:20–33. doi: 10.1016/j.isprsjprs.2012.07.004

Dong N, McMahan CM, Whalen MC, et al (2017) Transgenic guayule for enhanced isoprenoid production

Donner LJ, Wyman BL, Hemler RS, et al (2011) The dynamical core, physical parameterizations, and basic simulation characteristics of the atmospheric component AM3 of the GFDL global coupled model CM3. J Clim 24:3484–3519. doi: 10.1175/2011JCLI3955.1

Dufresne J-L, Foujols M-A, Denvil S, et al (2013) Climate change projections using the IPSL-CM5 Earth System Model: From CMIP3 to CMIP5. Clim Dyn 40:2123–2165. doi: 10.1007/s00382-012-1636-1

Dunford RW, Harrison PA, Bagstad KJ (2017) Computer modelling for ecosystem service assessment. In: Burkhard B, Maes J (eds) Mapping ecosystem services. Pensoft, Sofia, Bulgaria, pp 124–135

Evans HC (2002) Invasive neotropical pathogens of tree crops. In: Watling R, Frankland JC, Ainsworth AM, et al. (eds) Tropical mycology: Micromycetes. CABI Pub, Wallingford, Oxon, UK ; New York, pp 83–112

Fahrig L, Arroyo-Rodríguez V, Bennett JR, et al (2019) Is habitat fragmentation bad for biodiversity? Biol Conserv 230:179–186. doi: 10.1016/j.biocon.2018.12.026

Fan H, Fu X, Zhang Z, Wu Q (2015) Phenology-based vegetation index differencing for mapping of rubber plantations using landsat OLI data. Remote Sens 7:6041–6058. doi: 10.3390/rs70506041

Fang Y, Mei H, Zhou B, et al (2016) De novo Transcriptome Analysis Reveals Distinct Defense Mechanisms by Young and Mature Leaves of *Hevea brasiliensis* (Para Rubber Tree). Sci Rep 6:. doi: 10.1038/srep33151

FAOSTAT (2015) Food and Agriculture Organization of the United Nations. http://www.fao.org/faostat/en/#data/QC. Accessed 3 Feb 2015

FAOSTAT (2017) Food and Agriculture Organization of the United Nations. http://www.fao.org/faostat/en/#data/QC. Accessed 3 Sep 2017

FAOSTAT (2019) Food and Agriculture Organization of the United Nations. http://www.fao.org/faostat/en/#data/QC. Accessed 9 Jan 2019

Fernando THPS, Jayasinghe CK, Wijesundera RLC, Siriwardane D (2012) Some factors affecting in vitro production, germination and viability of conidia of *Corynespora cassiicola* from *Hevea brasiliensis*. J Natl Sci Found Sri Lanka 40:241. doi: 10.4038/jnsfsr.v40i3.4698

Fick SE, Hijmans RJ (2017) WorldClim 2: new 1-km spatial resolution climate surfaces for global land areas. Int J Climatol 37:4302–4315. doi: 10.1002/joc.5086

Fletcher RJ, Didham RK, Banks-Leite C, et al (2018) Is habitat fragmentation good for biodiversity? Biol Conserv 226:9–15. doi: 10.1016/j.biocon.2018.07.022

Fordham DA (2015) Mesocosms Reveal Ecological Surprises from Climate Change. PLOS Biol 13:e1002323. doi: 10.1371/journal.pbio.1002323

Fox J, Castella J-C (2013) Expansion of rubber (*Hevea brasiliensis*) in Mainland Southeast Asia: what are the prospects for smallholders? J Peasant Stud 40:155–170. doi: 10.1080/03066150.2012.750605

Fox J, Vogler JB, Sen OL, et al (2012) Simulating Land-Cover Change in Montane Mainland Southeast Asia. Environ Manage 49:968–979. doi: 10.1007/s00267-012-9828-3

Fox JM, Castella J-C, Ziegler AD, Westley SB (2014) Rubber Plantations Expand in Mountainous Southeast Asia: What Are the Consequences for the Environment? AsiaPacific Issues 1–8

Francl LJ (2001) The..Disease Triangle: A Plant Pathological Paradigm Revisited. Plant Health Instr. doi: 10.1094/PHI-T-2001-0517-01

Furtado EL, Cunha AR, Alvares CA, et al (2015) Ocorrência de epidemia do mal das folhas em regiões de "escape" do Brasil. Arq Inst Biológico 82:1–6. doi: 10.1590/1808-657000882013

Garcia D, Cazaux E, Rivano F, D'Auzac J (1995) Chemical and structural barriers to *Microcyclus ulei*, the agent of South American leaf blight, in *Hevea* spp. Eur J For Pathol 25:282–292. doi: 10.1111/j.1439-0329.1995.tb01013.x

Gasparotto L, Junqueira NTV (1994) Ecophysiological variability of *Microcyclus ulei*, causal agent of rubber tree leaf blight. Fitopatol Bras 19:22–28

Gent PR, Danabasoglu G, Donner LJ, et al (2011) The community climate system model version 4. J Clim 24:4973–4991. doi: 10.1175/2011JCLI4083.1

Getis A, Ord JK (1992) The Analysis of Spatial Association by Use of Distance Statistics. Geogr Anal 24:189–206. doi: 10.1111/j.1538-4632.1992.tb00261.x

Giorgetta MA, Jungclaus J, Reick CH, et al (2013) Climate and carbon cycle changes from 1850 to 2100 in MPI-ESM simulations for the Coupled Model Intercomparison Project phase 5. J Adv Model Earth Syst 5:572–597. doi: 10.1002/jame.20038

Global Witness (2013) Rubber barons: how Vietnamese companies and international financiers are driving a land grabbing crisis in Cambodia and Laos.

Golbon R, Cotter M, Sauerborn J (2018) Climate change impact assessment on the potential rubber cultivating area in the Greater Mekong Subregion. Environ Res Lett 13:084002. doi: 10.1088/1748-9326/aad1d1

Golbon R, Ogutu JO, Cotter M, Sauerborn J (2015) Rubber yield prediction by meteorological conditions using mixed models and multi-model inference techniques. Int J Biometeorol 59:1747–1759. doi: 10.1007/s00484-015-0983-0

Gonkhamdee S, Maeght J-L, Do F, Pierret A (2009) Growth dynamics of fine Hevea brasiliensis roots along a 4.5-m soil profile. Khon Kaen Agric J 37:265–276

Gouvêa LRL, Silva GAP, Verardi CK, et al (2013) Rubber tree early selection for yield stability in time and among locations. Euphytica 191:365–373. doi: 10.1007/s10681-013-0874-6

Grêt-Regamey A, Sirén E, Brunner SH, Weibel B (2017) Review of decision support tools to operationalize the ecosystem services concept. Ecosyst Serv 26:306–315. doi: 10.1016/j.ecoser.2016.10.012

Grogan K, Pflugmacher D, Hostert P, et al (2015) Cross-border forest disturbance and the role of natural rubber in mainland Southeast Asia using annual Landsat time series. Remote Sens Environ 169:438–453. doi: 10.1016/j.rse.2015.03.001

Grogan K, Pflugmacher D, Hostert P, et al (2019) Unravelling the link between global rubber price and tropical deforestation in Cambodia. Nat Plants 5:47. doi: 10.1038/s41477-018-0325-4

Groom QJ, Adriaens T, Desmet P, et al (2017) Seven Recommendations to Make Your Invasive Alien Species Data More Useful. Front Appl Math Stat 3:. doi: 10.3389/fams.2017.00013

Guardiola-Claramonte M, Troch PA, Ziegler AD, et al (2008) Local hydrologic effects of introducing non-native vegetation in a tropical catchment. Ecohydrology 1:13–22. doi: 10.1002/eco.3

Guardiola-Claramonte M, Troch PA, Ziegler AD, et al (2010) Hydrologic effects of the expansion of rubber (Hevea brasiliensis) in a tropical catchment. Ecohydrology 3:306–314. doi: 10.1002/eco.110

Gunasekera HKLK, Costa WAJMD, Nugawela A (2013) Canopy Photosynthetic Capacity and Light Response Parameters of Rubber (Hevea brasiliensis) with Reference to Exploitation. Curr Agric Res J 1:01–12

Guyot J, Condina V, Doaré F, et al (2014) Role of ascospores and conidia in the initiation and spread of South American leaf blight in a rubber tree plantation. Plant Pathol 63:510–518. doi: 10.1111/ppa.12126

Guyot J, Condina V, Doaré F, et al (2010) Segmentation applied to weather-disease relationships in South American leaf blight of the rubber tree. Eur J Plant Pathol 126:349–362. doi: 10.1007/s10658-009-9540-1

Guyot J, Le Guen V (2018) A Review of a Century of Studies on South American Leaf Blight of the Rubber Tree. Plant Dis 102:1052–1065. doi: 10.1094/PDIS-04-17-0592-FE

Hansen MC, Potapov PV, Moore R, et al (2013) High-Resolution Global Maps of 21st-Century Forest Cover Change. Science 342:850–853. doi: 10.1126/science.1244693

Hardanto A, Röll A, Hendrayanto, Hölscher D (2017) Tree soil water uptake and transpiration in mono-cultural and jungle rubber stands of Sumatra. For Ecol Manag 397:67–77. doi: 10.1016/j.foreco.2017.04.032

Haridas G (1985) Streamflow measurements in a small watershed to estimate evaporation from a stand of rubber. In: Proceedings of International Rubber Conference. Kuala Lumpur, Malaysia, pp 670–681

Harris NL, Goldman E, Gabris C, et al (2017) Using spatial statistics to identify emerging hot spots of forest loss. Environ Res Lett 12:024012. doi: 10.1088/1748-9326/aa5a2f

Hashim I (2012) South American Leaf Blight (*Microcyclus ulei*) of *Hevea* rubber. In: Protection against South American leaf blight of rubber in Asia and the Pacific region. FAO, Bangkok, Thailand, pp 21–133

Häuser I, Martin K, Germer J, et al (2015) Environmental and socio-economic impacts of rubber cultivation in the Mekong region: challenges for sustainable land use. CAB Rev Perspect Agric Vet Sci Nutr Nat Resour 10:. doi: 10.1079/PAVSNNR201510027

He P, Martin K (2015) Effects of rubber cultivation on biodiversity in the Mekong Region. CAB Rev 10:1–7. doi: 10.1079/PAVSNNR201510044

Hijmans RJ, Cameron SE, Parra JL, et al (2005) Very high resolution interpolated climate surfaces for global land areas. Int J Climatol 25:1965–1978. doi: 10.1002/joc.1276

Holliday P (1969) Dispersal of conidia of *Dothidella ulei* from *Hevea brasiliensis*. Ann Appl Biol 63:435–447. doi: 10.1111/j.1744-7348.1969.tb02840.x

Holliday P (1970) South American leaf blight (*Microcyclus ulei*) of *Hevea brasiliensis*. Phytopathol Pap

Hora Júnior BT da, de Macedo DM, Barreto RW, et al (2014) Erasing the Past: A New Identity for the Damoclean Pathogen Causing South American Leaf Blight of Rubber. PLoS ONE 9:e104750. doi: 10.1371/journal.pone.0104750

Hoskins AJ, Bush A, Gilmore J, et al (2016) Downscaling land-use data to provide global 30" estimates of five land-use classes. Ecol Evol 6:3040–3055. doi: 10.1002/ece3.2104

Hurvich CM, Tsai C-L (1989) Regression and time series model selection in small samples. Biometrika 76:297–307. doi: 10.1093/biomet/76.2.297

Ilut DC, Sanchez PL, Coffelt TA, et al (2017) A century of guayule: Comprehensive genetic characterization of the US national guayule (Parthenium argentatum A. Gray) germplasm collection. Ind Crops Prod 109:300–309. doi: 10.1016/j.indcrop.2017.08.029

IRSG (2014) Sustainable Natural Rubber Initiatives (SNR-i). In: Sustain. Nat. Rubber Initiat. SNR-I. http://www.snr-i.org/index.php. Accessed 15 Jan 2019

IRSG (2015) Statistical summary of world rubber situation. In: Int. Rubber Study Group. http://www.rubberstudy.com/statistics. Accessed 5 Feb 2015

IRSG (2017) Statistical summary of world rubber situation. In: Int. Rubber Study Group. http://www.rubberstudy.com/statistics. Accessed 3 Sep 2017

Jaimes Y, Rojas J, Cilas C, Furtado EL (2016) Suitable climate for rubber trees affected by the South American Leaf Blight (SALB): Example for identification of escape zones in the Colombian middle Magdalena. Crop Prot 81:99–114. doi: 10.1016/j.cropro.2015.12.016

Jayasooryan KK, Satheesh PR, Krishnakumar R, Jacob J (2015) Occurrence of extreme temperature events – A Probable risk on natural rubber cultivation. J Plant Crops 43:218–224. doi: 10.19071/jpc.2015.v43.i3.2856

Jiang A (1988) Climate and natural production of rubber (*Hevea brasiliensis*) in Xishuangbanna, southern part of Yunnan province, China. Int J Biometeorol 32:280–282. doi: 10.1007/BF01080028

Jongrungrot V, Thungwa S (2013) Resilience of Rubber-Based Intercropping System in Southern Thailand. Adv Mater Res 844:24–29. doi: 10.4028/www.scientific.net/AMR.844.24

Jongrungrot V, Thungwa S, Snoeck D (2014) Tree-crop diversification in rubber plantations to diversify sources of income for small-scale rubber farmers in Southern Thailand. BOIS FORETS Trop 321:21. doi: 10.19182/bft2014.321.a31214

Kajiura H, Suzuki N, Mouri H, et al (2018) Elucidation of rubber biosynthesis and accumulation in the rubber producing shrub, guayule (Parthenium argentatum Gray). Planta 247:513–526. doi: 10.1007/s00425-017-2804-7

Kennedy SF, Leimona B, Yi Z-F (2017) Making a green rubber stamp: emerging dynamics of natural rubber eco-certification. Int J Biodivers Sci Ecosyst Serv Manag 13:100–115. doi: 10.1080/21513732.2016.1267664

Kenney-Lazar M (2012) Plantation rubber, land grabbing and social-property transformation in southern Laos. J Peasant Stud 39:1017–1037. doi: 10.1080/03066150.2012.674942

Kenward MG, Roger JH (1997) Small Sample Inference for Fixed Effects from Restricted Maximum Likelihood. Biometrics 53:983–997. doi: 10.2307/2533558

Kirtman B, Power SB, Adedoyin AJ, et al (2013) Near-term Climate Change: Projections and Predictability. In: Stocker TF, Qin D, Plattner G-K, et al. (eds) Climate Change 2013: The Physical Science Basis. Contribution of Working Group I to the Fifth Assessment Report of the Intergovernmental Panel on Climate Change. Cambridge University Press, Cambridge, United Kingdom and New York, NY, USA, pp 953–1028

Kobayashi N, Kumagai T, Miyazawa Y, et al (2014) Transpiration characteristics of a rubber plantation in central Cambodia. Tree Physiol 34:285–301. doi: 10.1093/treephys/tpu009

Koedsin W, Huete A (2015) Mapping rubber tree stand age using pléiades satellite imagery: A case study in Thalang District, Phuket, Thailand. Eng J 19:45–56. doi: 10.4186/ej.2015.19.4.45

Kositsup B, Montpied P, Kasemsap P, et al (2009) Photosynthetic capacity and temperature responses of photosynthesis of rubber trees (*Hevea brasiliensis* Müll. Arg.) acclimate to changes in ambient temperatures. Trees - Struct Funct 23:357–365

Kossin JP, Emanuel KA, Camargo SJ (2016) Past and projected changes in western north pacific tropical cyclone exposure. J Clim 29:5725–5739. doi: 10.1175/JCLI-D-16-0076.1

Kou W, Liang C, Wei L, et al (2017) Phenology-Based Method for Mapping Tropical Evergreen Forests by Integrating of MODIS and Landsat Imagery. . Forests 8:1–14. doi: 10.3390/f8020034

Kou W, Xiao X, Dong J, et al (2015) Mapping deciduous rubber plantation areas and stand ages with PALSAR and landsat images. Remote Sens 7:1048–1073. doi: 10.3390/rs70101048

Kreuzberger M, Hahn T, Zibek S, et al (2016) Seasonal pattern of biomass and rubber and inulin of wild Russian dandelion (Taraxacum koksaghyz L. Rodin) under experimental field conditions. Eur J Agron 80:66–77. doi: 10.1016/j.eja.2016.06.011

Langenberger G, Cadisch G, Martin K, et al (2017) Rubber intercropping: a viable concept for the 21st century? Agrofor Syst 91:577–596. doi: 10.1007/s10457-016-9961-8

Langford MH (1945) South American leaf blight of Hevea rubber trees. US Dept. of Agriculture

Le Guen V, Garcia D, Mattos CRR, Clément-Demange A (2002) Evaluation of field resistance to *Microcyclus ulei* of a collection of Amazonian rubber tree (*Hevea brasiliensis*) germplasm. Cropp Breed Appl Biotechnol 2:141–148. doi: 10.12702/1984-7033.v02n01a18

Le Guen V, Guyot J, Mattos CRR, et al (2008) Long lasting rubber tree resistance to *Microcyclus ulei* characterized by reduced conidial emission and absence of teleomorph. Crop Prot 27:1498–1503. doi: 10.1016/j.cropro.2008.07.012

Le Guen V, Koop DM, Salgado LR, et al (2015) Genetic and genomic diversity response of rubber tree to a major fungal disease. In: The 11th International Congress of Plant Molecular Biology. IPMB2015, Foz do Iguaçu, Brazil

Le Guen V, Lespinasse D, Oliver G, et al (2003) Molecular mapping of genes conferring field resistance to South American Leaf Blight (*Microcyclus ulei*) in rubber tree. Theor Appl Genet 108:160–167. doi: 10.1007/s00122-003-1407-9

Le Guen V, Seguin M, Mattos CRR (2000) Qualitative resistance of *Hevea* to *Phyllachora huberi* P. Henn. Euphytica 112:211–217. doi: 10.1023/A:1003983902257

LebaiJuri M, Othman S, Wan Mashol WZ, Ismail R (1997) Comparative feasibility of gamma, electron beam and x-rays facilities at the Kuala Lumpur International airport (KLIA), Sepang, Malaysia. In: Proceedings of INC '97 - International Nuclear Conference: a new era in Nuclear Science and Technology - the challenge of the 21st century. Malaysian Inst for Nuclear Technology Research MINT, Bangi, Selangor, Malaysia, pp 173–185

Lewandowsky S, Risbey JS, Oreskes N (2016) The “pause” in global warming: Turning a routine fluctuation into a problem for science. Bull Am Meteorol Soc 97:723–733. doi: 10.1175/BAMS-D-14-00106.1

Li H, Aide TM, Ma Y, et al (2007) Demand for rubber is causing the loss of high diversity rain forest in SW China. Biodivers Conserv 16:1731–1745. doi: 10.1007/s10531-006-9052-7

Li P, Zhang J, Feng Z (2015) Mapping rubber tree plantations using a Landsat-based phenological algorithm in Xishuangbanna, southwest China. Remote Sens Lett 6:49–58. doi: 10.1080/2150704X.2014.996678

Li S, Zou F, Zhang Q, Sheldon FH (2013) Species richness and guild composition in rubber plantations compared to secondary forest on Hainan Island, China. Agrofor Syst 87:1117–1128. doi: 10.1007/s10457-013-9624-y

Li Z, Fox JM (2012) Mapping rubber tree growth in mainland Southeast Asia using time-series MODIS 250 m NDVI and statistical data. Appl Geogr 32:420–432

Li Z, Fox JM (2011a) Integrating Mahalanobis typicalities with a neural network for rubber distribution mapping. Remote Sens Lett 2:157–166. doi: 10.1080/01431161.2010.505589

Li Z, Fox JM (2011b) Rubber Tree Distribution Mapping in Northeast Thailand. Int J Geosci 2:573–584. doi: 10.4236/ijg.2011.24060

Lieberei R (2007) South American Leaf Blight of the Rubber Tree (*Hevea* spp.): New Steps in Plant Domestication using Physiological Features and Molecular Markers. Ann Bot 100:1125–1142. doi: 10.1093/aob/mcm133

Liu C, Guénard B, Blanchard B, et al (2016) Reorganization of taxonomic, functional, and phylogenetic ant biodiversity after conversion to rubber plantation. Ecol Monogr 86:215–227. doi: 10.1890/15-1464.1

Liu C, Men X, Chen H, et al (2018a) A systematic optimization of styrene biosynthesis in Escherichia coli BL21(DE3). Biotechnol Biofuels 11:14. doi: 10.1186/s13068-018-1017-z

Liu H, Zhu J, Ding H, et al (2018b) Foliar spray of growth regulators significantly increases trans-1,4-polyisoprene production from Eucommia ulmoides Oliver short-rotation coppice. Ind Crops Prod 113:383–390. doi: 10.1016/j.indcrop.2018.01.054

Liu J, Liu W, Zhu K (2018c) Throughfall kinetic energy and its spatial characteristics under rubber-based agroforestry systems. CATENA 161:113–121. doi: 10.1016/j.catena.2017.10.014

Liu J-J, Slik JWF (2014) Forest fragment spatial distribution matters for tropical tree conservation. Biol Conserv 171:99–106. doi: 10.1016/j.biocon.2014.01.004

Liu S, Zhou G, Fang S, Zhang J (2015a) Effects of future climate change on climatic suitability of rubber plantation in China. Ying Yong Sheng Tai Xue Bao J Appl Ecol Zhongguo Sheng Tai Xue Xue Hui Zhongguo Ke Xue Yuan Shenyang Ying Yong Sheng Tai Yan Jiu Suo Zhu Ban 26:2083–2090

Liu W, Hu H, Ma Y, Li H (2006) Environmental and Socioeconomic Impacts of Increasing Rubber Plantations in Menglun Township, Southwest China. Mt Res Dev 26:245–254. doi: 10.1659/0276-4741(2006)26[245:EASIOI]2.0.CO;2

Liu W, Li J, Lu H, et al (2014) Vertical patterns of soil water acquisition by non-native rubber trees (*Hevea brasiliensis*) in Xishuangbanna, southwest China. Ecohydrology 1234–1244. doi: 10.1002/eco.1456

Liu W, Luo Q, Li J, et al (2015b) The effects of conversion of tropical rainforest to rubber plantation on splash erosion in Xishuangbanna, SW China. Hydrol Res 46:168–174. doi: 10.2166/nh.2013.109

Liyanage A de S, Jacob CK (1992) Diseases of economic importance in rubber. In: Sethuraj MR, Mathew NM (eds) Developments in Crop Science. Elsevier, pp 324–359

Liyanage KK, Khan S, Ranjitkar S, et al (2018) Evaluation of key meteorological determinants of wintering and flowering patterns of five rubber clones in Xishuangbanna, Yunnan, China. Int J Biometeorol. doi: 10.1007/s00484-018-1598-z

Lotti C, Moreno RMB, Gonçalves P de S, et al (2012) Extensional rheology of raw natural rubber from new clones of Hevea brasiliensis. Polym Eng Sci 52:139–148. doi: 10.1002/pen.22056

Lu JN (2017) Tapping into rubber: China's opium replacement program and rubber production in Laos. J Peasant Stud 44:726–747. doi: 10.1080/03066150.2017.1314268

Maeght J-L, Gonkhamdee S, Clément C, et al (2015) Seasonal Patterns of Fine Root Production and Turnover in a Mature Rubber Tree (*Hevea brasiliensis* Müll. Arg.) Stand- Differentiation with Soil Depth and Implications for Soil Carbon Stocks. Front Plant Sci 6:. doi: 10.3389/fpls.2015.01022

Marattukalam JG, Saraswathyamma CK (1992) Propagation and planting. In: Sethuraj MR, Mathew NM (eds) Developments in Crop Science. Elsevier, pp 164–199

Martin GM, Bellouin N, Collins WJ, et al (2011) The HadGEM2 family of Met Office Unified Model climate configurations. Geosci Model Dev 4:723–757. doi: 10.5194/gmd-4-723-2011

McSweeney CF, Jones RG, Lee RW, Rowell DP (2015) Selecting CMIP5 GCMs for downscaling over multiple regions. Clim Dyn 44:3237–3260. doi: 10.1007/s00382-014-2418-8

Medhaug I, Stolpe MB, Fischer EM, Knutti R (2017) Reconciling controversies about the 'global warming hiatus.' Nature 545:41–47. doi: 10.1038/nature22315

Meinshausen M, Smith SJ, Calvin K, et al (2011) The RCP greenhouse gas concentrations and their extensions from 1765 to 2300. Clim Change 109:213. doi: 10.1007/s10584-011-0156-z

Men X, Wang F, Chen G-Q, et al (2019) Biosynthesis of Natural Rubber: Current State and Perspectives. Int J Mol Sci 20:50. doi: 10.3390/ijms20010050

Miedaner T (2017) Henry Ford musste kapitulieren. In: Pflanzenkrankheiten, die die Welt beweg(t)en. Springer Berlin Heidelberg, Berlin, Heidelberg, pp 211–234

Min S, Bai J, Huang J, Waibel H (2018) Willingness of smallholder rubber farmers to participate in ecosystem protection: Effects of household wealth and environmental awareness. For Policy Econ 87:70–84. doi: 10.1016/j.forpol.2017.11.009

Min S, Huang J, Waibel H, et al (2019) Rubber Boom, Land Use Change and the Implications for Carbon Balances in Xishuangbanna, Southwest China. Ecol Econ 156:57–67. doi: 10.1016/j.ecolecon.2018.09.009

Mittermeier R, Robles Gil P, Hoffmann M, et al (2004) Hotspots Revisited. CEMEX, Mexico City

Monteny BA, Barbier JM, Bernos CM (1985) Determination of the energy exchanges of forest type culture: *Hevea brasiliensis*. In: Hutchinson BA, Hicks BB (eds) Forest Atmospheric Interaction. Reidel, Dordrecht, Netherlands, pp 211–233

Montény BA, Barbier JM, Bernos CM (1985) Determination of the energy exchanges of a forest type culture: *Hevea brasiliensis*. In: Hutchinson BA, Hicks BB (eds) The Forest–Atmosphere Interaction. Reidel, Dordrecht, Netherlands, pp 211–233

Muggeo VMR (2003) Estimating regression models with unknown break-points. Stat Med 22:3055–3071. doi: 10.1002/sim.1545

Myers N, Mittermeier RA, Mittermeier CG, et al (2000) Biodiversity hotspots for conservation priorities. Nature 403:853. doi: 10.1038/35002501

NCEP (2018) NCEP global reanalysis daily surface relative humidity data. https://www.esrl.noaa.gov/psd/data/gridded/data.ncep.reanalysis.surface.html. Accessed 21 Aug 2018

Nelson TA, Boots B (2008) Detecting spatial hot spots in landscape ecology. Ecography 31:556–566. doi: 10.1111/j.0906-7590.2008.05548.x

Newbold T, Hudson LN, Arnell AP, et al (2016) Has Land use pushed terrestrial biodiversity beyond the planetary boundary? A global assessment. Science 353:288–291. doi: 10.1126/science.aaf2201

Nguyen BT, Dang MK (2016) Temperature dependence of natural rubber productivity in the southeastern Vietnam. Ind Crops Prod 83:24–30. doi: 10.1016/j.indcrop.2015.12.019

Nóia Júnior R de S, Pezzopane JEM, Vinco JS, et al (2018) Characterization of photosynthesis and transpiration in two rubber tree clones exposed to thermal stress. Braz J Bot 41:785–794. doi: 10.1007/s40415-018-0495-3

Novais SMA, Macedo-Reis LE, Neves FS (2017) Predatory beetles in cacao agroforestry systems in Brazilian Atlantic forest: a test of the natural enemy hypothesis. Agrofor Syst 91:201–209. doi: 10.1007/s10457-016-9917-z

NSO (1994) The forth Thailand agricultural census. In: Natl. Stat. Off. Thail. http://web.nso.go.th/eng/en/stat/agric/cont_e.htm. Accessed 20 Jun 2017

Omokhafe KO (2004) Interaction between flowering pattern and latex yield in *Hevea brasiliensis* Muell. Arg. Cropp Breed Appl Biotechnol 4:280–284. doi: 10.12702/1984-7033.v04n03a03

Ong SH, Othman R, Benong M (1998) Breeding and selection of clonal genotypes for climatic stress condition. In: Cronin ME (ed) Proceedings of the IRRDB Symposium. IRRDB. IRRDB, Hertford, pp 149–154

Onokpise O, Louime C (2012) The Potential of the South American Leaf Blight as a Biological Agent. Sustainability 4:3151–3157. doi: 10.3390/su4113151

Onokpise OU (2004) Natural Rubber, *Hevea Brasiliensis* (Willd. Ex A. Juss.) MüLl. Arg., Germplasm Collection In The Amazon Basin, Brazil: A Retrospective. Econ Bot 58:544–555. doi: 10.1663/0013-0001(2004)058[0544:NRHBWE]2.0.CO;2

Ord JK, Getis A (1995) Local Spatial Autocorrelation Statistics: Distributional Issues and an Application. Geogr Anal 27:286–306. doi: 10.1111/j.1538-4632.1995.tb00912.x

Ortolani AA, Sentelhas PC, Camargo MBP, et al (1998) Agrometeorological model for seasonal rubber tree yield. Ind J Nat Rubber Res 11:8–14

Panara F, Lopez L, Daddiego L, et al (2018) Comparative transcriptomics between high and low rubber producing Taraxacum kok-saghyz R. plants. BMC Genomics 19:. doi: 10.1186/s12864-018-5287-4

Partelli FL, Araújo AV, Vieira HD, et al (2014) Microclimate and development of "Conilon" coffee intercropped with rubber trees. Pesqui Agropecuária Bras 49:872–881. doi: 10.1590/S0100-204X2014001100006

Priyadarshan PM (2011) Biology of *Hevea* rubber. CABI, Wallingford, Oxfordshire, UK ; Cambridge, MA

Priyadarshan PM (2016) Genetic Diversity and Erosion in *Hevea* Rubber. In: Ahuja MR, Jain SM (eds) Genetic Diversity and Erosion in Plants. Springer International Publishing, Cham, pp 233–267

Priyadarshan PM, Goncalves P de S (2003) *Hevea* gene pool for breeding. Genet Resour Crop Evol 50:101–114

Priyadarshan PM, Hoa TTT, Huasun H, de Souza Gonçalves P (2005) Yielding potential of rubber (*Hevea brasiliensis*) in sub-optimal environments. J Crop Improv 14:221–247. doi: 10.1300/J411v14n01_10

Priyadarshan PM, Sasikumar S, Goncalves P de S (2001) Phenological changes in *Hevea brasiliensis* under differential geo-climates. The Planter 77:447–459

Pushparajah E (1983) Problems and potentials for establishing *Hevea* under difficult environmental conditions. Planter 242–251

Raj S, Das G, Pothen J, Dey SK (2005) Relationship between latex yield of *Hevea brasiliensis* and antecedent environmental parameters. Int J Biometeorol 49:189–196. doi: 10.1007/s00484-004-0222-6

Ramirez-Cadavid DA, Cornish K, Michel Jr. FC (2017) Taraxacum kok-saghyz (TK): compositional analysis of a feedstock for natural rubber and other bioproducts. Ind Crops Prod 107:624–640. doi: 10.1016/j.indcrop.2017.05.043

Ramirez-Villegas J, Jarvis A (2010) Downscaling Global Circulation Model Outputs: The Delta Method; decision and policy analysis working paper no 1.

Rao GP, Kole PC (2016) Evaluation of Brazilian wild Hevea germplasm for cold tolerance: genetic variability in the early mature growth. J For Res 27:755–765. doi: 10.1007/s11676-015-0188-8

Rao PS, Saraswathyamma CK, Sethuraj MR (1998) Studies on the relationship between yield and meteorological parameters of para rubber tree *Hevea brasiliensis*. 11

Rasutis D, Soratana K, McMahan C, Landis AE (2015) A sustainability review of domestic rubber from the guayule plant. Ind Crops Prod 70:383–394. doi: 10.1016/j.indcrop.2015.03.042

Ray D, Behera MD, Jacob J (2014) Indian Brahmaputra valley offers significant potential for cultivation of rubber trees under changed climate. Curr Sci 107:461–469

Ray D, Behera MD, Jacob J (2016a) Improving spatial transferability of ecological niche model of *Hevea brasiliensis* using pooled occurrences of introduced ranges in two biogeographic regions of India. Ecol Inform 34:153–163. doi: 10.1016/j.ecoinf.2016.06.003

Ray D, Behera MD, Jacob J (2016b) Predicting the distribution of rubber trees (*Hevea brasiliensis*) through ecological niche modelling with climate, soil, topography and socioeconomic factors. Ecol Res 31:75–91. doi: 10.1007/s11284-015-1318-7

Rembold K, Mangopo H, Tjitrosoedirdjo SS, Kreft H (2017) Plant diversity, forest dependency, and alien plant invasions in tropical agricultural landscapes. Biol Conserv 213:234–242. doi: 10.1016/j.biocon.2017.07.020

Renner SS (2007) Synchronous flowering linked to changes in solar radiation intensity. New Phytol 175:195–197. doi: 10.1111/j.1469-8137.2007.02132.x

Riahi K, Rao S, Krey V, et al (2011) RCP 8.5-A scenario of comparatively high greenhouse gas emissions. Clim Change 109:33–57. doi: 10.1007/s10584-011-0149-y

Righi CA, Bernardes MS, Lunz AMP, et al (2007) Measurement and simulation of solar radiation availability in relation to the growth of coffee plants in an agroforestry system with rubber trees. Rev Árvore 31:195–207. doi: 10.1590/S0100-67622007000200002

Righi CA, Campoe OC, Bernardes MS, et al (2013) Influence of rubber trees on leaf-miner damage to coffee plants in an agroforestry system. Agrofor Syst 87:1351–1362. doi: 10.1007/s10457-013-9642-9

Righi CA, Lunz AMP, Bernardes MS, et al (2008) Coffee water use in agroforestry system with rubber trees. Rev Árvore 32:781–792. doi: 10.1590/S0100-67622008000500001

Ritchie J, Dowlatabadi H (2017a) The 1000 GtC coal question: Are cases of vastly expanded future coal combustion still plausible? Energy Econ 65:16–31. doi: 10.1016/j.eneco.2017.04.015

Ritchie J, Dowlatabadi H (2017b) Why do climate change scenarios return to coal? Energy 140:1276–1291. doi: 10.1016/j.energy.2017.08.083

Rivano F, Maldonado L, Simbaña B, et al (2015) Suitable rubber growing in Ecuador: An approach to South American leaf blight. Ind Crops Prod 66:262–270

Rivano F, Mattos CRR, Cardoso SEA, et al (2013) Breeding *Hevea brasiliensis* for yield, growth and SALB resistance for high disease environments. Ind Crops Prod 44:659–670. doi: 10.1016/j.indcrop.2012.09.005

Rodrigo VHL (2007) Ecophysiological factors underpinning productivity of Hevea brasiliensis. Braz J Plant Physiol 19:245–255. doi: 10.1590/S1677-04202007000400002

Roy CB, Newby Z-J, Mathew J, Guest DI (2017) A climatic risk analysis of the threat posed by the South American leaf blight (SALB) pathogen *Microcyclus ulei* to major rubber producing countries. Eur J Plant Pathol 148:129–138. doi: 10.1007/s10658-016-1076-6

Sanjeeva Rao P, Vijayakumar KR (1992) Climatic requirements. In: Sethuraj MR, Mathew NM (eds) Developments in Crop Science. Elsevier, pp 200–219

Sarathchandra C, Dossa GGO, Ranjitkar NB, et al (2018) Effectiveness of protected areas in preventing rubber expansion and deforestation in Xishuangbanna, Southwest China. Land Degrad Dev 29:2417–2427. doi: 10.1002/ldr.2970

SAS (2011) SAS for Windows, version 9.3. SAS Institute, Cary

Satheesan KV, Rao GG, Sethuraj MR, Raghavendra AS (1984) Canopy Photosynthesis in Rubber (Hevea Brasiliensis): Characteristics of Leaves in Relation to Light Interception. In: Sybesma C (ed) Advances in Photosynthesis Research: Proceedings of the VIth International Congress on Photosynthesis, Brussels, Belgium, August 1–6, 1983. Volume IV. Springer Netherlands, Dordrecht, pp 125–128

Scholes RJ, Biggs R (2005) A biodiversity intactness index. Nature 434:45. doi: 10.1038/nature03289

Self SG, Liang K-Y (1987) Asymptotic Properties of Maximum Likelihood Estimators and Likelihood Ratio Tests under Nonstandard Conditions. J Am Stat Assoc 82:605–610. doi: 10.1080/01621459.1987.10478472

Semenov MA, Stratonovitch P (2010) Use of multi-model ensembles from global climate models for assessment of climate change impacts. Clim Res 41:1–14. doi: 10.3354/cr00836

Senevirathna AMWK, Stirling CM, Rodrigo VHL (2003) Growth, photosynthetic performance and shade adaptation of rubber (Hevea brasiliensis) grown in natural shade. Tree Physiol 23:705–712. doi: 10.1093/treephys/23.10.705

Senf C, Pflugmacher D, van der Linden S, Hostert P (2013) Mapping rubber plantations and natural forests in Xishuangbanna (Southwest China) using multi-spectral phenological metrics from modis time series. Remote Sens 5:2795–2812. doi: 10.3390/rs5062795

Shangphu L (1986) Judicious tapping with stimulation based on dynamic analysis of latex production. In: Pan Y, Zhao C (eds) Proceedings of the IRRDB Rubber Physiology and Exploitation Meeting. SCATC, Hainan, China, pp 230–239

Shuochang A, Yagang G (1990) Exploration of the high yield physiological regulation of *Hevea brasiliensis* in Xishuangbanna. In: Proceedings of the IRRDB Symposium on Physiology and Exploitation of *Hevea brasiliensis*. IRRDB, Kunming, China, pp 83–92

Silva KR da, Cecílio RA, Xavier AC, et al (2013) Zoneamento edafoclimático para a cultura da seringueira no Espírito Santo. Irriga 18:01. doi: 10.15809/irriga.2013v18n1p01

Silva JQ, Scaloppi Júnior EJ, Moreno RMB, et al (2012) Producción y propiedades químicas del caucho en clones de Hevea según los estados fenológicos. Pesqui Agropecuária Bras 47:1066–1076. doi: 10.1590/S0100-204X2012000800006

Snoeck D, Lacote R, Kéli J, et al (2013) Association of hevea with other tree crops can be more profitable than hevea monocrop during first 12 years. Ind Crops Prod 43:578–586. doi: 10.1016/j.indcrop.2012.07.053

Somboonsuke B, Wetayaprasit P, Chernchom P, Pacheerat K (2011) Diversification of Smallholding Rubber Agroforestry System (SRAS) Thailand. Kasetsart J 327–339

Soratana K, Rasutis D, Azarabadi H, et al (2017) Guayule as an alternative source of natural rubber: A comparative life cycle assessment with *Hevea* and synthetic rubber. J Clean Prod 159:271–280. doi: 10.1016/j.jclepro.2017.05.070

Steffen W, Richardson K, Rockström J, et al (2015) Planetary boundaries: Guiding human development on a changing planet. Science 347:1259855. doi: 10.1126/science.1259855

Steinbüchel A (2003) Production of rubber-like polymers by microorganisms. Curr Opin Microbiol 6:261–270. doi: 10.1016/S1369-5274(03)00061-4

Stephens EM, Edwards TL, Demeritt D (2012) Communicating probabilistic information from climate model ensembles-lessons from numerical weather prediction. Wiley Interdiscip Rev Clim Change 3:409–426. doi: 10.1002/wcc.187

Stewart RIA, Dossena M, Bohan DA, et al (2013) Mesocosm Experiments as a Tool for Ecological Climate-Change Research. In: Woodward G, O'Gorman EJ (eds) Advances in Ecological Research. Academic Press, pp 71–181

Stone M (1974) Cross-Validatory Choice and Assessment of Statistical Predictions. J R Stat Soc Ser B Methodol 36:111–147

Stonebloom SH, Scheller HV (2019) Transcriptome analysis of rubber biosynthesis in guayule (Parthenium argentatum gray). BMC Plant Biol 19:71. doi: 10.1186/s12870-019-1669-2

Stram DO, Lee JW (1994) Variance Components Testing in the Longitudinal Mixed Effects Model. Biometrics 50:1171–1177. doi: 10.2307/2533455

Su X, Yan X, Tsai C-L (2012) Linear regression. Wiley Interdiscip Rev Comput Stat 4:275–294. doi: 10.1002/wics.1198

Sugiura N (1978) Further analysts of the data by akaike' s information criterion and the finite corrections: Further analysts of the data by akaike' s. Commun Stat - Theory Methods 7:13–26. doi: 10.1080/03610927808827599

Tan Z-H, Zhang Y-P, Song Q-H, et al (2011) Rubber plantations act as water pumps in tropical China. Geophys Res Lett 38:. doi: 10.1029/2011GL050006

Tarigan S, Wiegand K, Sunarti, Slamet B (2018) Minimum forest cover required for sustainable water flow regulation of a watershed: a case study in Jambi Province, Indonesia. Hydrol Earth Syst Sci 22:581–594. doi: https://doi.org/10.5194/hess-22-581-2018

Thanichanon P, Schmidt-Vogt D, Epprecht M, et al (2018) Balancing cash and food: The impacts of agrarian change on rural land use and wellbeing in Northern Laos. PLOS ONE 13:e0209166. doi: 10.1371/journal.pone.0209166

Thompson RM, Beardall J, Beringer J, et al (2013) Means and extremes: Building variability into community-level climate change experiments. Ecol Lett 16:799–806. doi: 10.1111/ele.12095

Thomson AM, Calvin KV, Smith SJ, et al (2011) RCP4.5: a pathway for stabilization of radiative forcing by 2100. Clim Change 109:77–94. doi: 10.1007/s10584-011-0151-4

Thorne P (2017) Briefing: Global surface temperature records: an update. Proc Inst Civ Eng - Forensic Eng 170:50–53. doi: 10.1680/jfoen.17.00001

Thornton PE, Hasenauer H, White MA (2000) Simultaneous estimation of daily solar radiation and humidity from observed temperature and precipitation: an application over complex terrain in Austria. Agric For Meteorol 104:255–271. doi: 10.1016/S0168-1923(00)00170-2

Trisasongko BH (2017) Mapping stand age of rubber plantation using ALOS-2 polarimetric SAR data. Eur J Remote Sens 50:64–76. doi: 10.1080/22797254.2017.1274569

Václavík T, Langerwisch F, Cotter M, et al (2016) Investigating potential transferability of place-based research in land system science. Environ Res Lett 11:095002. doi: 10.1088/1748-9326/11/9/095002

van Beilen JB, Poirier Y (2007a) Establishment of new crops for the production of natural rubber. Trends Biotechnol 25:522–529. doi: 10.1016/j.tibtech.2007.08.009

van Beilen JB, Poirier Y (2007b) Guayule and Russian dandelion as alternative sources of natural rubber. Crit Rev Biotechnol 27:217–231. doi: 10.1080/07388550701775927

Varghese YA (1992) Germplasm resources and genetic improvement. In: Sethuraj MR, Mathew NM (eds) Developments in Crop Science. Elsevier, pp 88–115

Verbeke G, Molenberghs G (2000) Linear mixed models for longitudinal data. Springer, New York

Villamil-Otero GA, Zhang J, He J, Zhang X (2018) Role of extratropical cyclones in the recently observed increase in poleward moisture transport into the Arctic Ocean. Adv Atmospheric Sci 35:85–94. doi: 10.1007/s00376-017-7116-0

Wang J, Feng L, Tang X, et al (2017) The implications of fossil fuel supply constraints on climate change projections: A supply-side analysis. Futures 86:58–72. doi: 10.1016/j.futures.2016.04.007

Wang L, Du H, Wuyun T (2016) Genome-Wide Identification of MicroRNAs and Their Targets in the Leaves and Fruits of Eucommia ulmoides Using High-Throughput Sequencing. Front Plant Sci 7:. doi: 10.3389/fpls.2016.01632

Warren-Thomas E, Dolman PM, Edwards DP (2015) Increasing Demand for Natural Rubber Necessitates a Robust Sustainability Initiative to Mitigate Impacts on Tropical Biodiversity. Conserv Lett 8:230–241. doi: 10.1111/conl.12170

Watson GA, Weng WP, Narayanan R (1964) Effect of Cover Plants on Soil Nutrient Status and on Growth of Hevea III. A Comparison of Leguminous Creepers with Grasses and Mikania cordate? Mikania Cordata 18:80–95

Whaley WG (1948) Rubber-The Primary Sources For American Production. Econ Bot 2:198–216. doi: 10.1007/BF02859004

Wigboldus S, Hammond J, Xu J, et al (2017) Scaling green rubber cultivation in Southwest China—An integrative analysis of stakeholder perspectives. Sci Total Environ 580:1475–1482. doi: 10.1016/j.scitotenv.2016.12.126

Wolff M, Zhang L (2010) Soil classification in the Naban River Watershed National Nature Reserve. GRIN, Munich, Germany

Wolfinger R (1993) Covariance structure selection in general mixed models. Commun Stat - Simul Comput 22:1079–1106. doi: 10.1080/03610919308813143

Xiao C, Li P, Feng Z (2019) Monitoring annual dynamics of mature rubber plantations in Xishuangbanna during 1987-2018 using Landsat time series data: A multiple normalization approach. Int J Appl Earth Obs Geoinformation 77:30–41. doi: 10.1016/j.jag.2018.12.006

Xin X, Zhang L, Zhang J, et al (2013) Climate change projections over east asia with BBC_CSM1.1 climate model under RCP scenarios. J Meteorol Soc Jpn 91:413–429. doi: 10.2151/jmsj.2013-401

Xu J, Grumbine RE, Beckschäfer P (2014) Landscape transformation through the use of ecological and socioeconomic indicators in Xishuangbanna, Southwest China, Mekong Region. Ecol Indic 36:749–756. doi: 10.1016/j.ecolind.2012.08.023

Yamashita S, Yamaguchi H, Waki T, et al (2016) Identification and reconstitution of the rubber biosynthetic machinery on rubber particles from Hevea brasiliensis. eLife 5:e19022. doi: 10.7554/eLife.19022

Yang J, Xian M, Su S, et al (2012) Enhancing Production of Bio-Isoprene Using Hybrid MVA Pathway and Isoprene Synthase in E. coli. PLOS ONE 7:e33509. doi: 10.1371/journal.pone.0033509

Yang X, Blagodatsky S, Lippe M, et al (2016) Land-use change impact on time-averaged carbon balances: Rubber expansion and reforestation in a biosphere reserve, South-West China. For Ecol Manag 372:149–163. doi: 10.1016/j.foreco.2016.04.009

Yeang H-Y (2007) Synchronous flowering of the rubber tree (*Hevea brasiliensis*) induced by high solar radiation intensity. New Phytol 175:283–289. doi: 10.1111/j.1469-8137.2007.02089.x

You Q, Min J, Lin H, et al (2015) Observed climatology and trend in relative humidity in the central and eastern Tibetan Plateau. J Geophys Res Atmospheres 120:3610–3621. doi: 10.1002/2014JD023031

Yu H, Hammond J, Ling S, et al (2014) Greater diurnal temperature difference, an overlooked but important climatic driver of rubber yield. Ind Crops Prod 62:14–21

Yukimoto S, Adachi Y, Hosaka M, et al (2012) A new global climate model of the Meteorological Research Institute: MRI-CGCM3: -Model description and basic performance-. J Meteorol Soc Jpn 90A:23–64. doi: 10.2151/jmsj.2012-A02

Zhai D-L, Yu H, Chen S-C, et al (2017) Responses of rubber leaf phenology to climatic variations in Southwest China. Int J Biometeorol. doi: 10.1007/s00484-017-1448-4

Zhang C, Wang Y (2017) Projected future changes of tropical cyclone activity over the Western North and South Pacific in a 20-km-Mesh regional climate model. J Clim 30:5923–5941. doi: 10.1175/JCLI-D-16-0597.1

Zhang M, Chang C, Quan R (2017) Natural forest at landscape scale is most important for bird conservation in rubber plantation. Biol Conserv 210:243–252. doi: 10.1016/j.biocon.2017.04.026

Ziegler AD, Fox JM, Xu J (2009) The rubber juggernaut. Science 324:1024–1025

Zomer RJ, Trabucco A, Wang M, et al (2014) Environmental stratification to model climate change impacts on biodiversity and rubber production in Xishuangbanna, Yunnan, China. Biol Conserv 170:264–273

Appendix

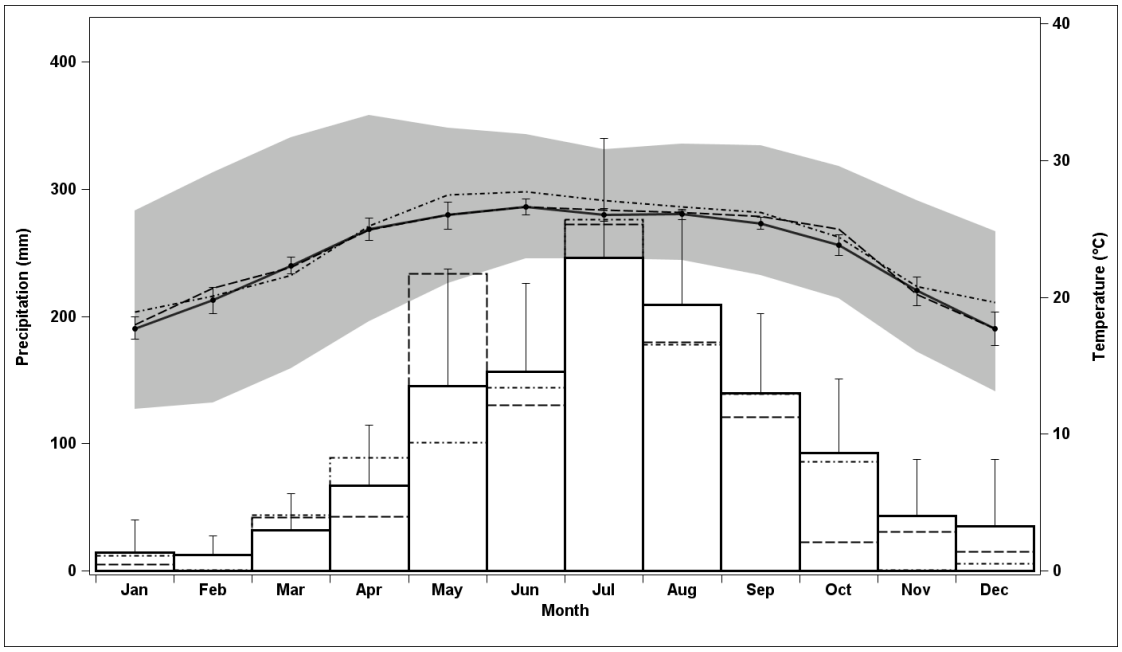

Figure A2.1 Comparison of monthly weather conditions in the study site during the data collection period with the local historical climatic records
Solid lines and error bars are the mean and standard deviation of 20 years (1989-2008) of mean monthly climatic records (XSBN Airport data), dashed lines and dash-dotted lines show the 2009 and 2010 weather conditions, respectively. Rainfall is shown as vertical bars and temperature conditions as a curvilinear plot

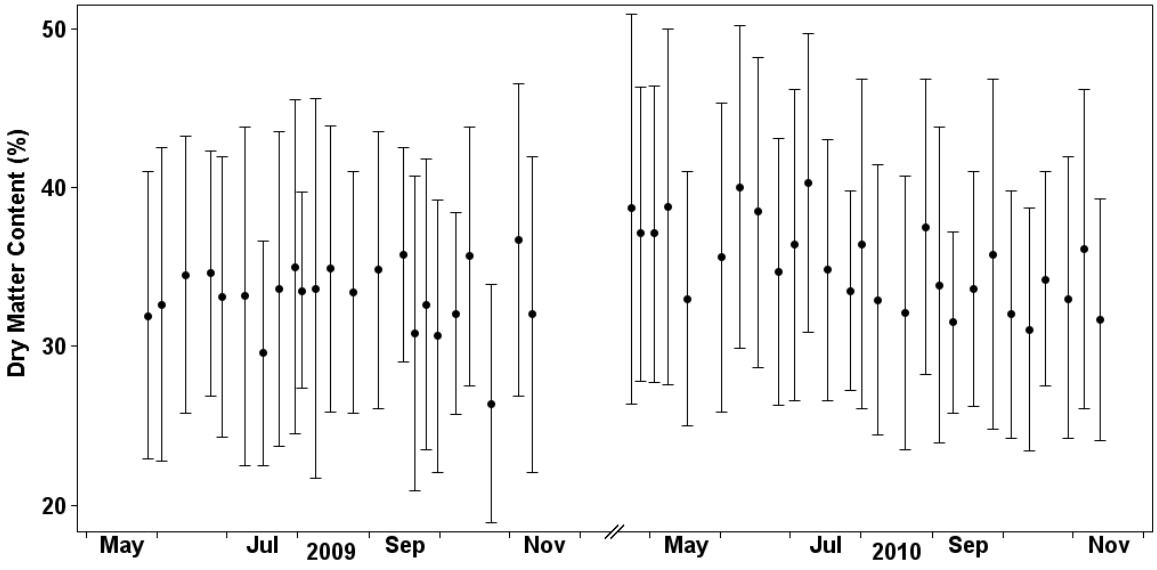

Figure A2.2 Temporal variation in the Latex dry matter content of the weekly dried samples across the 2009 and 2010 data collection
Error bars show the standard deviation of the weekly records

Table A2.1 Coefficient estimates for the fixed effects

	Fixed effect	Coefficient estimate	SE	95% confidence interval		DF	T-value	P>|T|
				Lower	Upper			
raw variables	Intercept	23.593	1.875	19.915	27.271	1965.1	12.58	5.8×10^{-35}
	MnT(30,0)	-0.366	0.038	-0.441	-0.292	1895.2	-9.63	1.8×10^{-21}
	MxT(30,0)	-0.051	0.013	-0.077	-0.025	1908.6	-3.91	0.0001
	MxRH(30,0)	-0.109	0.021	-0.151	-0.067	1869.8	-5.11	3.6×10^{-7}
	P(30,0)	0.633	0.185	0.27	0.997	1952.4	3.42	0.0007
	MnT(30,0)*P(30,0)	-0.028	0.008	-0.045	-0.011	1946.4	-3.29	0.001
standardized variables	Intercept	4.733	0.234	4.24	5.226	17	20.25	2.5×10^{-13}
	MnT(30,0)	-29.859	3.1	-35.939	-23.78	1895.2	-9.63	1.8×10^{-21}
	MxT(30,0)	-6.068	1.551	-9.111	-3.026	1908.6	-3.91	0.0001
	MxRH(30,0)	-12.884	2.523	-17.831	-7.937	1869.8	-5.11	3.6×10^{-07}
	P(30,0)	84.151	24.64	35.827	132.474	1952.3	3.42	0.0007
	MnT(30,0)*P(30,0)	-83.725	25.434	-133.606	-33.844	1946.4	-3.29	0.001

Coefficients estimated for selected model parameters (daily precipitation (P), minimum daily temperature (MnT), maximum daily temperature (MxT) and maximum relative humidity (MxRH) averaged over 30 days leading to the tapping event with no lag (30,0)). Coefficients for z-scores were calculated after standardizing the raw covariates to zero mean and unit variance. The t-statistic is the estimate divided by its standard error. The significance column shows the two-tailed p-value corresponding to the t-value and associated degrees of freedom (identical to the Kenward-Roger denominator degrees of freedom used in the F-tests). Confidence intervals equal the estimate ± 2×standard error.

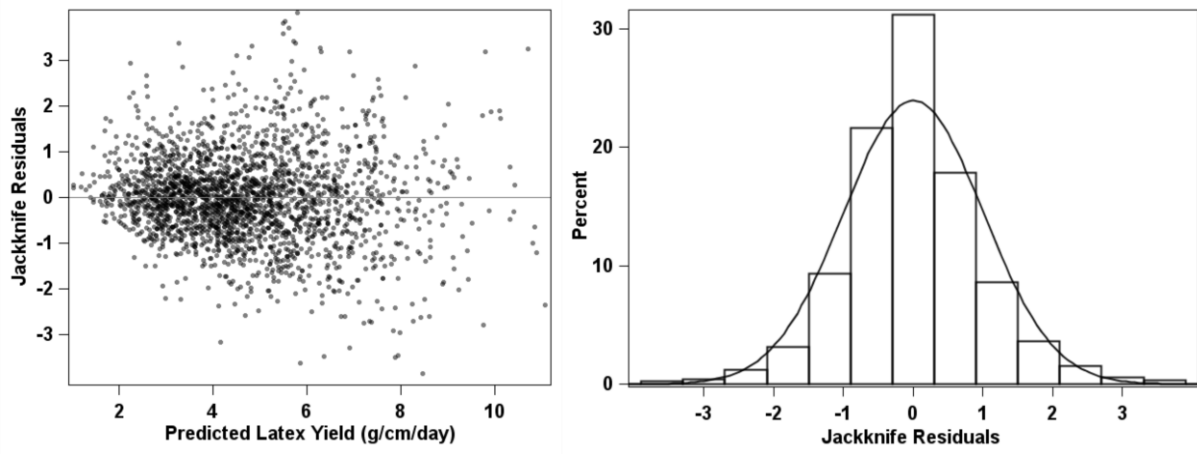

Figure A2.3 Regression diagnostics for the final model
Studentized deleted residuals (jackknife residuals) are used to generate the graphs

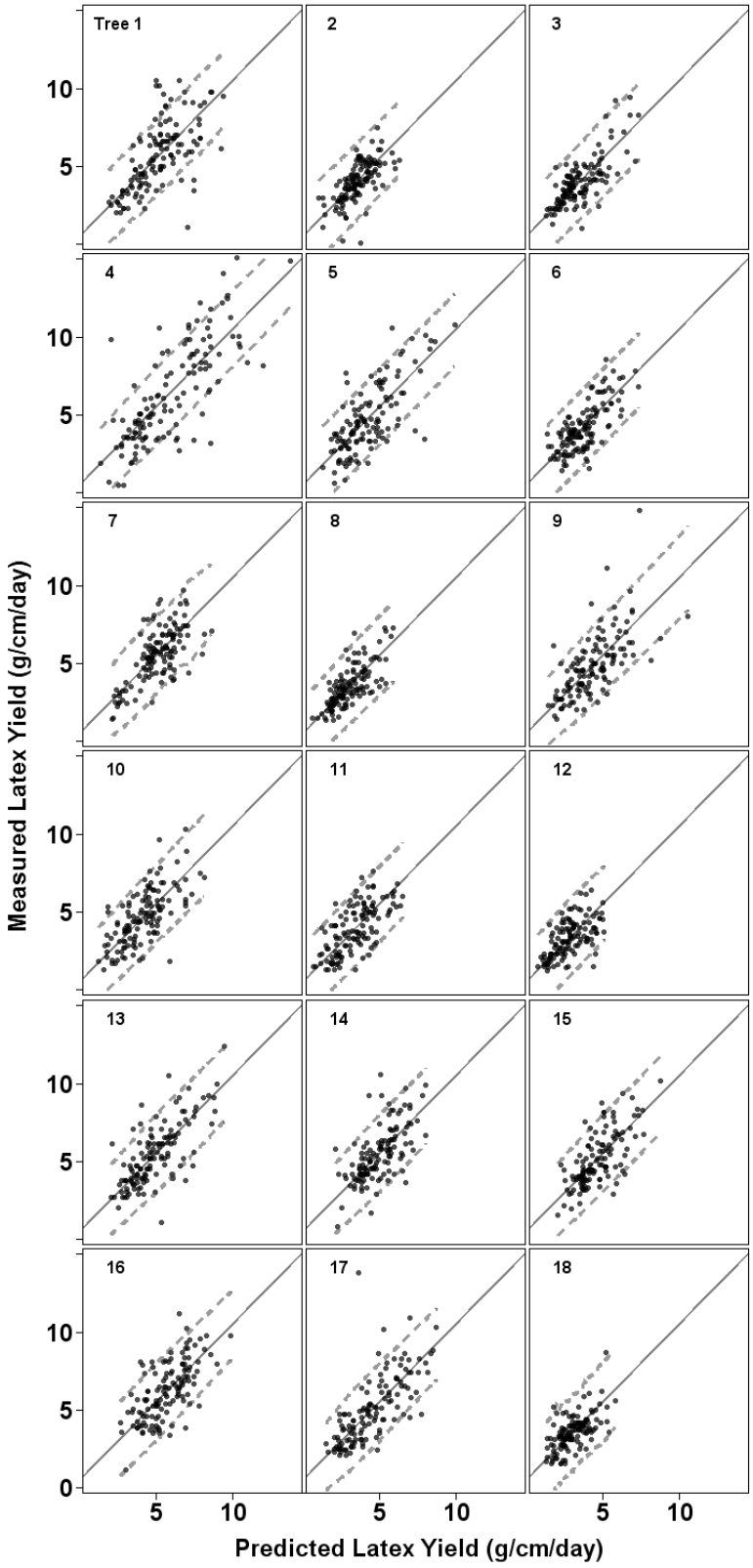

Figure A2.4 Rubber tree specific scatter plots of the predicted vs. measured latex yield obtained by leave-one-out cross-validation on the training dataset

Dashed lines are the smoothed 95% pointwise confidence bands obtained by leave-one-out cross-validation .

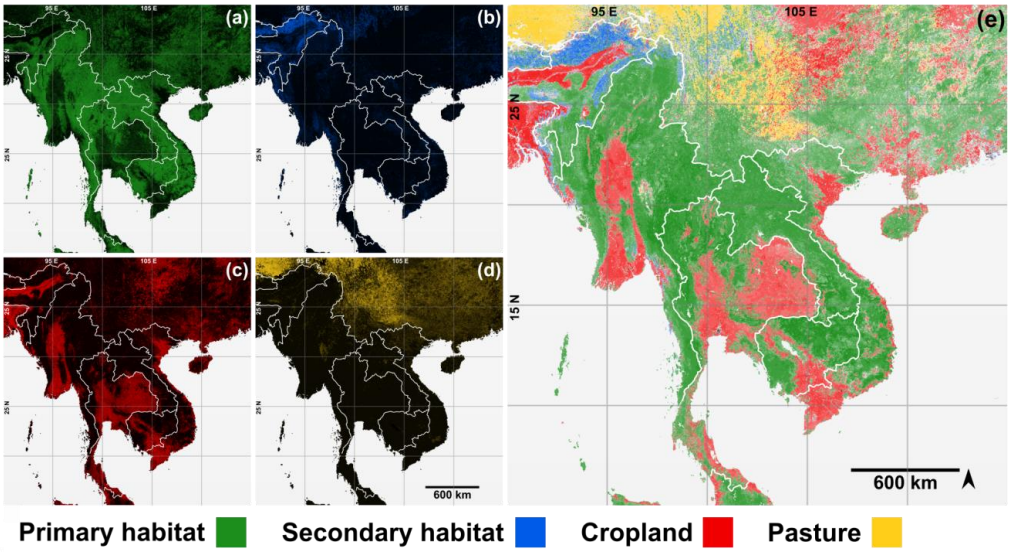

Figure A3.1 Land use composition of the study area in 2005

Gridded data provided by (Hoskins et al. 2016) were used to generate this figure. Originally, the data are composed of five layers (we have left out the urban land use) which sum up to 100 % for each grid cell. Grid cells from the panels (a) to (d) with minimum value of 40 (%) have been integrated to the panel (e) to produce a map reflecting the dominant land use. Terms primary and secondary habitat represent 'undisturbed natural' and 'recovering, previously disturbed natural' habitats respectively.

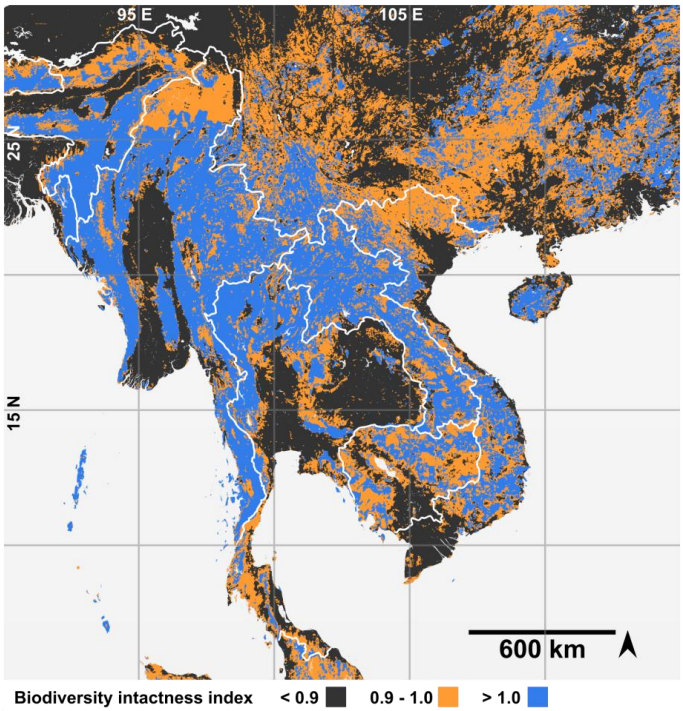

Figure A3.2 Biodiversity intactness in the study area

Biodiversity Intactness Index (BII) is a measure of habitat disturbance defined as the "total abundance of originally occurring species, as a percentage of their total abundance in minimally disturbed primary vegetation" (Newbold et al. 2016) based on the original concept by (Scholes and Biggs 2005). A safe limit of 0.9 (maximum 10% decline) has been proposed for BII (Steffen et al. 2015). We have used the gridded data produced by (Newbold et al. 2016) to generate this map in ArcGIS 10.2.2. Inkscape 0.92 was used for visual optimization.

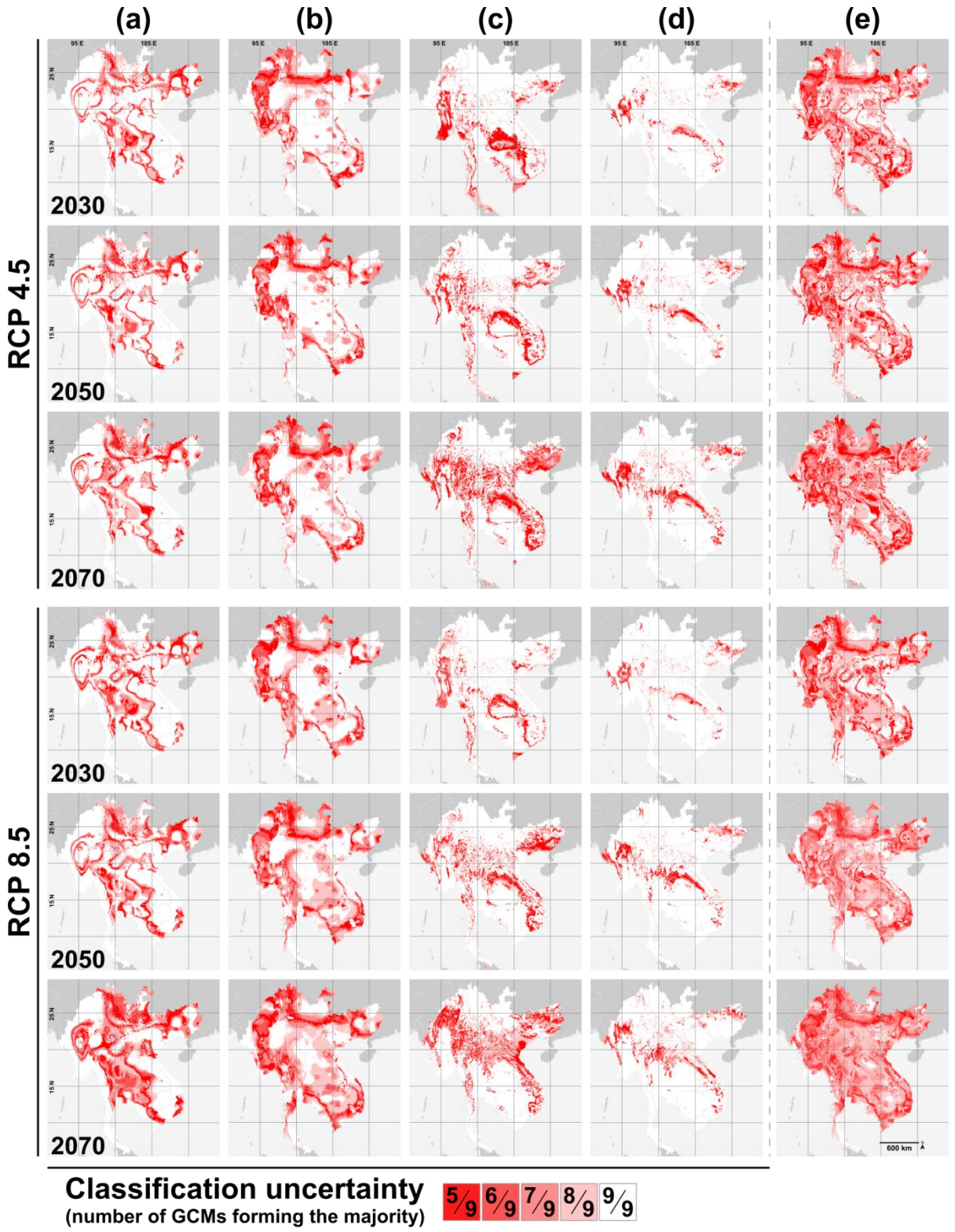

Figure A3.3 Uncertainty in climatic projections for GMS

Number of GCMs forming the majority (ensemble) outcome for each grid cell for the four climatic factors: (a) annual precipitation, (b) intra-annual precipitation distribution, (c) annual mean temperature and (d) intra-annual temperature distribution aggregating to (e) which is their overlaid semitransparent product.

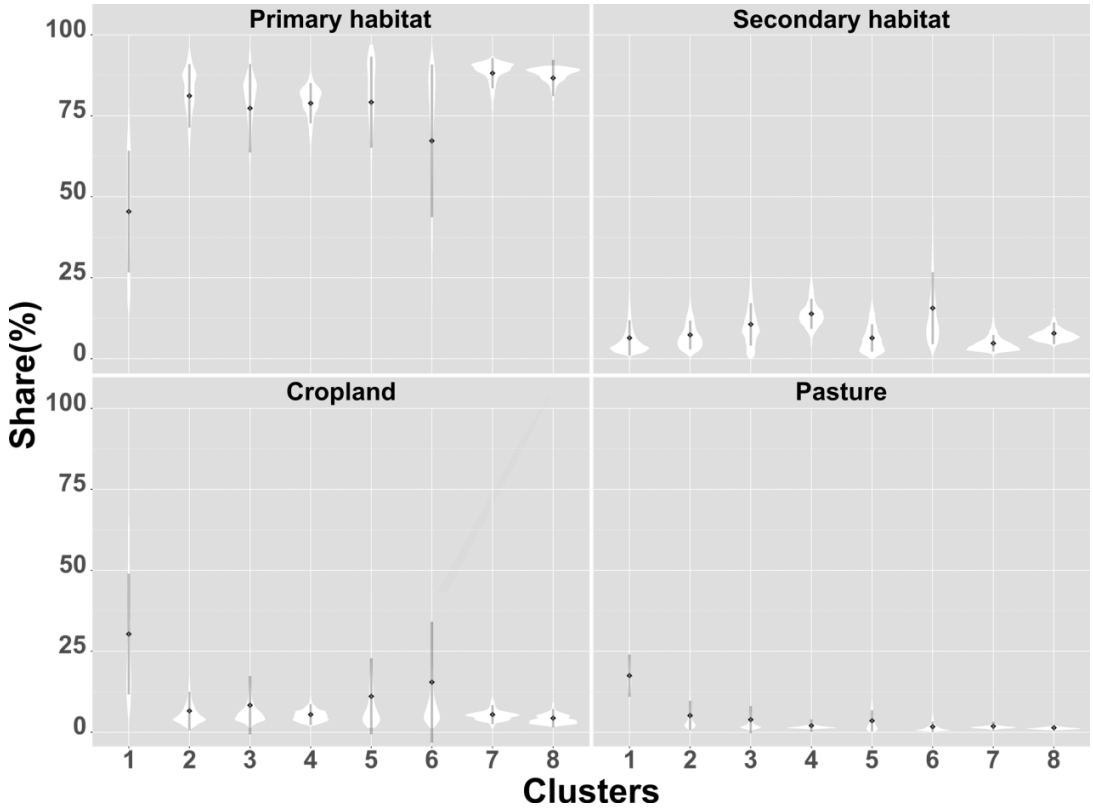

Figure A3.4 Land use composition of the clusters

Terms primary and secondary habitat represent 'undisturbed natural' and 'recovering, previously disturbed natural' habitats respectively. Diamonds and whiskers reflect mean and standard deviation respectively. R package 'ggplot2' 2.1.0 was used to generate this figure.

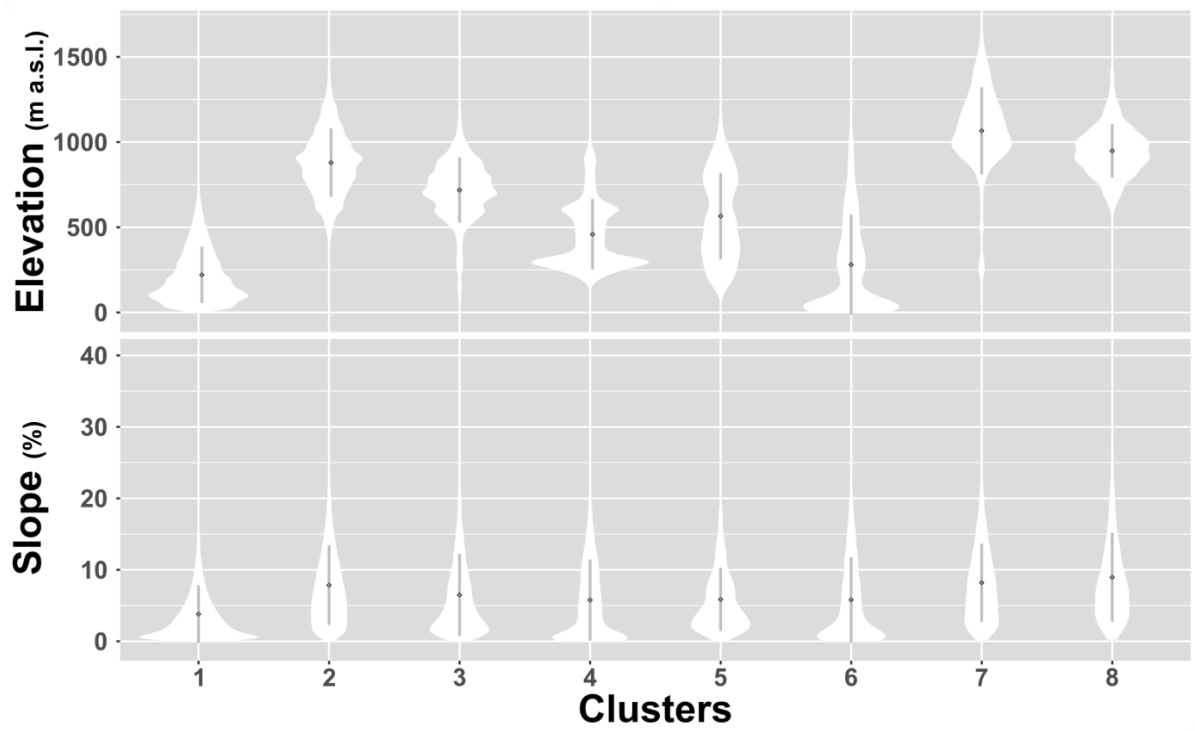

Figure A3.5 Physiographic conditions of the clusters

Diamonds and whiskers reflect mean and standard deviation respectively. R package 'ggplot2' 2.1.0 was used to generate this figure.

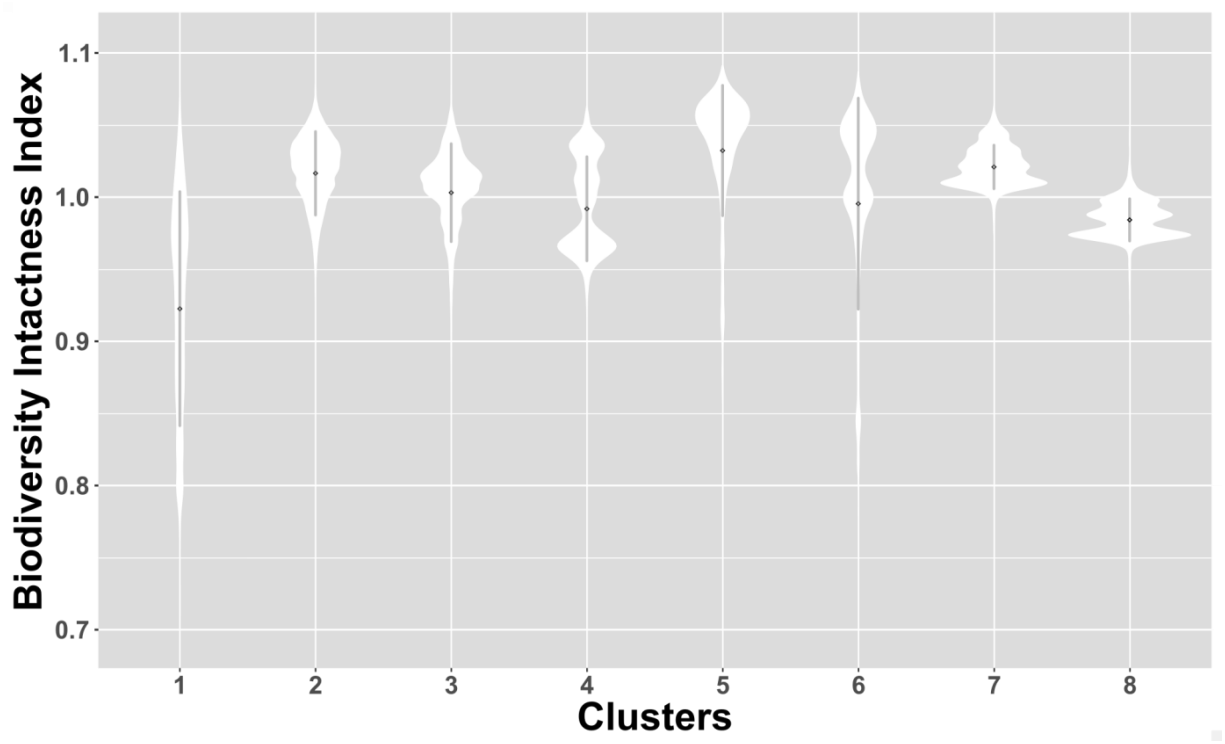

Figure A3.6 Biodiversity intactness index (BII) in clusters
Diamonds and whiskers reflect mean and standard deviation respectively. R package 'ggplot2' 2.1.0 was used to generate this figure.

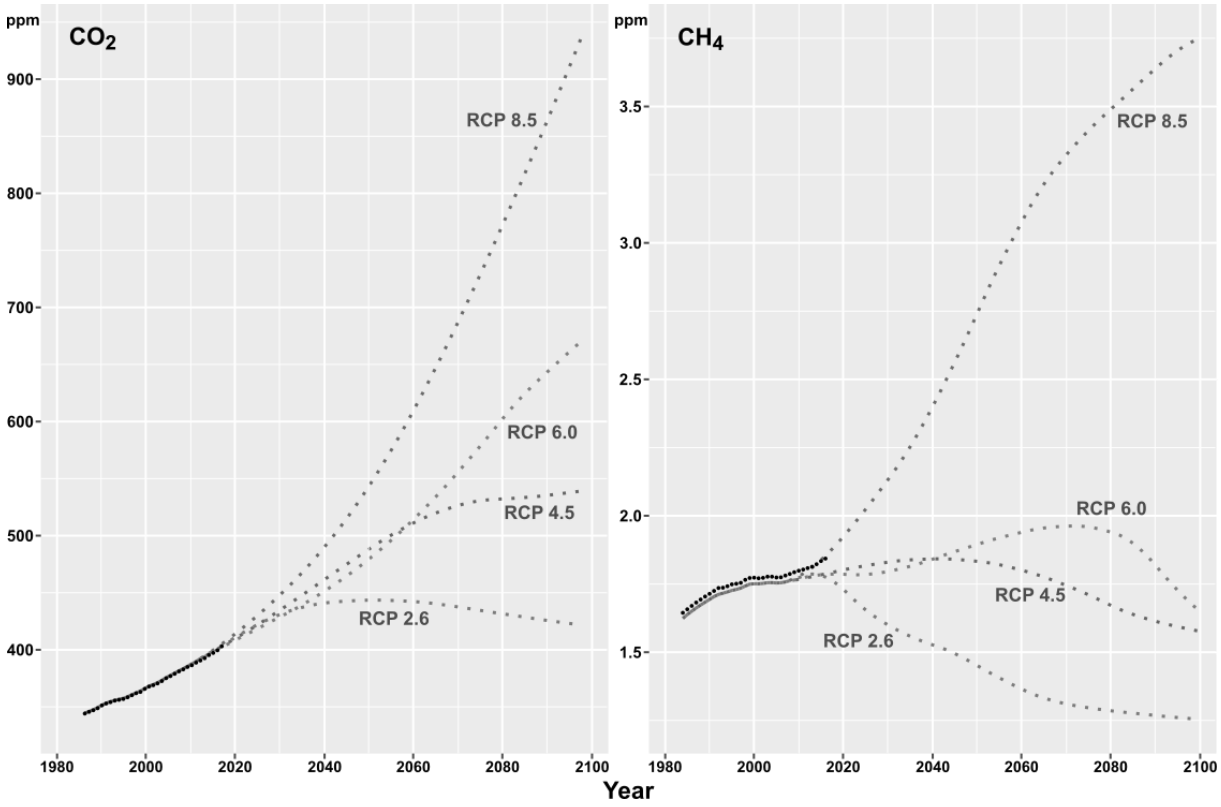

Figure A3.7 Historic and projected trajectories for the main GHGs
Historic (1984 - 2016) global emission records (black dots) for CO_2 (Dlugokencky and Tans 2017) and CH_4 (Dlugokencky 2017) vs. AR5 projections (Meinshausen et al. 2011)

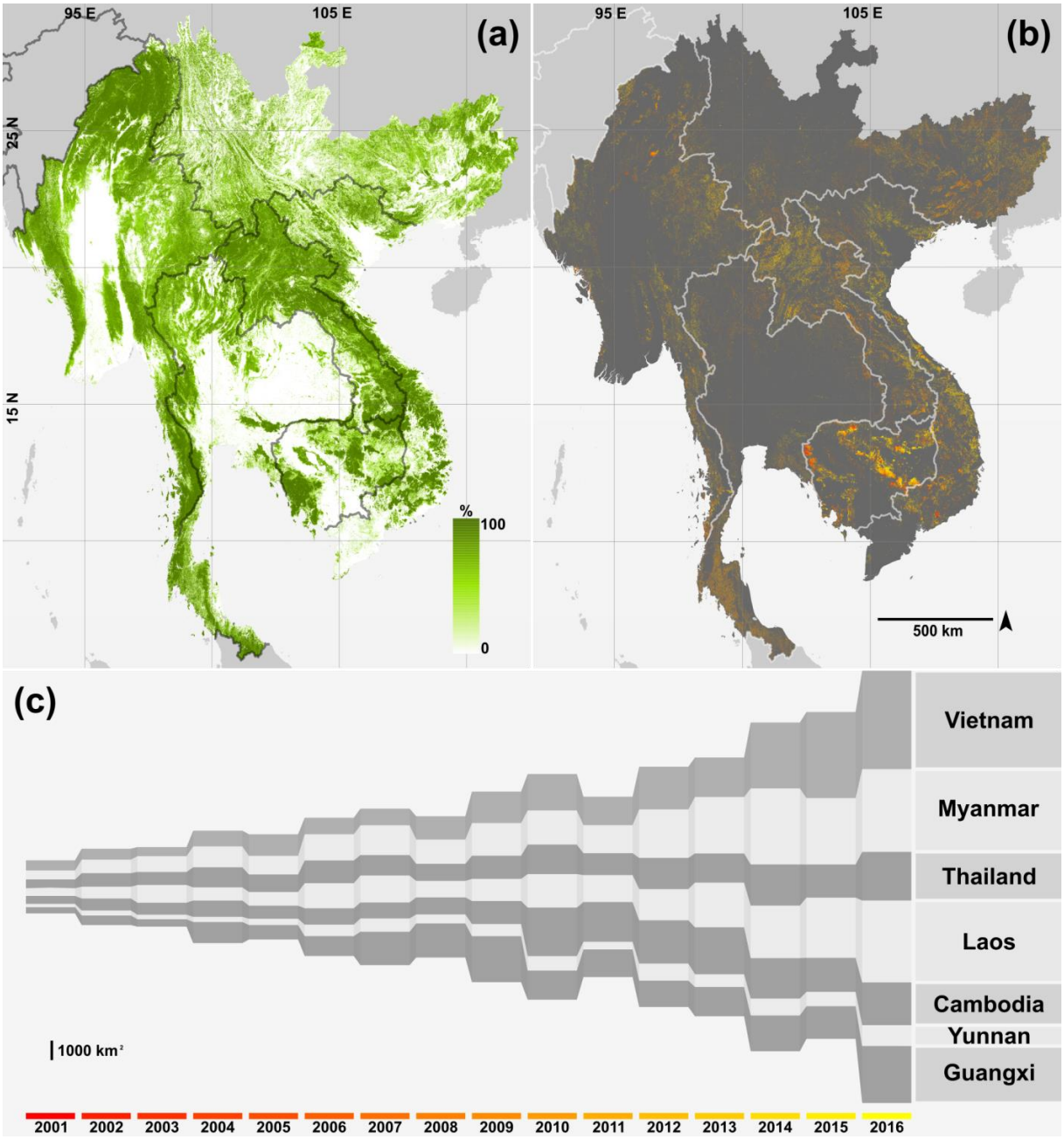

Figure A3.8 Forest cover (2000) and deforestation (2001-2016) in GMS

Produced from the Global Forest Change data (Hansen et al. 2013) version 1.4 (2017 update, available at http://earthenginepartners.appspot.com/science-2013-global-forest/download_v1.4.html) which extends the temporal coverage of the remote sensing to 2016. Panel Ⓐ shows the forest cover in year 2000 with the color ramp reflecting the canopy closure for grid cells. Panel Ⓑ illustrates the forest cover loss and its spatiotemporal trend since 2000. Panel Ⓒ reflects the annual increments of the newly deforested area for each year broken down by the administrative divisions (not cumulative).

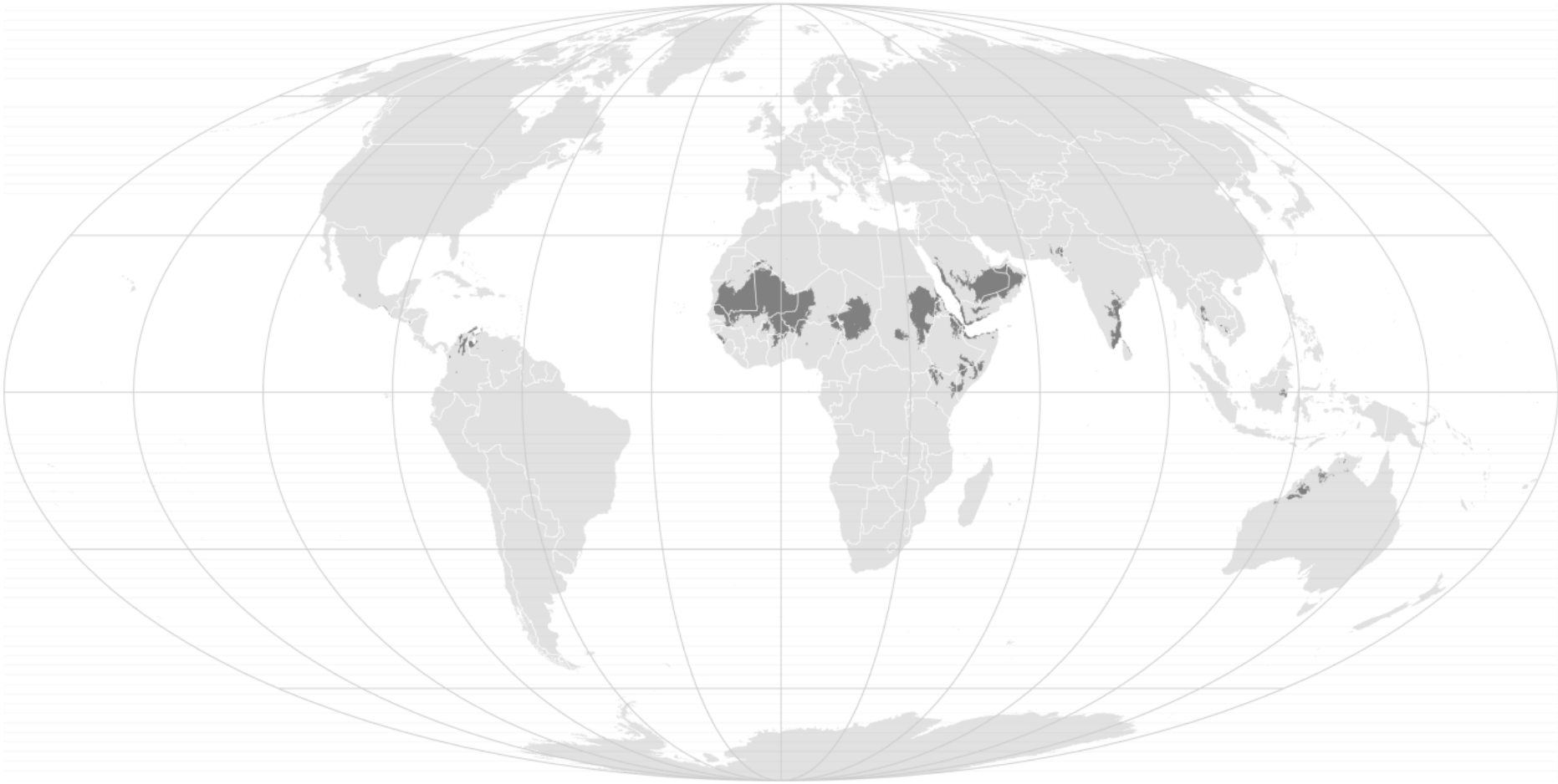

Figure A3.9 Global distribution of annual mean surface temperature above 28°C
This figure is generated from WorldClim 2.0 data (Fick and Hijmans 2017) using ArcGIS 10.2.2 and visually optimized in Inkscape 9.1.

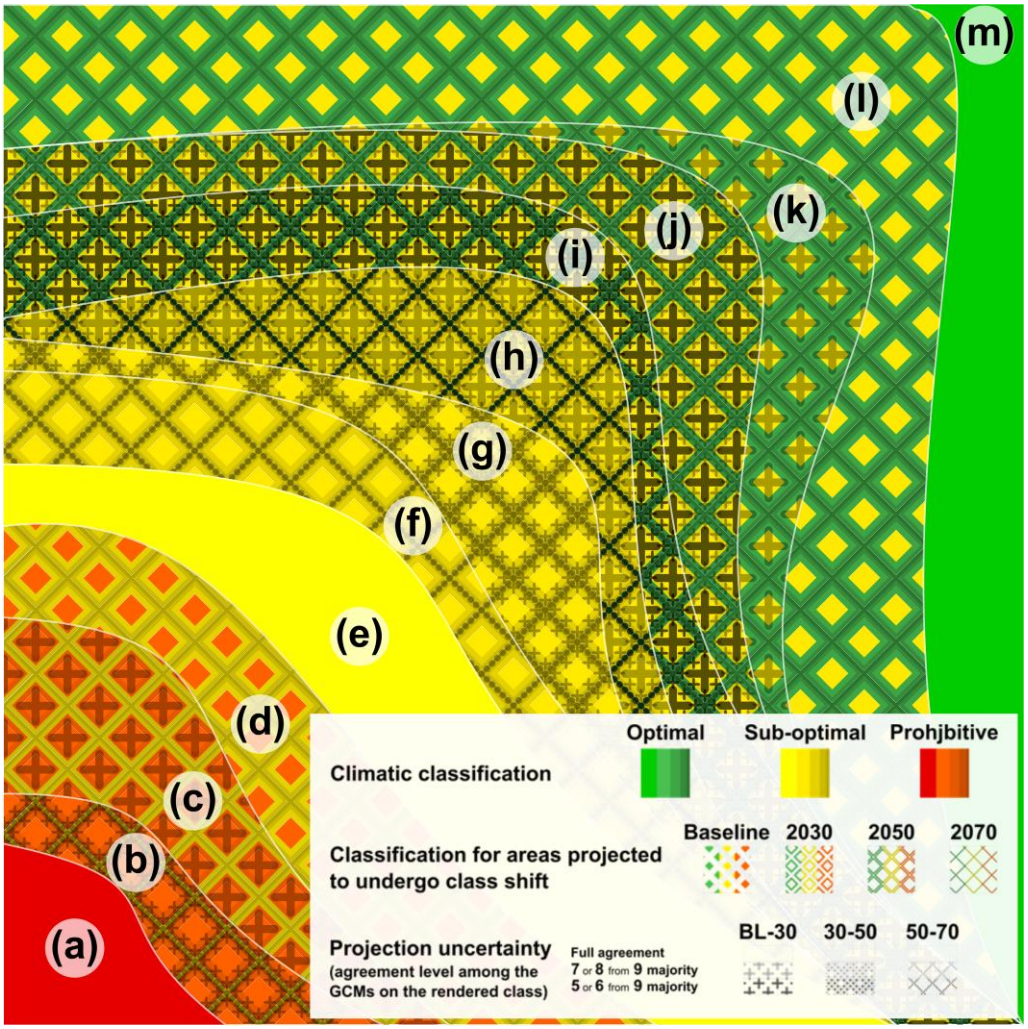

Figure A3.10 Ilustration consept used in climatic class dynamics maps

This schematic diagram provides supplementary examples to further clarify the innovative graphical concept used in the illustration of the maps presented in Figures 3.5, 3.7 and 3.11. Sections denoted by (a), (e) and (m) are projected to retain the baseline climatic class across the whole time span covered in this study with all involved GCMs agreeing upon the classification outcome. In other parts of the diagram, the diamond-shaped pattern suggests a projected change in class by time, absence of full agreement in the ensemble or a combination the two. The solid diamonds reflect the baseline class, while the hollow diamonds wrapping the solid diamonds delineate the future projections. Wherever a class shift is projected by a non-consensus ensemble majority, the concerned projected transition is overlaid with crosses or dots partially covering the two involved periods (the respective diamonds). Compared with the section (a), section (b) is projected to shift from Prohibitive class to Suboptimal first at the 2050 to 2070 time step, while projections associated with time sections after 2030 are both based on a (7 or 8 from 9) strong majority. For section (c) this transition is projected to happen one time period earlier (2030 to 250 time step) with full ensemble agreement (hence the absence of crosses), while a strong majority suggests the Prohibitive class to be retained until the end of the 2030 period. In section (d), transition from Prohibitive to Suboptimal class at the 2030 time step is projected with full ensemble agreement. Section (f) is projected to retain its Sup-optimal class by 2070, with full ensemble agreement until 2050 and with strong majority at the 2050 to 2070 time step. Compared with section (f), section (g) loses the full agreement at the 2030 to 2050 time step to strong majority which for section (h), covers the baseline to 2030 time step. Section (h) is also assigned the Optimal class by 2070 by a weak (5 or 6 from 9) majority. For zones marked with (i) and (j), transition to Optimal class is Projected to occur one time step earlier (2030 to 2050), both projected with weak majority to retain their Suboptimal class by 2030, while the 2030 to 2050 transition from Suboptimal to Optimal class is supported by weak ensemble majority for (i) and strong majority for (j). Zones (k) and (l) are projected to transit from Suboptimal to Optimal by 2030, with strong majority transition projection for (k) and full ensemble agreement for (l). They both are projected with full ensemble agreement to retain their Optimal status thereafter. Inkscape 9.2 was used to generate this figure.

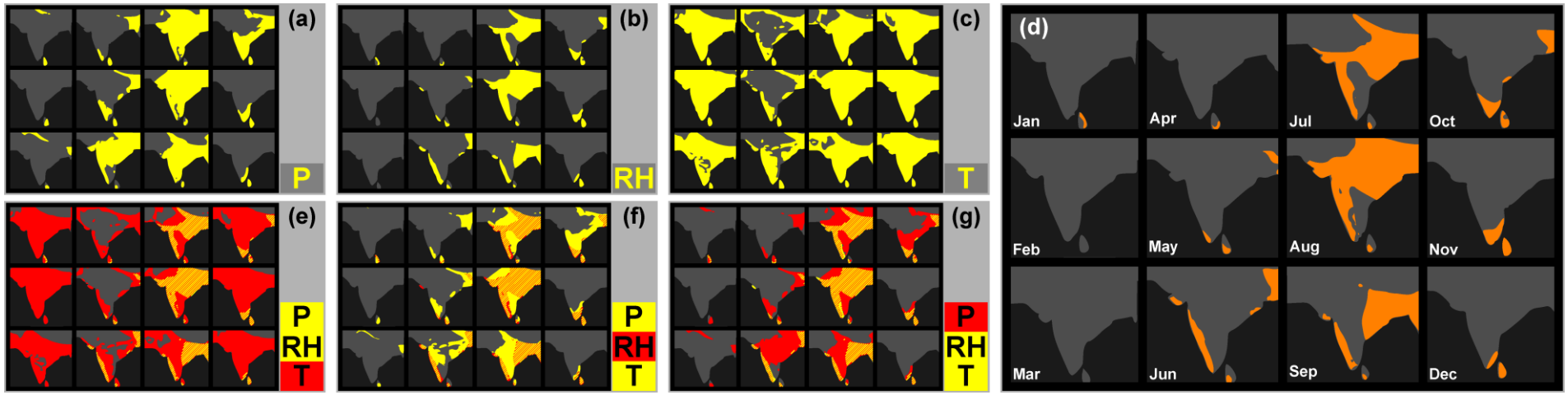

Figure A4.1 The de facto redundancy of monthly mean temperature in detection of areas climatically suitable for formation of South American Leaf Blight (SALB)

This figure based on Roy et al. (2017), maps the potential area climatically conducive to rubber for the Indian subcontinent. The following criteria and thresholds were considered by Roy et al. (2017) to be necessary for SALB infection: monthly total precipitation ($P \geq 63$ mm), monthly mean relative humidity ($RH > 65$ %) and monthly mean temperature ($18.5°C \leq T < 36.5°C$). The area accommodating each single criterion for each month of the year is reflected in panels (a) to (c) and the area matching all three criteria yields panel (d). We have produced panels (e) to (g) which evaluate the relevance/redundancy of the variables by checking the area rendered by a subset of two criteria at each turn against the third criterion. It can be seen in panel (e) that the area of red shade (related to variable 'T') completely engulfs the area retuned by the two other criteria and therefore has no contribution to the determination of the spatial span of the final outcome. Inkscape 0.92 has been used for the vectorization of the source image and also for its further processing.

Please consult the electronic (PDF) version of this thesis or

https://doi.org/10.3390/f10030203 or

https://doi.org/10.5281/zenodo.2576857

Video A4.1 Trends for humidity and precipitation in relation to outbreak risk of South American Leaf Blight
Spatiotemporal patterns demonstrated here are extracted from 30 years of gridded historical data using Emerging Hot Spot Analysis. Applied thresholds stand for conditions leading to continuous leaf wetness which paves the way to South American Leaf Blight outbreak. Still frames were generated using ArcGIS Desktop 10.6 and rendered to video using Blender 2.79.

Please consult the electronic (PDF) version of this thesis or

https://doi.org/10.3390/f10030203 or

https://doi.org/10.5281/zenodo.2576857

Video A4.2 Simplified trends for humidity and precipitation in relation to outbreak risk of South American Leaf Blight
This is a simplified view of Video 1 in which the variables behind the patterns are not distinguished. HS, CS and NS stand for 'hot spot', 'cold spot' and 'no pattern/pattern not significant' respectively. Still frames were generated using ArcGIS Desktop 10.6 and rendered to video using Blender 2.79.

Please consult the electronic (PDF) version of this thesis or

https://doi.org/10.3390/f10030203 or

https://doi.org/10.5281/zenodo.2576857

Video A4.3 Significant risk cold spots for South American Leaf Blight outbreak overlaid with climatically optimal and suboptimal areas for rubber cultivation
This is a simplified view of Videos 1 and 2 overlaid with the geographical extents of climatically optimal and suboptimal areas for rubber cultivation (see Figure 4.1). Area×day combinations for which at least one of the two criteria considered in this study (relative humidity and precipitation) is found by Emerging Hot Spot Analysis to be a significant cold spot (as defined in the methods section 4.2.2), and thus potentially low risk 'points in time' for South American Leaf Blight are reflected in brown. Still frames were generated using ArcGIS Desktop 10.6 and rendered to video using Blender 2.79

This PhD thesis focuses on three climate-related aspects of Para rubber (*Hevea brasiliensis*) cultivation in areas where altitudes and latitudes higher than its endemic range create conditions which are labeled nontraditional, suboptimal or marginal for rubber cultivation: 1. rubber yield in relation to the meteorological conditions preceding harvest events, 2. potential geographical shifts in rubber cultivation through climate change and 3. assessment of climate driven susceptibility to South American leaf blight (*Pseudocercospora ulei*) of rubber.

UNIVERSITÄT HOHENHEIM